ERIM
FORMERLY WILLOW RUN LABORATORIES, THE UNIVERSITY OF MICHIGAN

STUDY FOR AN OPTICAL PROCESSOR SYSTEM FOR VLA RADIOTELESCOPE DATA

April 1977

123400-8-F

PREFACE

This report describes the results of a seven-month study at the Environmental Research Institute of Michigan (ERIM) for a coherent optical processor system intended for Fourier transform processing of VLA radio telescope visibility function data. The work was performed for the National Radio Astronomy Observatory (NRAO) under Contract VLA-215. The NRAO Project Manager for this effort was L. Somers. The Principal Investigator for this study at ERIM was I. Cindrich and ERIM staff members participating in this program were C. Aleksoff, J. Fienup, A. Klooster and R. Dallaire.

CONTENTS

LIST OF ILLUSTRATIONS

VLA OPTICAL PROCESSOR STUDY

1
INTRODUCTION

A central aspect of radio astronomy is the determination of the distribution of radiated power from celestial sources with the radio telescope. This power distribution or sky brightness, B, is a measure of the power per unit area and per unit solid angle for the temporal frequency band under observation. The sky brightness data obtained serves a primary role in the scientific research on the physics of radio sources and the structure of stars and the universe more generally.

Radio telescopes have evolved over the past few decades from radio receivers of modest performance having simple antennas of limited angular resolution. Present day technology provides receivers of high sensitivity and stability with fine angular resolution obtained by synthetic aperture antenna concepts which utilize a large array of antennas operated in interferometer pairs that scan celestial radiation fields by means of earth's rotation.

The very large array radio telescope (VLA) currently under development by the National Radio Astronomy Observatory (NRAO) employs the aperture synthesis concept. This system provides as its output a signal history called the visibility function V. It is related to the desired measure of the sky brightness function B through the Fourier transform. Thus, Fourier transform post processing of the radio telescope output V allows recovery of a measured version of B.

The purpose of the ERIM VLA optical processor study described in this report was to make an initial assessment of the feasibility of performing Fourier transform post processing of the VLA radio telescope output data using a coherent optical processor system. This study was performed for the NRAO and is directed toward use with the 27-element VLA radio telescope being developed at the Socorro, New Mexico site. The results of the study indicate that optical processing of the VLA radio telescope data is feasible and would provide a method for Fourier transform processing having a large number of input data points and good processing speed and accuracy. Of the four antenna array configurations (A,B,C,D) for the radio telescope, the 72 KM A-array poses the most demanding requirements for processor performance because its visibility data has the largest space-bandwidth product of 3000 cycles. The B, C and D arrays are much less demanding with their reduced u, v plane sizes of 21.92 KM, 6.67 KM and 2.03 KM and the correspondingly smaller space-bandwidth products of 912, 278 and 84.

The material in this report consists of five sections which provide an overview of the salient properties of the optical processor system concepts and a recommended system design configuration. A more detailed treatment of important signal properties and system design considerations is given in a four-part appendix which is included in this report.

2
OPTICAL PROCESSING

The optical processor system is comprised of a coherent optical processing channel, together with provisions for entering visibility data at its input and provisions for observing and removing sky brightness data at its output.

The coherent optical chnnel will be described briefly in this section with a detailed discussion of the entire system given in Appendices A, B, C and D.

The optical channel provides for the rapid computation of the Fourier transform of a large number of sample points of the visibility function when it is entered at the processor input plane as a two-dimensional spatial recording. Figure 1 depicts the general input and output planes of the optical processor.

Several arrangements of the optical elements and the relative locations of the input and output planes is possible; however, they all fall into either of two basic configurations shown in Figure 2. The difference in these arrangements being the location of the input data plane, being before the Fourier lens or after the Fourier lens. The input recorded data must be in a form which causes either an amplitude (transmittance) or phase variation of the field of the light beam wavefront illuminating the input plane. The illuminating beam, after passing through the input data, emerges with a wavefront modulation proportional to the recorded input data and is then diffracted in correspondence to this modulation as it continues to propagate.

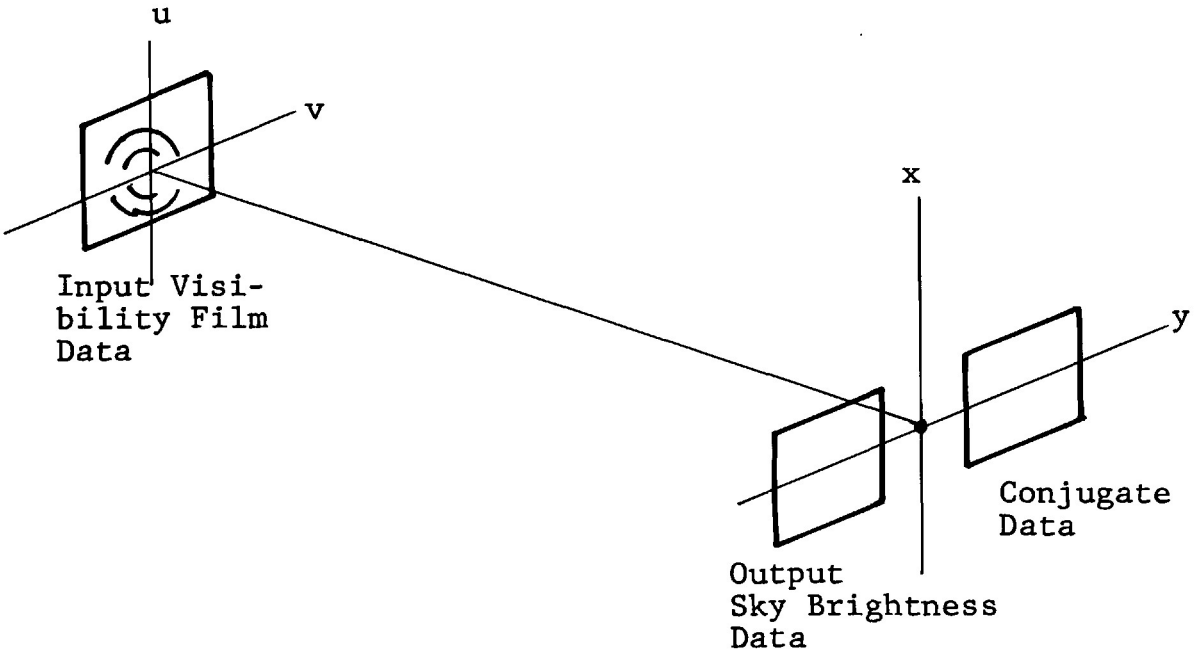

Figure 1. Optical Processor Input and Output Data Planes (Optical Components not Shown).

Simply stated, the basic notion of the optical Fourier transformation process is that of causing a diffracted wave due to any sinusoidal component at the input data u, v plane to focus to a point (spot) of light at the output x,y plane. The location of that point at the output plane is proportional to the frequency of the input sinusoid. The local distribution of the output spot is defined by the Fourier transform of the input data aperture, including any amplitude weighting over the aperture.

The Fourier relationship between the input and output plane of the optical processor is realized in terms of the "field" of the light beam. Since, as a practical matter, the light intensity rather than the light field is accessible for use at the processor output, the optical processing channel will provide the absolute value squared of the desired Fourier transform rather than the Fourier transform, per se. The desired Fourier transform is readily provided, however, with the addition of a reference light beam at the output plane, as shown in Figure 2.

The optical processing channel arrangement shown in Figure 2 simply adds a reference light wave to the normally available Fourier transform light field at the output. The light intensity at the processor output is then the absolute value squared of this sum of reference and Fourier fields which contains a term proportional to the desired output.

Consider the film recorded input data t(u,v) at the processor input plane which is illuminated with the light wave $U_i(u,v)$. The light beam passing through the input plane data is

$$U_i(u,v)\ t(u,v)$$

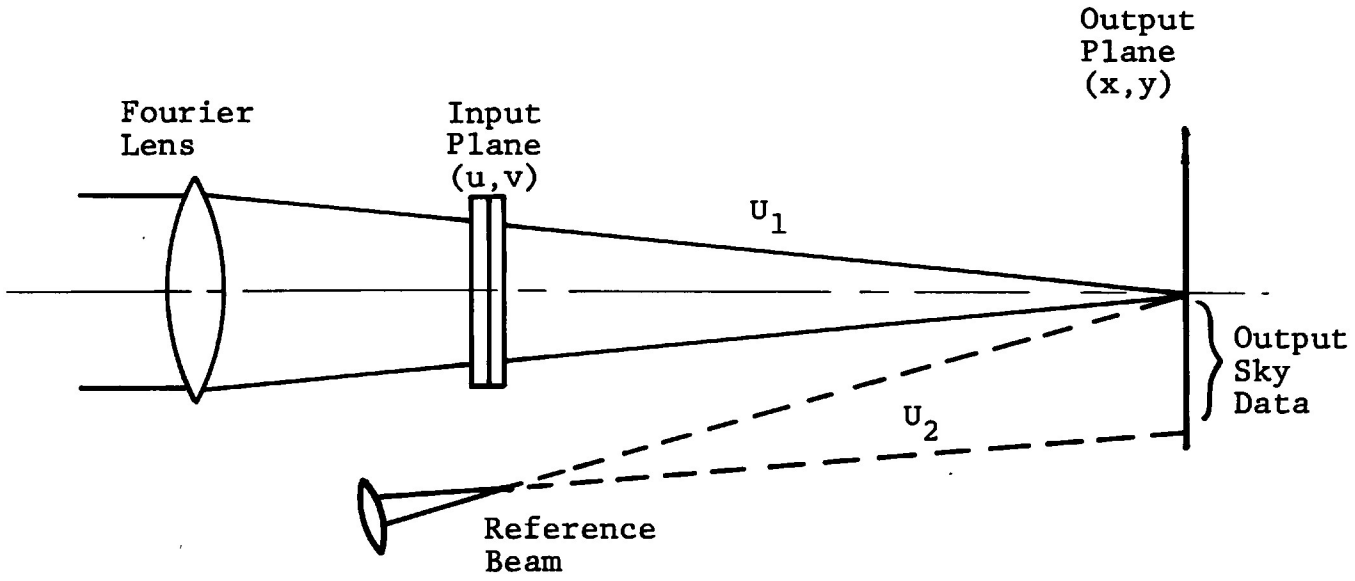

(a) After-the-Lens Input Optical Processing Channel

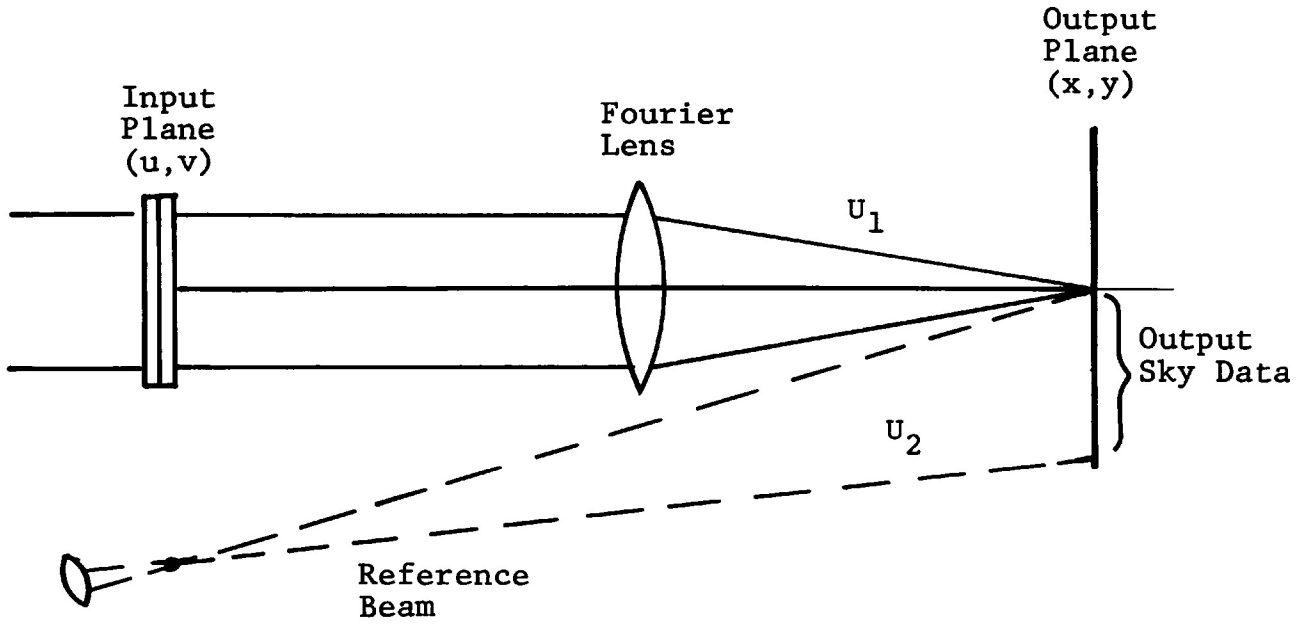

(b) Before-the-Lens Input Optical Processing Channel

Figure 2. Optical Processing Channel Configuratins.

Assuming the case where the illuminating wave has constant amplitude, then at the output plane we have the optical Fourier transform field $U_1(x,y)$ which can be expressed as

$$U_1(x,y) = A_1 e^{j\theta_1(x,y)} F[t(u,v)]$$

$\theta_1(x,y)$ is a residual phase term which typically has quadratic variation with x and y and A_1 is essentially constant. The Fourier transform term F[t] has the explicit form

$$F[t(u,v)] = \iint t(u,v) e^{-j\frac{2\pi}{\lambda z}(xu+uv)} du,dv$$

Here z is the processor working focal length, λ the optical wavelength, and $x/\lambda z$ and $y/\lambda z$ are spatial frequency coordinate at the output plane of the optical channel.

Using a reference wave $U_2(x,y)$ of the form

$$U_2(x,y) = A_2 e^{j\theta_2(x,y)}$$

the optical processing channel output light intensity distribution will be

$$I(x,y) = |U_1(x,y) + U_2(x,y)|^2$$

$$= 2A_1A_2\ F[t(u,v)]\ \cos\ (\theta_1 - \theta_2)$$

$$+ |U_1|^2 + |U_2|^2$$

The output of interest in the general form of the above expression is the Fourier transform term F[t]. It is available multiplied by the constant $2A_1A_2$ and a function cos $(\theta_1 - \theta_2)$, where $(\theta_1 - \theta_2)$ can have a prescribed phase. Of the undesired or extraneous terms, $|U_1|^2$ contains the modulus squared of F[t] and $|U_2|^2$ is the modulus squared of the reference wave. These extraneous terms are to be avoided. This is accomplished by a two step process in which we generate the output twice, each one differing by the value of the phase of $(\theta_1 - \theta_2)$, followed by subtraction of these two outputs. Denoting the output as $I_1(x,y)$ when $(\theta_1 - \theta_2) = 0$ and $I_2(x,y)$ when $(\theta_1 - \theta_2) = \pi$, then the difference $I_1 - I_2$ removes the extraneous terms and gives the desired sky brightness output B(x,y) as

$$B(x,y) = I_1(x,y) - I_2(x,y)$$

$$= 4A_1A_2\ F[t(u,v)]$$

We realize the desired sky brightness map as the Fourier transform F[t] of the spatially recorded version of the visibility function t. As discussed in Appendix B, the recorded data t(u,v) will contain a conjugate pair of the visibility functions as well as a constant bias level. At the output of the processor we use only that part of F[t] which corresponds to the Fourier transform of one of the conjugate pair of visibility functions. It is converted to an electronic signal with a scanning photodetector and then digitized, thus providing digital sky brightness map data to the astronomer for computer analysis and display. The other image is spatially separated and is used for direct viewing of the sky map by the processor system operator.

The complete processor system is comprised of a pre-filter, optical recorder, optical-processing channel, output image photodetector, analog-to-digital converter and a system control unit as depicted in the functional block diagram of Figure 3. The pre-filter serves to convert digital visibility data into an analog form suited to operation of the optical film recorder. Recorded visibility data is entered into the optical-processing channel input u,v plane, processed, read out with a scanning photodetector, digitized and the scan difference computed. The entire operating sequency is automated to a large extent, including the handling of visibility function film recordings.

With the response properties of the total processor system taken into account, the sky brightness data will have the form

$$B(x,y) = 4A_1A_2k_rk_d\left\{F[t(u,v)]G_r(x,y) \otimes g_d(x,y)\right\} \cdot \pi\left(\frac{x}{d_x}\right) \cdot \pi\left(\frac{y}{d_y}\right)$$

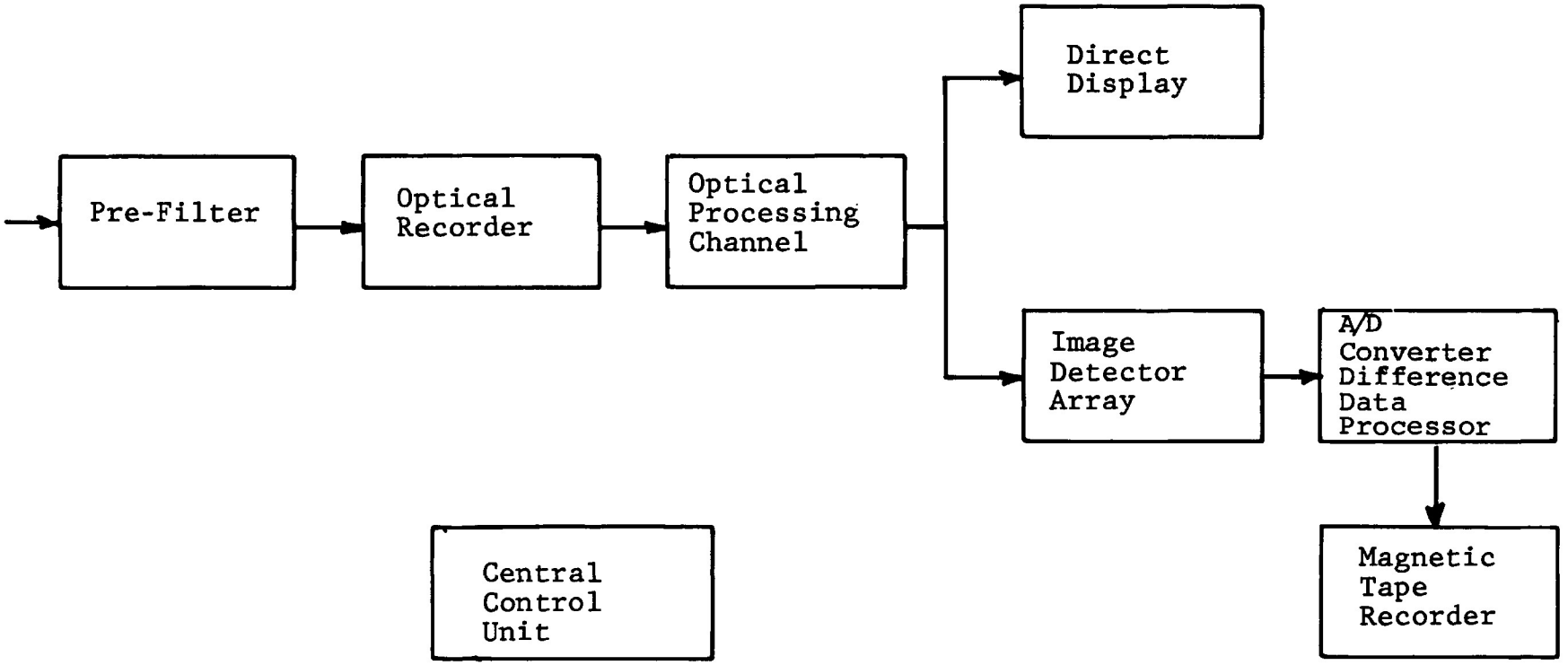

Figure 3. Processor System Functional Diagram.

The output is scaled by $4A_1A_2k_rk_d$ which now includes the optical recorder gain k_r and photodetector gain k_d. It is also weighted by the recorder frequency response function G_r, smoothed by the photodetector spatial response function g_d and sampled by the photodetector as indicated by the sampling functions Ш, with sampling periods d_x and d_y. The derivation of these system response characteristics and a system design and performance analysis is given in Appendix B.

3
EXPERIMENTAL RESULTS

An experimental breadboard of the Fourier transform processing channel was assembled to demonstrate and verify the merit of the basic processing concept.

A diagram of the optical channel is shown in Figure 4. It consisted of an after-the-lens input gate for entry of input data-film recordings. The input-to-output plane spacing or working focal length was 3.3 m. Illumination with a He-Ne laser beam (λ = .6328) was provided by focusing the laser beam onto a pinhole filter and then imaging the pinhole (point source) onto the output plane of the processor with an aspheric Fourier lens. A diverging spherical reference was used originating from a focal point located at the center of the input film plane. This wave was generated by collecting a small portion of the Fourier lens output beam with a lens, which then focused the light to a point at the center of the input plane. The relative phase between the reference beam and the Fourier beam was shifted between 0 and π by changing the length of the optical path of the reference beam. This was accomplished by mounting a flat glass plate in the reference wave just before the reference wave lens. An electronic actuator rotated the plate between two positions of a slightly different angle which caused the reference wave to experience slightly different optical path lengths which were set to correspond to a phase of 0 and π relative to the Fourier beam. This change of phase was synchronized to the output photodetector scan period to allow readout at the brightness plane with two successive scans, which

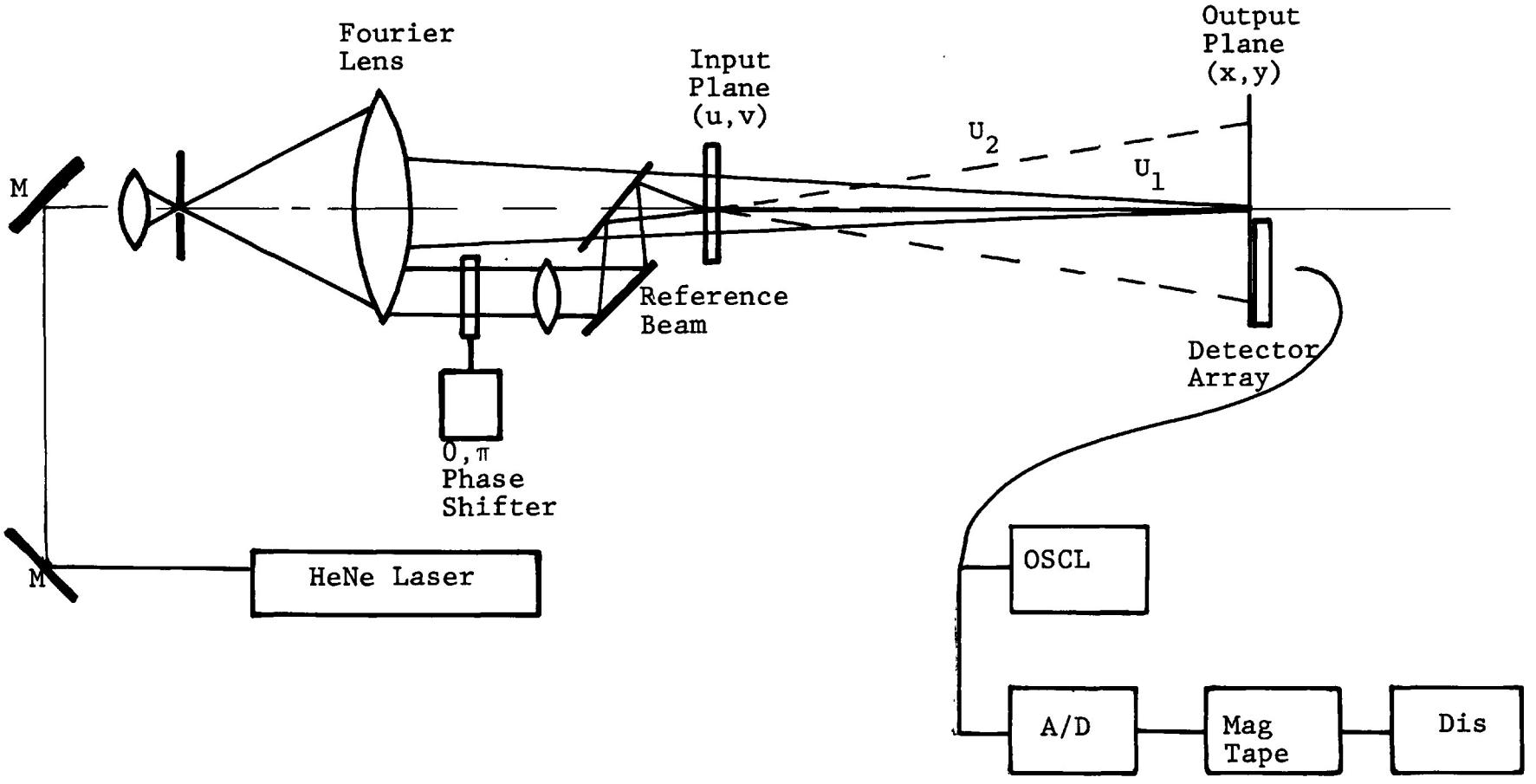

Figure 4. Experimental Optical Processing Channel.

correspond to the 0 and π phase condition. The two scans were then subtracted to obtain sky brightness data as discussed previously in Section 2.

Sample input data for the processing experiments was generated with a precision CRT/film recorder system. Recordings of simple sinusoidal rasters and also of simulated VLA data were made. Simulated VLA data of a point source was provided by the NRAO in the form of computer compatible magnetic tape recordings with the data in a raster format. These tapes were converted to analog electronic data with an appropriate bias level, carrier frequency and synchronization trigger pulses and then recorded on the CRT/film recorder using the ERIM special-purpose data-processing facilities.

A Reticon 1024 element linear photodetector array was used to scan the output sky-brightness plane. Scanning was done electronically along the length of the linear array and the array was moved mechanically in the direction perpendicular to the array length with a precision stepping motor and drive assembly. Data readout at the output plane was viewed on a special-purpose oscilloscope/scan recorder system and it was also digitized and recorded on magnetic tape for viewing on a Ramtek TV-type display which is part of an ERIM computer facility.

Examples of the experimental data obtained at the output of the breadboard optical channel are shown in Figures 5 through 7. Figure 5 shows the results (which do not include compensation of pattern defects in the photo detector) for a one-dimensional scan through the output obtained when the u,v plane input is a clear circular aperture. Data is shown for both single scans through the processor output (a)

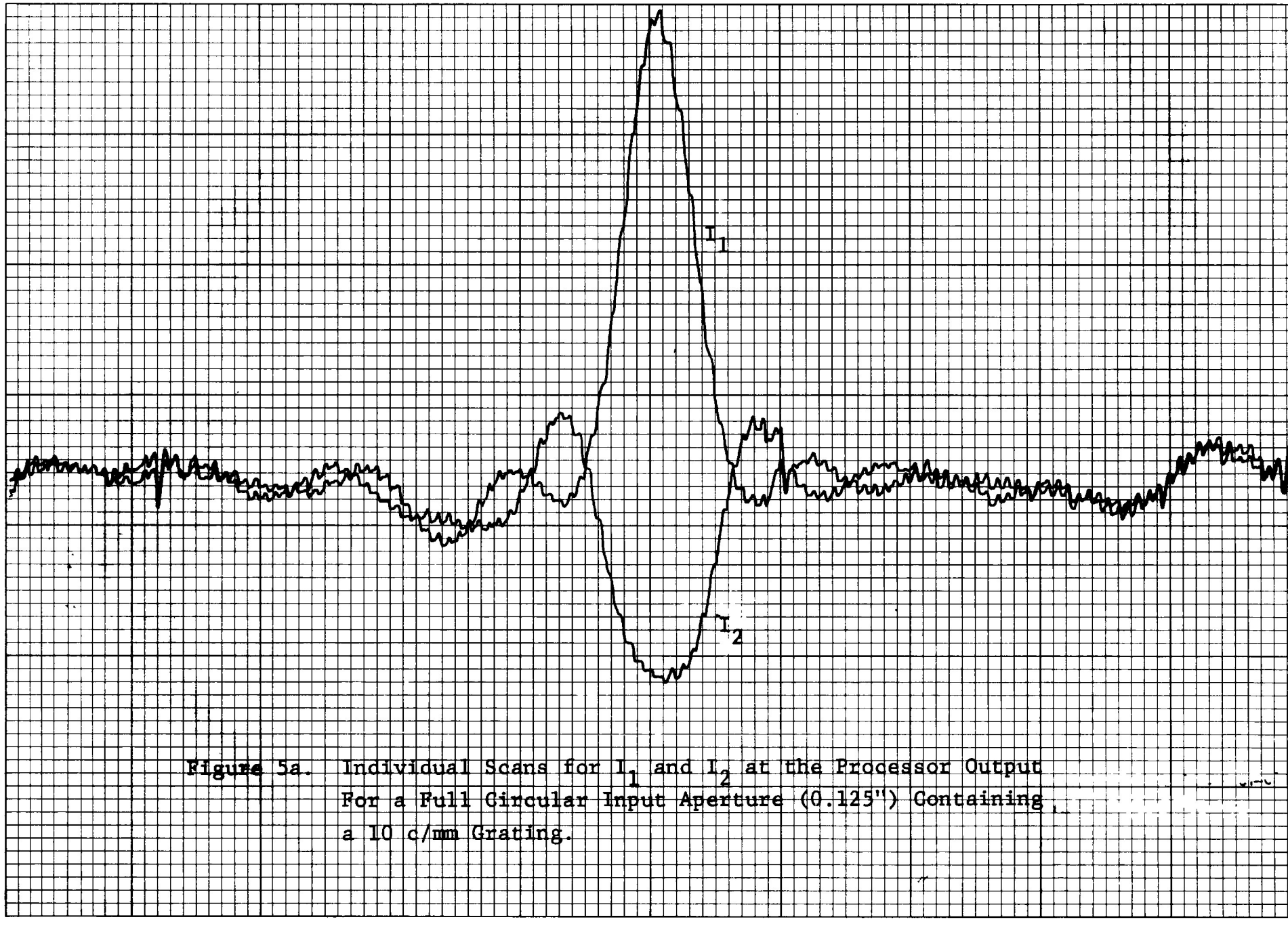

Figure 5a. Individual Scans for I_1 and I_2 at the Processor Output For a Full Circular Input Aperture (0.125") Containing a 10 c/mm Grating.

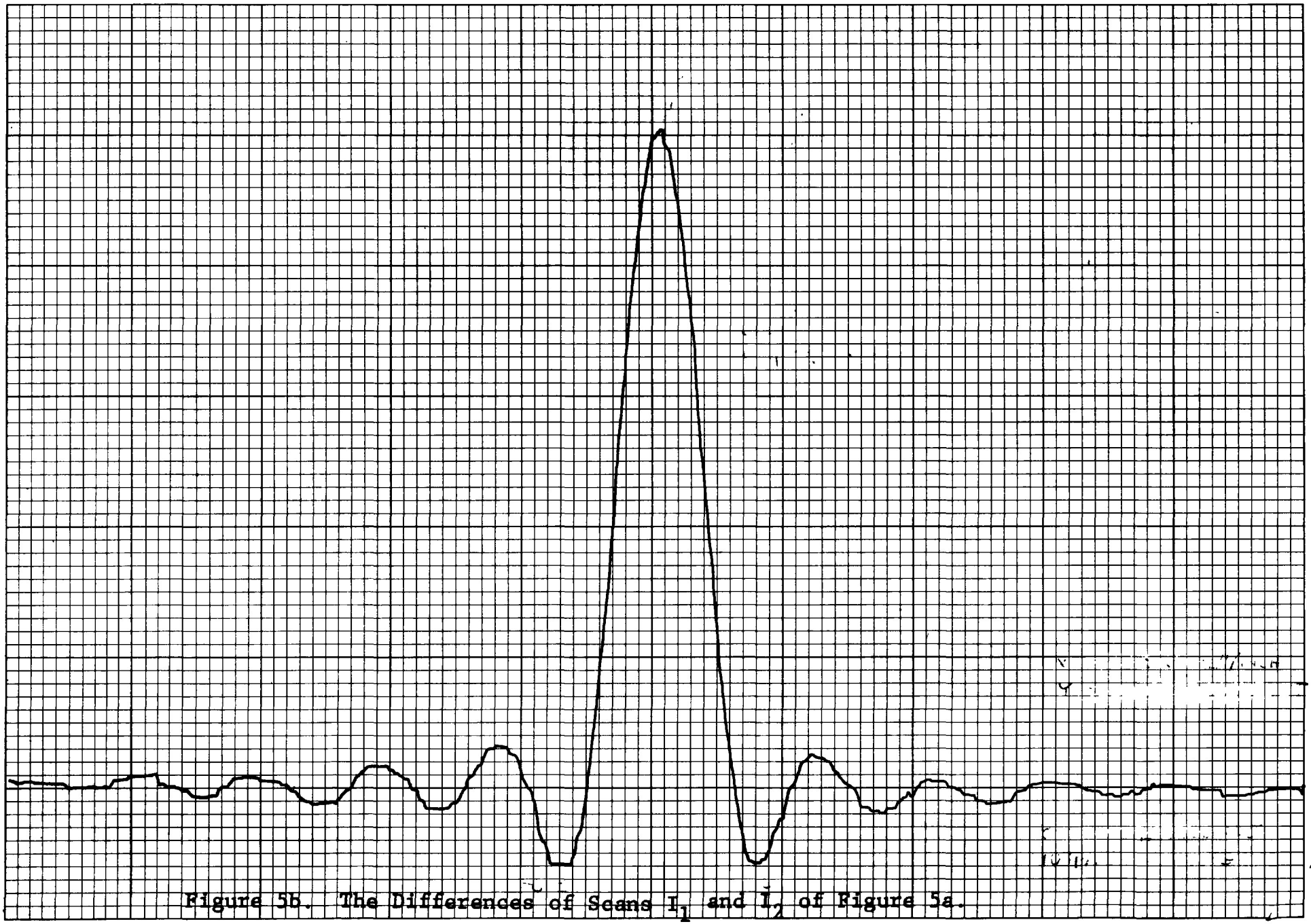

Figure 5b. The Differences of Scans I_1 and I_2 of Figure 5a.

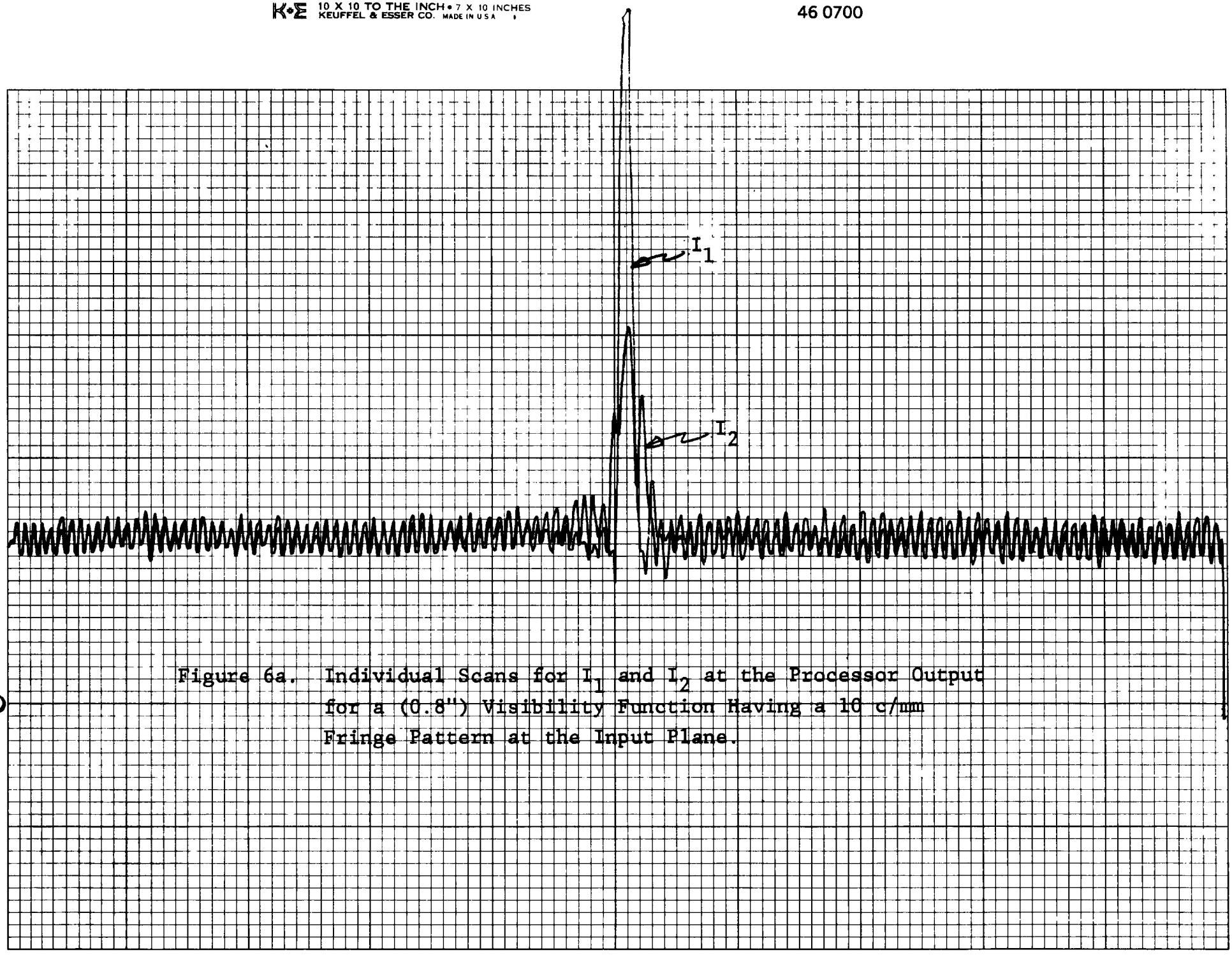

Figure 6a. Individual Scans for I_1 and I_2 at the Processor Output for a (0.8") Visibility Function Having a 10 c/mm Fringe Pattern at the Input Plane.

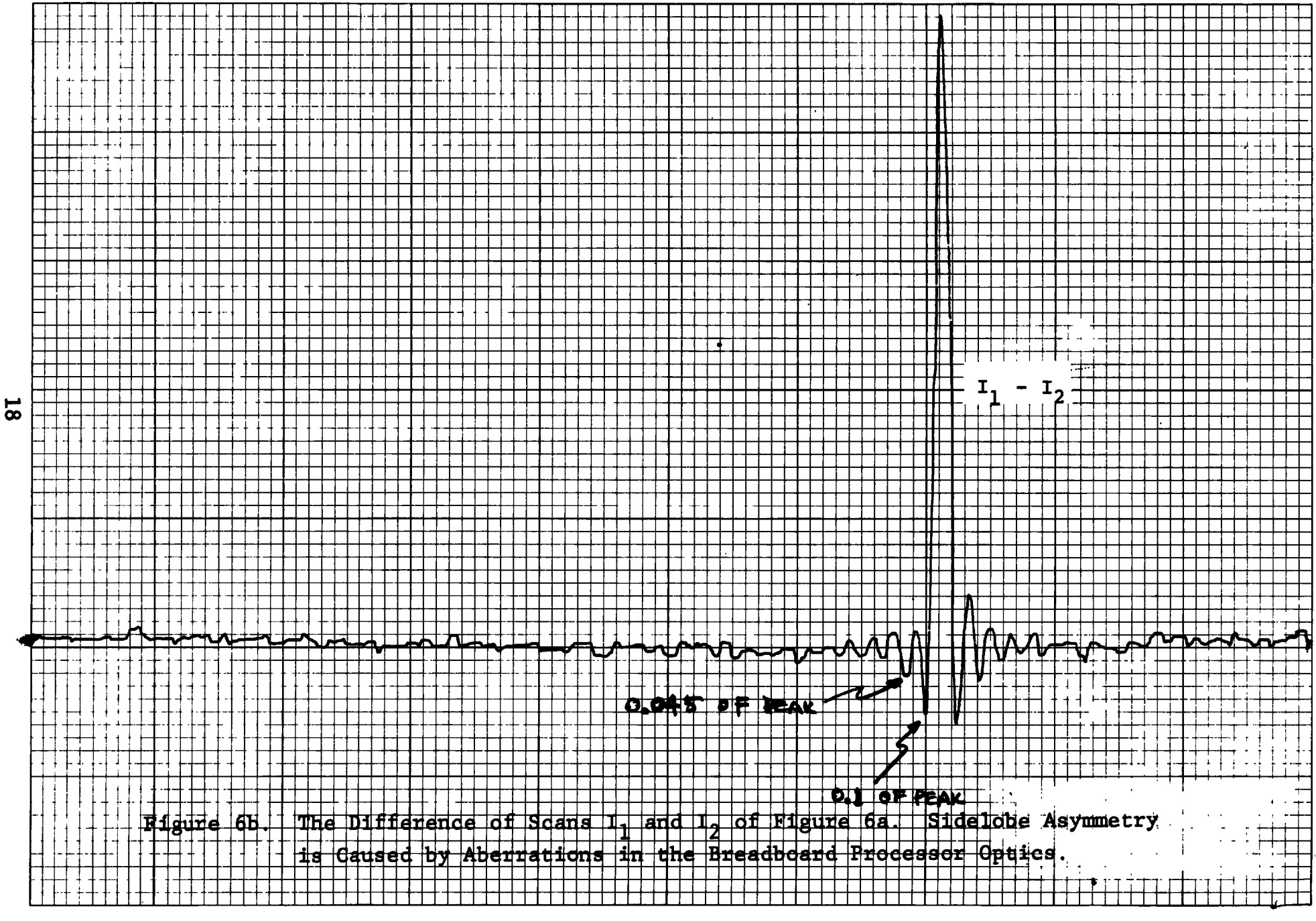

Figure 6b. The Difference of Scans I_1 and I_2 of Figure 6a. Sidelobe Asymmetry is Caused by Aberrations in the Breadboard Processor Optics.

and (b) for the difference of two scans with the subtracted scans differing by the θ and π phase change between reference and Fourier beams in the optical channel. Figure 6 gives similar uncompensated data for a synthetic beam at the processor output when the input u,v plane film data is a CRT/film recording of a simulated visibility function of a point source.

The data of Figures 5 and 6 both do not have photodetector defect compensation. In addition, the data of Figure 6 was obtained using a larger u,v plane aperture than that of Figure 5 and the modest quality of the breadboard processor over this larger aperture caused the nonsymmetric side-lobe error seen in Figure 6(b).

Figure 7 shows a photograph of the sky-brightness plane data seen on the ERIM Ramtek display for the case of a clear square u,v plane input aperture. This data was obtained by a sequence of steps starting with photodetector readout of the processor sky-brightness output plane. Two successive readouts were made. Each was a two-dimensional scan obtained with the Reticon photodetector array. The outputs differed by the 0, π phase conditions within the optical channel of the processor. Each scanned output was digitized, recorded on magnetic tape and compensated for fixed-pattern variations caused by the photodetector (an example of which is seen in Figure 5). The magnetic tape data was then used as the input for a computer subtraction of the two scans (0, π) to give the desired sky-brightness data which was then displayed on a Ramtek (TV) display, as shown in Figure 7. Again a nonsymmetric side-lobe structure can be seen in one dimension because of optical quality limitation over the increased u,v plane aperture used in obtaining this data.

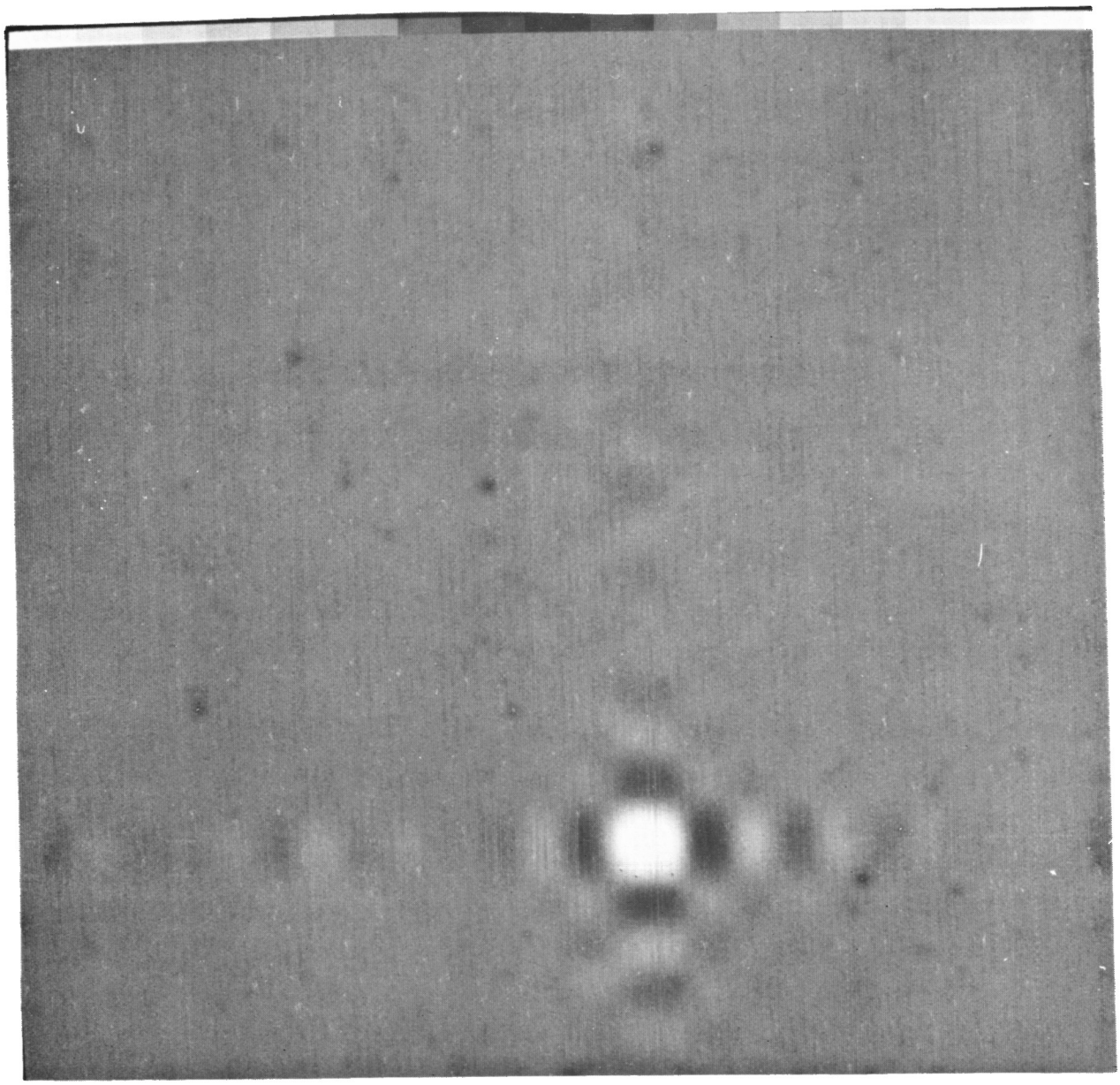

Figure 7. Experimental Optical Processor Output Viewed on a Ramtek TV Display After Detector Readout and Digitization.

The experimental results verify the basic processing concept and demonstrate high-quality, sky-brightness output capability (one percent accuracy) when using restricted u,v plane aperture sizes consistent with the quality available with the breadboard processor system. High-quality, sky-brightness outputs of one percent accuracy are achievable over the required u,v plane apertures with proper design. A configuration suited to the performance requirements for VLA processing is summarized in Section 4.0 and discussed in detail in the Appendices.

4
RECOMMENDED DESIGN AND OPERATING FEATURES

In this section, a summary overview of a recommended design for the VLA optical processor system is given. A discussion of design details is given in Appendices A through D. The recommended VLA optical processor system is comprised of the following subsystems:

Prefilter
Optical recorder (film)
Optical processing channel
Readout detector array
Analog-to-digital converter/processor
System control unit

A plan view of the system is shown in Figure 8 and the flow diagram of Figure 9 indicates the path of data through the system.

We will trace the data flow through the system to establish an awareness of its major functional elements. The pre-filter modifies the digital visibility data made available from the telescope disc storage to an analog form suited for optical recording. A cathode-ray tube optical recorder, writing on photographic film, converts the visibility data to optical transmission variations in the film. Automated film-handling provisions then transport the film from the optical recorder through a rapid film development station and into the input plane of the optical processing channel. Once the visibility function film recording enters the processing channel, its optical Fourier transformation is performed instantaneously providing a light intensity distribution at the processor

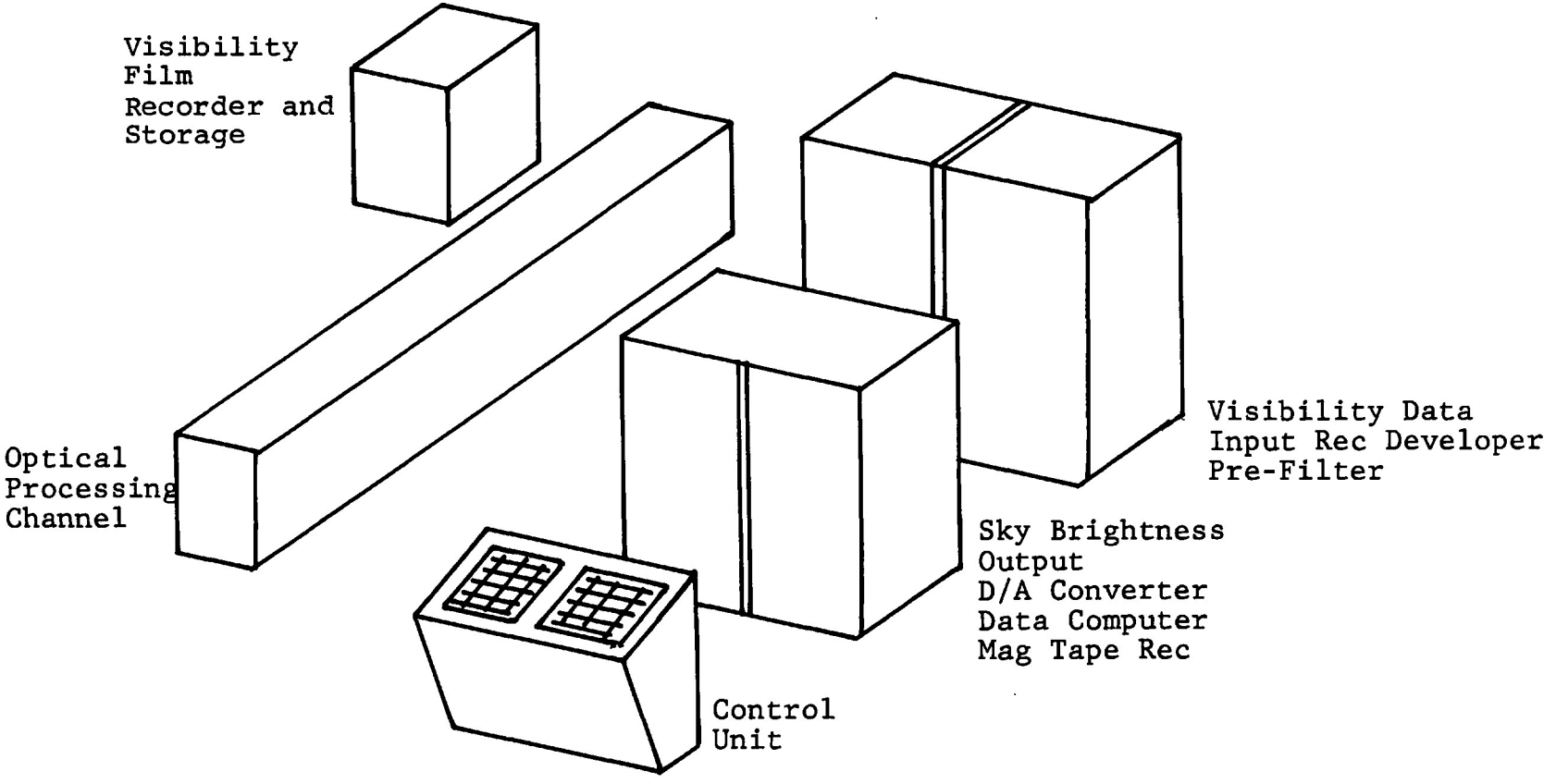

Figure 8. Optical Processor System Plan View

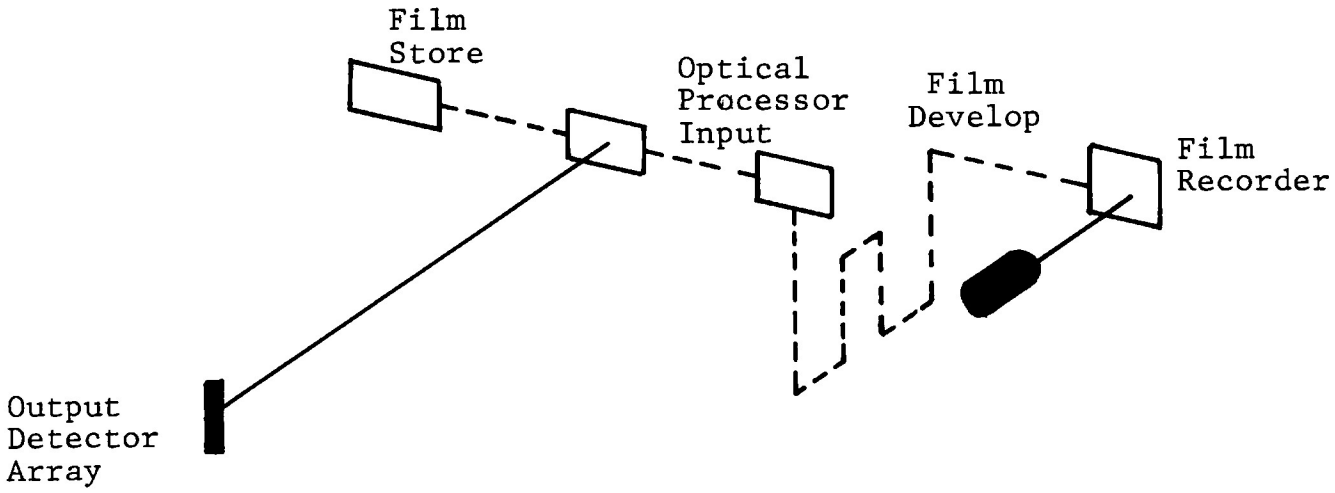

Figure 9. Processor System Data Flow.

output plane which contains the sky brightness data. The output is scanned twice with a photodetector array. The detector array sky-brightness and position data are fed to the A/D converter/processor. The sky data output is digitized and the data obtained from the two scans of the processor output plane are subtracted. These outputs differ for each of the two scans by a prescribed change in the optical phase between reference and Fourier waves in the optical channel. The double scan and subtraction of the outputs is done on a line-by-line basis rather than after a full scan of the processor output plane. The A/D converter/processor provides the desired digital sky-brightness and position data output.

Visibility data processing is done on a frame basis, each frame being identified with a single spectral line or frequency band of the radio telescope. Individual frames are optically recorded on film in 20 seconds or less, depending on scan format. Automatic handling of the film from the recorder through a rapid film developer and into the processor input plane is accomplished on a continuous flow basis but with a 20-second lag time between exposure of the film in the recorder and entry to the processor. Photodetector readout of the sky-map data and conversion to digital form is done in 15 seconds. The observer will have a display of the sky-map data at the processor control unit the moment a visibility data film frame enters the optical processing channel. It is important to note that this display provides full sky-map resolution and full dynamic range. It is made available as an optical projection of the modulus squared of sky-brightness data which is readily available at the processor output.

The A-array visibility function was taken to have a space bandwidth product of 3000 as a design guideline. This corresponds to a totally filled input aperture. The processor output for filled input aperture will have 1230 x 1230 resolvable elements measured between first zeros of its "Airy disc" impulse response function. Photodector readout at the processor output will provide six samples per processor impulse response function. For actual inputs from the VLA A-array aperture, about 10 samples per synthesized beam will be realized.

4.1 DESIGN RATIONALE

The system is designed to accept visibility data without pre-sorting and to provide highly sampled sky-map data of one per cent accuracy for the A-array of the radio telescope. The B, C, and D arrays present less stringent processing demands and are readily accommodated.

To provide one per cent accuracy performance for A-array data requires a close tolerance on sources of processor defects and the use of built-in calibration provisions. Optical processing channel phase defects, spherical wave defects and data position defects have been analyzed to determine performance requirements consistent with obtaining sky-map data of one per cent accuracy.

Phase defects of the spatially slow varying type are the main concern with the cubic phase defect found to require the tightest constraint. A linear phase defect causes a simple shift of position in the output data which is compensated for during calibration of the processor

output plane scale factor. Quadratic phase errors cause a defocusing of the processor output and must be adequately constrained. Higher order phase defects are more tolerable and of a level which does not cause map degradation.

The spherical wave defect, which is deterministic and frame-to-frame repeatable, gives rise to both phase and amplitude defects for which compensation provisions are incorporated. Phase defect compensation is provided by a slight tilt of the plane in which the detector array is scanned and by use of a prescribed and built-in phase variation of the optical channel illuminating beam at the processor input plane.

Recorded data position defects, also expected to be slowly varying spatial functions, must be kept below a peak value of 0.005 per cent of the recorded data aperture width to assure a tolerable effect on output data accuracy.

Variations of system amplitude gain and bias level settings also impact on the accuracy of the system output. Design for one-tenth per cent or better stability for gain and bias control will be provided and the effect of slow variations from the desired gain and bias levels will be corrected by system calibration. System amplitude noise at the processor output must be kept low relative to sky brightness data. Film and photodetector noise, which are expected to be the major noise contributors at the output plane, can be kept low enough to provide a peak signal to RMS noise ratio of about 2000:1.

The output of the processor can contain extraneous data not part of the desired sky brightness information. The system is designed to suppress these data to a negligible level. These extraneous terms, inherent to the optical channel, are comprised of undiffracted or zero order light and a background consisting of the modulus squared of the Fourier and the reference light waves. The zero order is suppressed by use of destructive interference between the zero order and the reference wave and by the use of complementary weighting in the u,v plane. Background terms are cancelled in the double scan and subtract procedure used to readout sky map data.

Calibration of the geometric scale factor at the system output will accommodate scale changes and map-position shifts caused by film shrinkage and linear position defects in the recorder. Net optical linear phase defects will also be removed with this calibration.

4.2 OPERATING PROCEDURES

System operation is largely automated with operating controls provided in a central control unit. One operator of the well-trained technician classification is required to be available to assist the observer and to provide routine maintenance for the system.

The central control unit provides for normal turn-on and activitation of automatic checkout and calibration sequences of the system. The operator is required to make a short routine daily check of the condition of the CRT/film recorder and film developer. The automated system calibration sequence consists of test signal generation, test data

processing and automatic evaluation of the resultant output for recorded data quality, gain and geometric scale factors. Deficient operation is identified as to inadequate recorded data quality or out of tolerance subsystem operation with an indication of such conditions being given at the control unit.

Once the general system checkout and calibration procedure is completed, the system is in a ready condition. In the ready condition, the processor system is prepared to receive and process visibility data from the radio telescope output storage device. Upon activiation of a data dump from the telescope, the prefilter and optical recorder automatically proceed in the process of recording visibility data on film. Recorded film data is automatically handled through the system from the recorder, through the film developer, into the optical processor input gate. At this time the "frame to frame" self calibration cycle occurs to accommodate residual effects due to recorder sensitometry after which film visibility data is processed, read out, digitized and stored. Upon completion of processing and readout the film data is moved automatically to a storage bin from which it can be retrieved for re-processing or removed for retention by the system user.

Should a system malfunction occur, an indicator at the central control unit will indicate the likely subsystem(s) which require attention.

The system is maintained in a ready condition on a 24 hour per day basis. A single switch turn-off will shut the system down. Override control will be available for each subsystem to allow individual subsystem observation for testing and maintenance.

4.3 INSTALLATION FACILITY

The entire system must be located in a room which is temperature and humidity controlled and is kept reasonably free of dust and dust-producing materials. The optical channel and all film transport paths are enclosed. A ventilation exhaust to remove any extraneous fumes from the optical channel liquid gate and the film developer would be required. The entire processor system would require a room having a floor space of about 20 ft by 20 ft.

4.4 CONFIGURATION SUMMARY

A summary of the recommended VLA Hybrid Optical Processor configuration on a system and subsystem basis is provided in tabular form on the pages which follow.

PROCESSOR SYSTEM

DATA INPUT

Data dump format:	b-t-f and t-b-f
Data content:	16 bit word for R, I, u, v
Data dump rate:	2×10^5 words/sec per channel
Data recording format:	Random access and continuous (elliptical)
Data recorder encoding:	Analog on a carrier
Space-bandwidth product:	3000
Weighting provisions:	Gaussian, "Uniform" (optical)

DATA OUTPUT

Electronic Readout

Resolution:	1230 x 1230 PSF (null-null)
Map size:	103 mm x 103 mm
Sampling:	10points per A-Array synthesized beam (null to null)
Total samples:	7200 x 7200 max
Map accuracy:	A-array 1%, B,C,D array $\leq$ 1%
Auxiliary data:	Telescope parameters, date

Direct Viewed Display

Map size:	400 mm x 400 mm
Screen type:	Liquid crystal
Resolution:	Full
Dynamic range:	Full

PROCESSOR SYSTEM (continued)

DATA PROCESSING RATES

Twenty seconds per map (continuous)

Fifty-five seconds per map (single map)

AUTOMATIC CALIBRATION

System gain factor

System spatial scale factor

PRE-FILTER

TYPE

This is a special purpose electronic device which must provide the following functions.

Digital R/I visibility data conversion to analog form

Digital u,v position data conversion to analog form

Injection of a prescribed carrier frequency into the analog visibility data

Interfacing analog visibility data and u,v position data with the optical recorder

INPUT

16 bit digital R/I visibility data

16 bit digital u,v position data

PERFORMANCE

Analog visibility data

Conversion accuracy:	13 bit equivalent
Carrier frequency accuracy:	$\leq 0.02\%$
Carrier phase stability:	$\leq \pi/50$

Analog u,v position data

Conversion accuracy:	16 bit equivalent

OPTICAL RECORDER

TYPE

Cathode ray tube recorder working into silver halide film.

Major components are:

- CRT and electronic controls
- Projection lens
- Film transport and electronic controls

PERFORMANCE

Film plane writing aperture:	50 mm x 50 mm
Film frame size:	70 mm x 70 mm
Film plane spatial bandwidth:	60 c/mm at 50% response
Scan linearity and accuracy*:	$\leq 1.7 \times 10^{-3}$ mm PP errors (frame basis)
Recorded data amplitude linearity:*	0.1% for $0.1 \leq T < 0.9$
Bias stability:	0.1%
Temporal bandwidth:	10 MHz to 50% response
Scan settling time:	≤ 5.0 μsec

LOCAL CONTROL AND MONITORS

Scan linearity	(Closed loop calibration)
Beam focus	(Dynamic correction)
Beam bias	(Closed loop control)

*With calibration included.

OPTICAL PROCESSING CHANNEL

TYPE

After-the-lens coherent optical Fourier transform processing channel with on axis reference wave. Major components are:

- Fourier lens with spherical wave defect compensation
- Input film liquid gate, liquid supply and automatic film feed mechanism
- Film centering control
- Fourier beam-forming optics
- Reference wave beam-forming optics
- Output plane projected image display optics and viewing screen
- Output plane relative optical phase sensor and control system
- Output plane readout photodetector array mounting and transport provisions
- Output plane energy-based exposure control
- Laser light power monitor and control
- Fourier wave light power monitor and control
- Reference wave light power monitor and control
- Enclosed optical mounting table for integrated assembly of the entire optical channel

PERFORMANCE

Processor input aperture:	65 mm x 65 mm
Working focal length:	3,300 mm
Fourier and reference wave relative phase:	$+90^{o} \pm 1^{o}$ $-90^{o} \pm 1^{o}$
Sensing and readout for:	Reference wave power, Fourier wave power, Laser output power, Calibration

OPTICAL PROCESSING CHANNEL (continued)

PERFORMANCE (continued)

Spherical wave defect: Phase defects: Amplitude defects:	To be limited or compensated for to an extent which allows one percent sky-brightness data (measured relative to the map data peak and first side lobe of a synthetic beam) for a 50 x 50 mm u,v plane input aperture. See Appendix C for defect tolerances.

SKY BRIGHTNESS READOUT PHOTODETECTOR

TYPE

Solid state array using combined electronic and mechanical scan.

PERFORMANCE

Spatial sampling:	7200 x 7200 rectangular grid
Sample spacing:	15 μm ± 1.0 μm
Scan time:	≤ 15 sec for 7200 x 7200
Scan format:	7200 samples/line
Dynamic range:	≥ 2500
Linearity*:	0.05%
Pattern noise*:	0.05%
Saturation blooming:	adjacent cell limited

*Including calibration

SKY-BRIGHTNESS READOUT PROCESSING

TYPE

This device consists of the following functional parts:

Analog-to-digital conversion sky brightness and position data

Digital subtraction for two 7200 word lines of sky-brightness data

Digital x,y position data

Buffer line storage of subtracted data lines and corresponding x,y position data

Calibration sequence control of the photo-detector and calibration, data storage and insertion

Outputs consisting of 13-bit sky-brightness data, 16-bit position data and auxiliary defining data, telescope scan and operating parameters and data-processor parameters

CONTROL UNIT

This unit provides for central control of the hybrid optical processor system. It will include the following provisions:

System on, ready, off control

Subsystem decoupling control

Subsystem errors and go-no-go monitor

System calibration indications

Laser, Fourier and reference wave light power indicators and adjustment control

Sky-brightness (modulus squared) display

5
SYSTEM DEVELOPMENT PLAN

The study reported here served as an initial assessment of the feasibility of an optical processor system for VLA data processing. A program for design, fabrication, and operating site installation of an optical processor system would consist of the following program elements:

1) Preparation of a finalized detailed design, design specifications and system costing ($60K).
2) Fabrication of subsystems and subsystem testing ($1.0M).
3) Operating site facility construction ($40K).
4) System integration and testing ($100K).
5) Finalized system installation and checkout at the operating site ($20K).
6) System documentation preparation ($10K).

Our current estimate is that this program could be accomplished in 22 months at a cost of $1.23M. The cost estimate for the separate program elements is shown in the above list.

APPENDIX A
SKY BRIGHTNESS AND VISIBILITY FUNCTION CHARACTERISTICS

A.1 SKY BRIGHTNESS

The sky brightness is taken as a two-dimensional spatial distribution B(x,y) for the purposes of this study. The x and y variables define orthogonal spatial angular position coordinates relative to a fixed reference direction within the field of observation of the radio telescope. B(x,y) has physical units of power per unit area and per unit solid angle for the location (x,y). It is a real valued function and its spatial variation encompasses point-like (stars) as well as highly dispersed distributions. The magnitude of the brightness function must be generated with an accuracy of one per cent of its peak value. An example of sky brightness map data is shown in Figure A.1.

A.2 VISIBILITY FUNCTION

The measured visibility function V, available at the radio telescope system output, is a composite of signals. We will discuss some of the salient properties of V pertinent to post processing; the derivation of V is described in the literature[1,2,3]. Each signal of this composite is derived from correlation processing of the reception from selected pairs of antennas of the 27 element array. Correlation is performed over a succession of short time intervals thus causing V to be a sampled function. Signals from 351 antenna pairs, $\frac{1}{2}(n)(n-1)$ for $n = 27$, which are generated simultaneously in parallel channels of the radio telescope system constitute V. The time history of V corresponds to the movement of the antenna array due to the earth's rotation. Typically during

Figure A.1. Copy from the Work of A. Rots.

the observation interval over which the visibility function is being collected, data is accumulated in buffer storage. It is then read out of buffer storage over a short time interval for post-processing to generate the sky-brightness map B. The broad temporal bandwidth of the radio telescope can be divided into as many as 256 individual narrow spectral bands or lines with a visibility function generated for each line. Fewer bands of broader bandwidth, about eight, may also be generated and are referred to as the continuum case.

As will be explained in greater detail below, the visibility function may be considered as a time varying signal and, more appropriate to the post-processing of V, as a spatially varying signal defined in a (u,v) spatial domain. A simulated example of V(u,v) is shown in Figure A.2 where each individual signal,of the total composite of 351 signals which make up V, occurs along one of the curved paths shown.

The ratio of the maximum value to the minimum value (noise) of the magnitude of V will be about 10:1 or less for about two-thirds of the spectralline visibility functions expected. Normally the remaining third of the expected visibility functions will have a ratio of 100:1 or less. The normal A-array space bandwidth product of V for a viewing field extending of the - 3 dB width of the telescope antenna is 3000 in each of its two dimensions.

The time domain representation of the visibility function will be written as

$$V(t) \sum_{k=1}^{351} V_k(t_n)$$

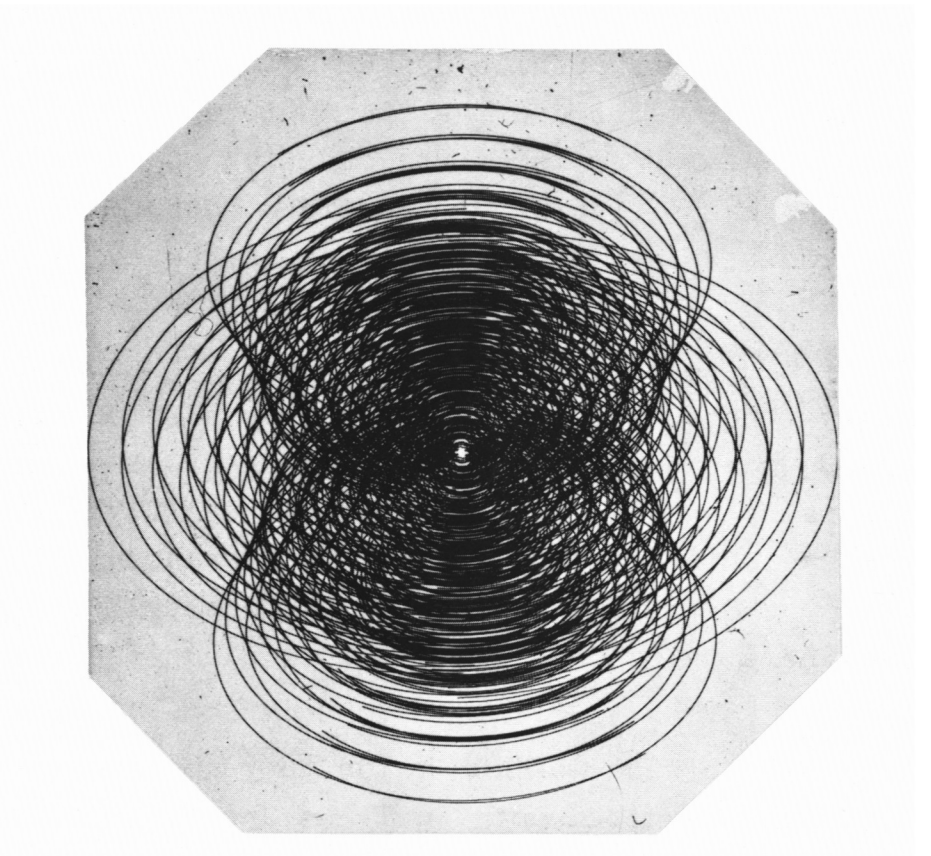

Figure A.2. An Example of the Visibility Function (simulated).

where k identifies an antenna pair of a particular baseline (separation) length and t_n the n-th discrete sample of the continuous succession of equally spaced samples in each V_k.

More appropriate to the Fourier transform processing to be performed on V is the spatial domain representation of the visibility function, V(u,v), which we can write as

$$V(u,v) = \sum_{k=1}^{351} V_k(u_n, v_n)$$

The variables u,v have the form of a distance normalized by the operating wavelength of the radio telescope, λ. More specifically, the radio telescope spatial domain related to u and v is a plane that is normal to the reference pointing direction of the radio telescope. Defining orthogonal coordinate unit vectors $\bar{u}$ and $\bar{v}$ in this plane, we have u as the normalized component of an antenna baseline in the $\bar{u}$ direction. Similarly for v. Each value of u and v corresponds to the position coordinate λu and λv in the u,v plane.

The signal history of the visibility function in the spatial domain falls along a set of elliptical paths, one path for each of the 351 baselines (antenna pairs). The $\bar{u},\bar{v}$ plane paths are well defined in terms of the earth's rotational angle (hour angle h), the declination angle of the reference pointing direction of the radio telescope (δ), the latitude angle of the antenna site (ℓ), and the east-west and north-south component lengths of the antenna baseline at the earth's surface (B_{EW} and B_{SN}). The path position coordinates in the $\bar{u},\bar{v}$ plane are given by the following expressions.

$$\lambda u = B_{EW} \cos h + B_{SN} \sin \ell \sin h$$

$$\lambda v = -B_{EW} \sin h \sin \delta + B_{SN} \sin \ell \cos h \sin \delta + B_{SN} \cos \ell \cos \delta$$

The locus of the points $\lambda u, \lambda v$ as time (or hour angle h) varies will in general be an ellipse. Solving the above expressions for $(\lambda u)^2 + (\lambda v)^2$ allows formulation of the equation for the elliptical path, i.e.,

$$\frac{(\lambda u)^2}{(B_{EW}^2 + B_{SN}^2 \sin^2 \ell)} + \frac{(\lambda v - B_{SN} \cos \ell \cos \delta)^2}{\sin^2 \delta (B_{EW} + B_{SN} \sin^2 \ell)} = 1$$

The ellipse has the following parameters

λu major axis:	$[B_{EW}^2 + B_{SN}^2 \sin^2 \ell]^{\frac{1}{2}}$
λv minor axis:	$[\sin^2 \delta (B_{EW}^2 + B_{SN}^2 \sin^2 \ell)]^{\frac{1}{2}}$
center at:	$\lambda u = 0$
	$\lambda v = B_{SN} \cos \ell \cos \delta$

Note that the elliptical paths can have the degenerate forms of circles when $\delta = \pi/2$ and lines when $\delta = 0$.

A simulated example of the visibility function is given in Figure A.2 where the elliptical paths along which this function lies are quite evident. It will be useful to recognize the elliptical tracks themselves as an aperture or mask function having a finite track width. The amplitude and phase variation of the visibility function V occurs within this aperture function, varying along the track length.

The visibility function made available for post processing will be complex, i.e.,

$$V(t_n) = |V(t_n)|e^{j\phi(t_n)}$$

or

$$V(u_n,v_n) = |V(u_n,v_n)|e^{j\phi(u_n,v_n)}$$

More specifically the values for the complex visibility function in phase and quadrature parts $V_i(u_n,v_n)$; $V_q(u_n,v_n)$ and the corresponding position coordinates (u_n,v_n) will be provided in digital form at the radio telescope output buffer store.

It should be noted that since B(x,y) is real then its Fourier transform, the complex visibility function, will be Hermitian, i.e.,

$$V(u,v) = V^*(-u,-v)$$

A.3 VISIBILITY FUNCTION DATA SEQUENCE

The visibility function is placed in buffer storage, most likely disc, at the output of the radio telescope. It is entered into storage as a sample sequence natural to the manner in which it is generated. Assuming frequency separation; at each time t_n, 351 data points (one for each baseline) are entered into storage. Note that for any one time t_n the corresponding u,v plane locations, which are known, will in general be different since u and v are dependent on baseline length and geometric location.

When the visibility function is read out of buffer storage for post processing the sequence preferred by the NRAO is along a common time sample, or, along baselines. A third possibility is defined in terms of the u,v position coordinates of the visibility function. It is a raster sequence in which data is read out over adjacent lines of constant u (or v). The raster format is quite common to optical recording and display devices but would not be used because of the extensive reformatting needed to realize raster data.

A.4 BRIGHTNESS FUNCTION OF A POINT SOURCE

The measured sky brightness for a single point source (star) obtained by Fourier transformation of the corresponding visibility function for that source, characterizes the impulse response of the total system. The point source visibility function is a linear grating fringe pattern seen through the aperture defined by the composite of elliptical tracks as shown in Figure A.2. The Fourier transform of

this visibility function has a spatial distribution which is defined by the transform of the elliptical track aperture function as shown in Figure A.3, with a location which is proportional to fringe frequency. This spatial distribution or impulse response is often called the synthetic beam and sometimes the dirty beam.

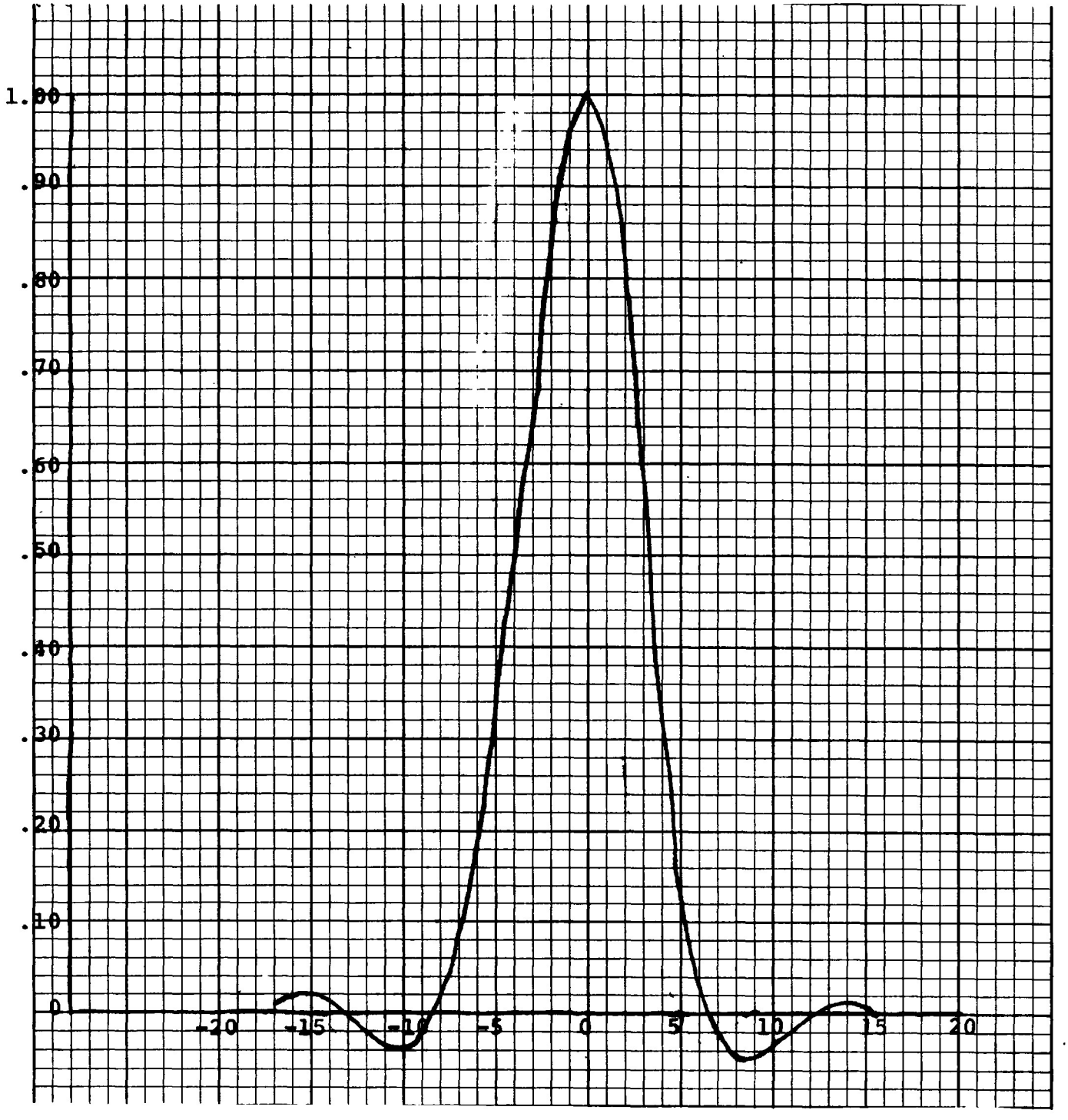

Figure A.3. Sky Brightness for a Point Source (simulated).

APPENDIX B
OPTICAL PROCESSOR SYSTEM

The optical processor system consists of a coherent optical processing channel in which the optical Fourier transform computation is accomplished, together with provisions for generating an optical recording of the visibility function at the input, and provisions for viewing and extracting the sky brightness map at the output. The functional parts of the system are the pre-filter, optical recorder, optical processing channel, scanning photodetector, analog to digital converter, difference data processor and a system control unit which are shown in the block diagram of Figure B.1.

The system input consists of digital visibility function data, its position coordinates, and auxiliary data (such as spectral band, telescope mode, date, etc), i.e.,

$$V_i(u,v), V_q(u,v), u, v, \text{Aux data}$$

The system provides two forms of outputs, directly viewable sky brightness map data available as the light intensity distribution at the processor output plane; and an electronic version of sky map data obtained by photodetector scanning of the light intensity at the optical channel output.

Subsystems of the processor system are described in the following sections.

B.1 PRE-FILTER

The major elements of the system shown in Figure B.1 start with the pre-filter. It serves to convert the digital visibility function and position data to a signal form suited to the optical recorder. This requires conversion to an analog form appropriate to the recorder encoding and spatial writing format. Several encoding and scan formats have been considered[7,8]. The choice is influenced mainly by the data sequence available from radio telescope buffer storage and the available optical recording techniques. The approach recommended for recording, that of continuous writing on a succession of elliptical paths (one path at a time) with the visibility function taken as a real analog video signal on a carrier frequency, requires an output from the pre-filter having the spatial form

$$|V_k(u,v)| \cos [\omega_1 u + \omega_1 v + \phi_k(u,v) + \theta_o]$$

The term $\omega_1(u + v)$ represents the phase of a spatial carrier frequency with a component ω_1 in the u and v dimensions. Though the cosine is shown the sine may be used or the fixed phase θ_o may be given a value best suited to the choice of map data processing techniques in the optical channel. Selection of ω_1 is based upon the need to separate the map data from extraneous unused data at the processor output plane. The value of ω_1 is about 1.05 times the highest u or v dimension frequency. Rather than the two dimensional carrier a one dimensional carrier could be used depending on details of the optical processing procedures.

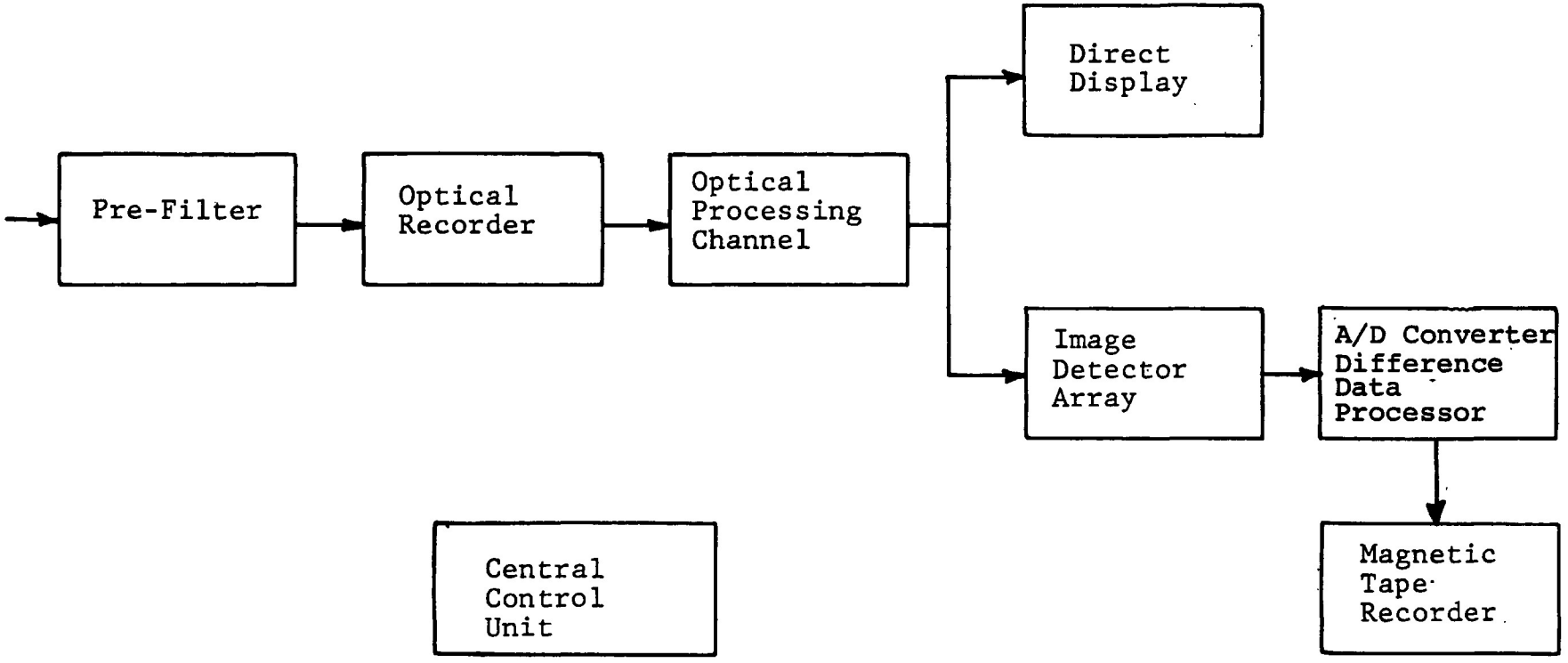

Figure B.1. Processor System Functional Diagram.

The prefilter consists of a digital to analog converter and circuitry for converting the in-phase and quadrature visibility components to a real signal on a carrier. Conversion of u,v positional information would also be accomplished in the prefilter with this output used for control of the optical recorder writing beam position. A prefilter of similar design has been highly developed and is in regular use as part of a synthetic aperture radar data processing facility at ERIM.

The signal that is actually to be recorded must be defined in further detail in two important respects related to the optical recording process. They are the representation of the spatial tracks along which the visibility function is recorded, and, the bias level that is used because available optical recording materials are not bipolar. We will denote the visibility data in the form in which it is to be recorded as $\underline{s}(u,v)$, which is expressed as

$$\underline{s}(u,v) = a(u,v)\Big\{a_t(u,v)\,[b_t + |V| \cos(\omega_1 u + \phi(u,v) + \theta_o)] + b[1 - a_t(u,v)]\Big\}$$

The elliptical tracks of the visibility function are defined explicitly by the function $a_t(u,v)$ which equals 1 along the tracks and zero otherwise. b_t is a constant bias level along the tracks relative to which the plus and minus excursions of V can vary. $[1 - a_t]b$ has zero value along the tracks and has the bias value b off the tracks. a(u,v) describes an aperture or frame function which encompasses the visibility function and is 1 for u,v within the aperture and zero for

u,v outside the aperture. The tracks $a_t(u,v)$ fall within the boundary aperture function $a(u,v)$.

A sketch of $\underline{s}(u,v)$, with $V = 0$, is shown in Figure B.2. The bias levels b and b_t and the aperture functions a and a_t are realized through control of the writing beam intensity and control of the writing beam position, respectively.

It will be convenient to re-arrange $\underline{s}(u,v)$ into a bias term s_o and conjugate pairs of the visibility function terms as follows

$$\underline{s}(u,v) = s_o(u,v) + s(u,v) + s_*(u,v)$$

$$s_o(u,v) = a(u,v)[b + a_t(u,v)(b_t - b)]$$

$$s(u,v) = \frac{1}{2} a_t(u,v)|V|e^{j[\omega_1 u + \phi(u,v) + \theta_o]}$$

$$s_*(u,v) = \frac{1}{2} a_t(u,v)|V|e^{-j[\omega_1 u + \phi(u,v) + \theta_o]}$$

Note that if $b = b_t$ then the bias term appears with the aperture function $a(u,v)$ only.

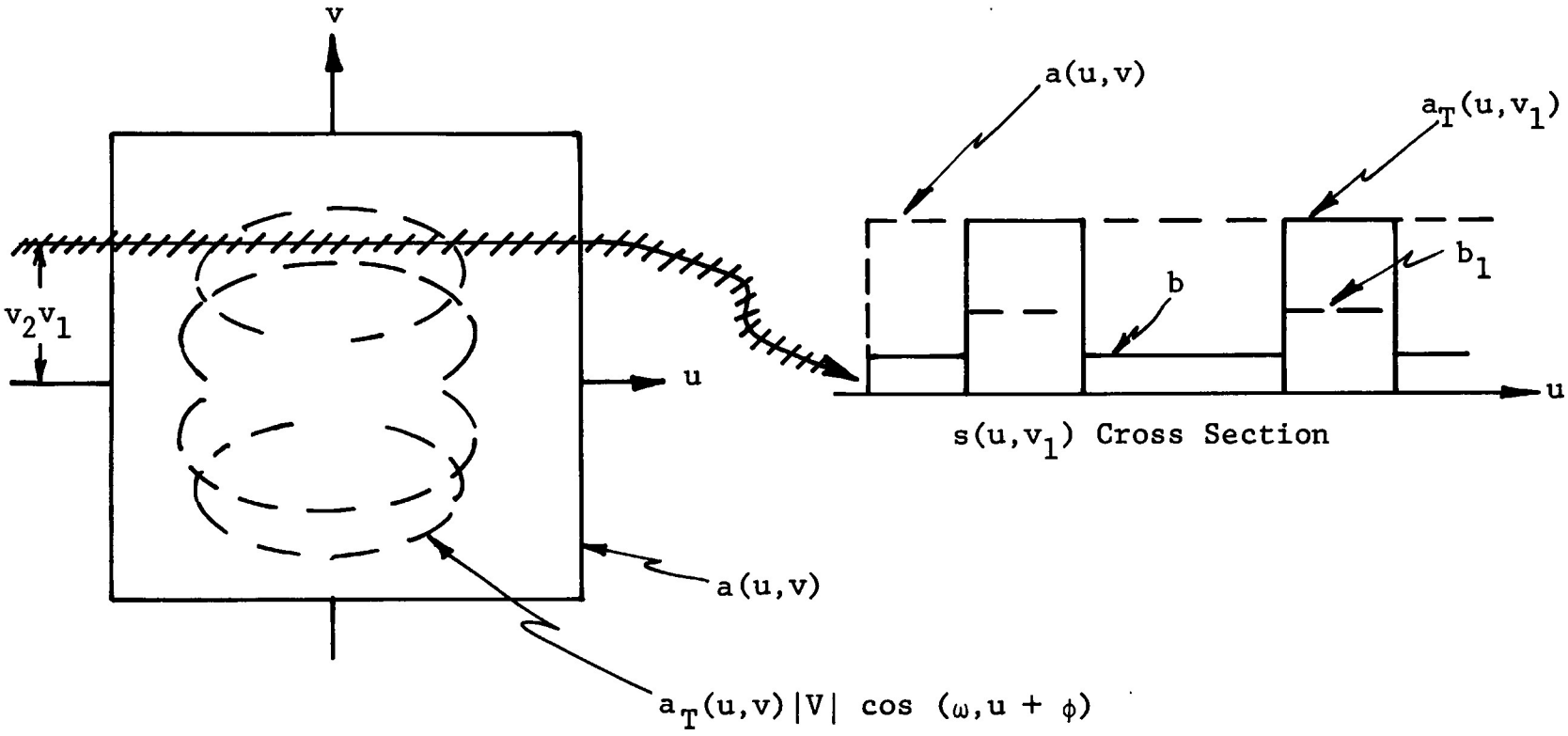

Figure B.2. s(u,v) Data Frame Properties.

B.2 OPTICAL RECORDER

The optical recorder serves to convert visibility function data to a spatial recording which acts as the input to the optical processing channel. The spatial domain of the recording material is a scaled version of the radio telescope $\bar{u},\bar{v}$ plane. The visibility function data may be viewed as a frame of data comprised of a composite of 351 elliptical tracks as shown previously in Figure A.2. A separate data frame is recorded for each of up to 256 spectral bands that can be observed with the radio telescope.

General Properties

In a general functional sense the recorder is comprised of a writing beam and a recording material. The writing beam is modulated in proportion to the visibility function while the beam position is scanned to the appropriate u,v plane location. The recording material is thus exposed. Upon exposure and development the recording material responds with a change of optical transmission (amplitude or phase depending upon choice of recording material) according to the writing beam intensity.

The essential performance properties of the optical recorder can be characterized in the context of the above functional description. The case of amplitude recording will be considered in further detail as it is a primary candidate for recording at the present state-of-the-art of recording devices. Other recording concepts, including phase recording on plastics, offer an attractive potential given proper engineering development. We will

consider the case of recording on photographic film with an intensity modulated writing beam. Denoting the input to the recorder as $\underline{s}(u,v)$, the exposure of recording material as $e(u,v)$, and the recorded data as the amplitude transmission variation $\underline{t}(u,v)$, the recording process can be expressed by the following convolution relations

$$\underline{e}(u,v) = \underline{s}(u,v) \circledast h_b(u,v)$$

$$\underline{t}(u,v) = \underline{e}(u,v) \circledast h_f(u,v)$$

Here h_b represents the spatial distribution of the writing beam (light power or beam current) scaled by scan speed or dwell time at the surface of the recording material, and h_f is the spatial distribution of the response of the recording material (film, etc.) to an exposure at a single point. The h_b and h_f are impulse response functions. The overall input to output relation for the optical recorder is given by

$$\underline{t}(u,v) = \underline{s}(u,v) \circledast h_b(u,v) \circledast h_f(u,v)$$

It will be convenient to recognize an impulse response function h_r which represents the impulse response of the overall recording process where $h_r = h_b \circledast h_f$. Further, recall the notation for the input signal $\underline{s}(u,v)$ where we identified a bias component $s_o(u,v)$ and the conjugate

pairs $s(u,v)$ and $s_*(u,v)$ which contained the visibility function data. Using this notation we can write the recorded data as consisting of three terms as follows

$$\underline{t}(u,v) = t_o(u,v) + t(u,v) + t_*(u,v)$$

with

$$t_o(u,v) = s_o(u,v) \otimes h_r(u,v)$$

$$t(u,v) = s(u,v) \otimes h_r(u,v)$$

$$t_*(u,v) = s_*(u,v) \otimes h_r(u,v)$$

The modulation transfer function (MTF) or frequency response of the recorder is the product of the Fourier transforms of h_b and h_f., i.e., the transform of h_r.

Though not shown explicitly, the temporal response of the input amplifier and writing beam modulator circuiting can be modeled in terms of a time equivalent spatial variable and will have an impulse response of finite extent along the writing beam scan path. It has not been included explicitly as it is not expected to have a significant affect for the limited temporal response required of the optical recorder for the VLA application. It can be viewed as a part of the beam function h_b in the above analysis.

It should be noted that the recorded film transmission $\underline{t}$ can, at most, vary between values of 0 and 1. Typically, to maintain linear operation, the film transmission variation is restricted further to about the range 0.1 to 0.9. The bias level t_o will be set at mid-range $t_o = 0.5$ with the visibility function data causing variations about the bias. Since the visibility function V(u,v) can have a peak to minimum value range which may differ, depending upon the nature of the radiating sources seen by the radio telescope (star fields versus distributed sources), the gain of the optical recorder input amplifier will be programmed to spread the visibility function data over the available range of film transmission variation. The gain would be fixed for visibility data obtained from any one scan made by the radio telescope. Information on which to base the gain setting could be generated automatically as the visibility is put into buffer storage prior to Fourier processing or it could be selected by the system operator. Gain setting information would be sent automatically to the processor readout device so that this gain can be properly accounted for in the output sky map data.

The recorder impulse response functions require further detailed consideration. They have the form of a product of a gain factor K and a spatial distribution factor g(u,v), i.e.,

$$h_b = K_b \, g_b(u,v)$$

$$h_f = K_f \, g_f(u,v)$$

The spatial functions have a bell-shaped distribution, generally, and the gain factors are ideally constants, but only over a finite range of variation of the respective inputs s and e. Departure from the ideal constant (linear) gain factor will cause K to be a function of input signal magnitude, however, with calibration highly linear operation is possible. K_b has dimensions of exposure density per volt of input signal and K_f has dimensions of optical transmission per unit of exposure energy density. g_b and g_f are dimensionless distribution functions. The general nature of these functions is sketched in Figure B.3.

Errors in the location of the recorded data from the correct u,v position can be characterized by writing beam position and recording material distortion error functions. In the case of the beam position variables an error $\varepsilon_u(u,v)$ and $\varepsilon_v(u,v)$ from the proper location u,v will be represented in the beam impulse response function as

$$h_b = K_b\, g(u + \varepsilon_u,\ v + \varepsilon_v)$$

$$= K_b\, g(u,v) \circledast \delta_b(u + \varepsilon_u,\ v + \varepsilon_v)$$

Recorded data position errors caused by localized distortion within the recording material, denoted $m_u(u,v)$ and $m_v(u,v)$, modify the film response as follows

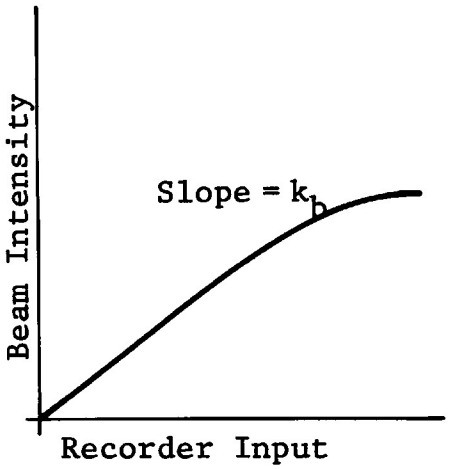

Write Beam Gain

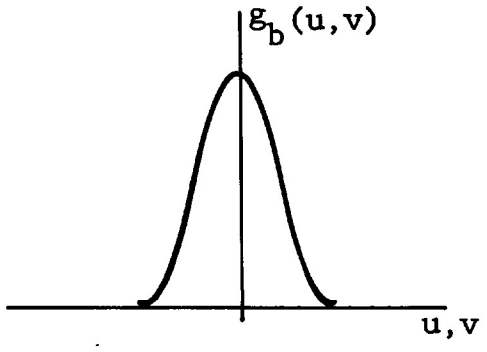

Write Beam Spatial Response

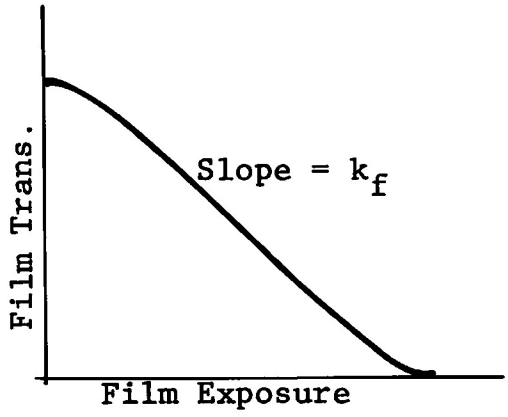

Film Gain

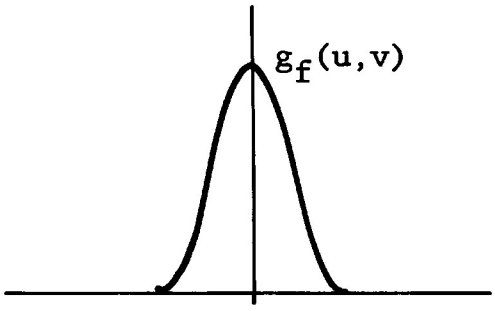

Film Spatial Response

Figure B.3. Optical Film Recorder Response Functions.

$$h_f = K_f\, g(u + m_u,\ v + m_v)$$

$$= K_f\, g(u,v) \circledast \delta_f(u + m_u,\ v + m_v)$$

With both film and beam errors included, the recorder response is expressed as

$$\underline{t}(u,v) = \underline{s}(u,v) \circledast h_b(u,v) \circledast h_f(u,v) \circledast \delta_b(u \pm \varepsilon_u, v \pm \varepsilon_r) \circledast \delta_f(u \pm m_u, v \pm m_v)$$

For compactness of notation we will define $\delta_r = \delta_b \circledast \delta_f$ as the recorder scan defect term and with $h_r = h_b \times h_f$ the recorder data will be written as

$$\underline{t}(u,v) = \underline{s}(u,v) \circledast h_r(u,v) \circledast \delta_r(u,v)$$

Note that the formulation of $\underline{t}(u,v)$ into three basic terms, a bias term and a conjugate pair, will also follow for the above case where the recorder error functions are included.

Noise in the recorded data can occur as small random variations of optical amplitude transmission or as a departure from uniformity of the optical material (thickness variation caused during manufacture or damage in handling). Amplitude transmission noise must be made sufficiently small relative to the recorded data, while thickness nonuniformity or surface imperfections in the photographic

recording film can be compensated for by use of a liquid gate. The liquid gate is discussed further in later sections.

Amplitude noise can be caused by noise in the writing beam used to expose the film and by the inherent microscopic graininess of the silver particles which serve as the basic mechanism for the recorded optical transmission variation in the film. We will denote beam noise as η_b and recording material (film) amplitude noise as η_f. It is convenient to assess the noise caused by both η_b and η_f in terms of the noise frequency spectrum of recorded data. It should be noted that the power spectral density of noise in recorded data is readily measured as a light power distribution normally available at the output of an optical Fourier transform channel when such recorded data is placed at the input. With stationarity the mean square measure of the recorded noise over a specified spatial bandwidth is equal to the integral of the noise power spectrum over that bandwidth, i.e.,

$$\overline{\eta^2(u,v)} = \iint S(f_x, f_y)\, df_x df_y$$

The spectral densities will, by the nature of the output of the VLA optical processing channel, be useful as a measure of the recorder noise in the sky brightness plane at the processor output.

The discussion of optical recording has thus far been quite general to allow a more comprehensive overview of

the essential performance considerations that apply to several possible hardware implementations of a recorder. Based upon relative cost and state-of-development, recording on silver halide film with either a laser beam, CRT light beam or direct electron beam are the primary candidates for an optical recorder intended for near term operational use. Each of these types of recorders is expected to be suitable to the task of VLA data recording for coherent optical processing. The use of a CRT or direct electron beam offers well developed methods for electronic control of beam scanning which is more flexible than methods readily available for laser bean scan control. CRT systems have a space-bandwidth product capability, with high spatial fidelity, of about 3000 in each direction of a 100 x 100 mm data frame allowing 36×10^6 input data points to be recorded. A laser or direct electron beam writing device can provide a space-bandwidth product of 8,000 in each dimension for the same size data aperture, which will allow 2.5×10^8 data points to be recorded.

Scan position linearity of at least 1 part in 20,000 is available with all three of these devices when special purpose high accuracy monitoring and correction of the scan position of the writing beam is utilized. A potential for improvement by a factor of about 1.5 to 2 exists.

Recording dynamic range, which is governed mainly by the inter-related combination of available writing beam intensity, film sensitivity, and recording noise properties can be as high as about 2×10^4 for laser and direct electron beam devices while the CRT provides about 5×10^3. This measure of dynamic range is taken in the domain of the Fourier transform of the recorded data on a resolution cell basis.

Throughput rate of the recorder is governed by the recorder writing speed and the film handling speed. When recording with continuous scan along elliptical tracks at a 4 MHz bandwidth, a frame is recorded in about 0.5 seconds. Special purpose rapid film development[9] and film handling provisions will allow development and movement of the film to the optical channel input in about 20 seconds, although the direct electron beam device requires special consideration for film removal from the vacuum envelope in which recording takes place. The entire recording and film development process for 8 frames of continuum data would require 24 seconds while 256 frames of spectral line data would require 148 seconds. Recording with a random access discrete position scan will take slightly longer because of the need for a beam settling time for each position.

The cost of design and fabrication of these types of recorders is expected to be lowest for a CRT/film device, with the direct electron beam the next highest and the laser beam device the highest. A major part of the cost difference would be due to non-recurring engineering costs; however, the laser and direct electron beam device would likely be somewhat higher than the CRT device in basic fabrication cost.

It should be noted that use of one type of optical recorder initially would not preclude a change to another type of recorder at a later time, while retaining essentially all of the other parts of the overall optical processor system.

Film handling provisions can be designed to accomodate film strips or individual film frames. The individual

frame basis is natural to the visibility function data and is preferred because film can be prepared as individual frames or slides and automatically fed into the recorder and then successively to the film developer and the optical processing channel. A frame of film measuring 70 × 70 mm would serve as a reasonable standard with the central 50 × 50 mm used for visibility function recording. The remaining area would be available for calibration signals and a small portion would be used for data annotation.

Control of the bias level b in the area of the u,v data frame where the visibility function tracks do not occur can be done in several ways. If a negative working film is used, then not exposing the off-track area will make this area clear giving b = 1. With a positive film the off-track area will be dark, b = 0, if it is not exposed. Exposure of the off-track area would be required in order to realize a prescribed bias value for b other than zero or one. This can be accomplished by scanning the recorder writing beam over the off-track areas after recording the visibility data or by use of a mask which when illuminated with an expanded light beam will expose the off-track areas while masking the region containing the visibility function. A mask can be generated on-line by exposing an electro-optic storage device with the track function $a_t(u,v)$ as written on the CRT. The electro-optic device would serve simply to provide a reversed image of the track function, i.e., dark tracks on a bright background, which would be projected onto the film to establish a bias exposure for the off-track region.

The CRT/film recorder properties will be discussed further since it is a good candidate for the VLA optical

processor system because of combined cost and performance features available at the present state-of-the-art.

B.2.1 CRT/Film Recording

Optical recording with a cathode ray tube is accomplished by projection of the light spot emitted from the CRT phosphor faceplate onto the recording film. A system diagram is given in Figure B.4. The projected spot of light serves as the writing beam which is intensity modulated in proportion to the input visibility signal, $\underline{s}(u,v)$, and is scanned in correspondence to the position defined by the visibility track function $a_t(u,v)$.

The CRT light beam is derived from an electron beam generated within the CRT electron gun triode structure. Thermionic emission from an oxide coated cathode passes through an apertured first grid. Variation of the voltage between the cathode and first grid causes modulation of the electron beam current passing through the first grid. The triode structure comprised of cathode and apertured first and second grids provides for initial focusing of the electron beam. An additional focusing stage is provided and serves to project the electron beam onto the phosphor screen. The temporal modulation bandwidth for the electron beam is governed by the performance of the video amplifier which must drive the capacitive impedance presented by the grid-cathode modulation electrodes. The grid-cathode capacitance is in the range of 5$\mu\mu$f and modulation over a video temporal bandwidth of many tens of megahertz is readily provided if needed. Gamma correction of the input voltage amplitude is used to maximize the linearity of the overall recording process. This is accomplished by

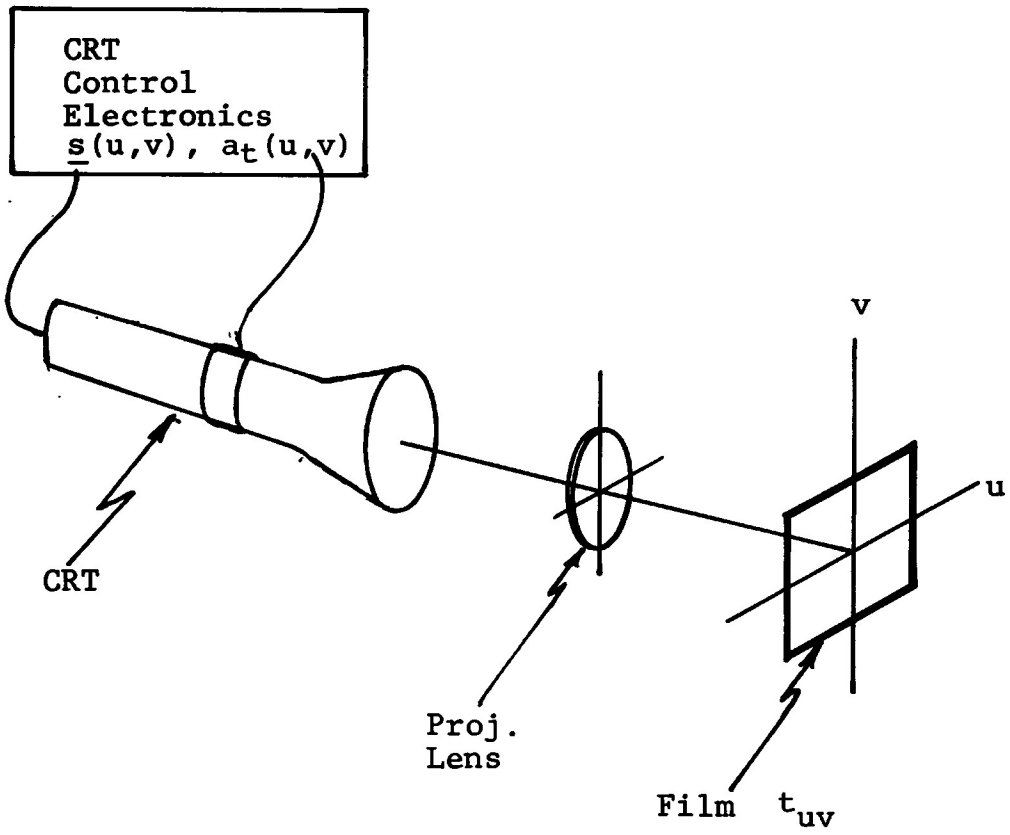

Figure B.4. Sketch of a CRT/Film Recorder.

making the beam gain constant K_b dependent on the input voltage $\underline{s}$ in a prescribed manner.

Electron beam scanning is provided by a magnetic field generated with deflection coils. Various scan formats such as discrete pointwise scanning or continuous scanning as along the elliptical tracks of the visibility function are readily provided. Settling time between scans will be negligible compared to the duration of a scan along the elliptical data paths for continuous scanning.

Scan accuracy will be dependent on noise in the deflection coil drive circuits which can be as small as 5×10^{-6} of the maximum scan drive signal.

Scan linearity can be made quite good for small to medium sized apertures. Linearity correction circuits, currently available, are capable of providing linearity of at least 1 part in 20,000 over the total scan length. To realize such performance requires special means to observe or sense the beam location so that the linearity adjustment can be made. This provision in the recorder is essential for the VLA application. This is accomplished by a procedure in which the CRT light beam is projected onto a precision reference grating while the beam is being intensity modulated at a precise frequency. The beat or fringe pattern between the modulated light beam and the reference grating allows observation of the departure from a truly linear scan. Scan linearity errors are slowly varying with position over the faceplate of the CRT and can be kept quite stable with time. The linearity adjustment provision can be automated and be made part of an automatic calibration cycle incorporated in the recording system.

A one-dimensional open loop linearity correction of this type has been designed at ERIM. Recording results obtained with this device are discussed later in this section. This particular design was made for a CRT with a 40^{o} deflection angle. Lower deflection angles ($\simeq 20^{o}$) for the same output recording aperture can be realized and would enhance the potential for further improvements in scan linearity. It should be noted that observation of scan linearity would be made at the plane of the recording film, thereby including correction for effects due to the projection lens as well as the CRT beam deflection system.

The phosphor light spot of commercially available high resolution cathode ray tubes can be as small as 12 μm with an intensity high enough for recording on film suited to this application. A high quality imaging lens with an f-number of about 3 and operated at a demagnification of 2 would be used to project a 100 × 100 mm writing area at the CRT phosphor onto a 50 × 50 mm recording area at the film surface. The light spot at the film surface will be 6 μm, allowing a recorded spot size of about 8 μm when the film response is included.

Several films are available for recording with the cathode ray tube. Film selection is based on the need for a suitably high sensitivity for the available light level of the CRT light beam and suitable performance in terms of impulse response or MTF, noise level and compatibility with rapid film development techniques. Films such as Kodak Microfile, Dacomat G and Minicard are appropriate candidates for this application.

The photographic recording film can experience a

small amount of physical distortion between the time of the recording (exposure) and the completion of film development. The distortion consists of two types: (1) a uniform change of size resulting in a simple scale change, and (2) the more objectionable localized variations (m_u, m_v) which can degrade the signal properties of the recorded visibility data. The scale change is readily compensated by calibration of the processor output. The localized distortion must be kept suitably small. It is expected to have a peak value of about 0.5×10^{-3} mm which is smaller than the expected beam scan errors ($\varepsilon_u, \varepsilon_v$) for a 50 × 50 mm data aperture. The use of individual film frames rather than continuous film rolls or strips is expected to help minimize localized film distortions.

We will consider an example of recordings made with a line scan CRT/film recorder used on-line in optical data processing activities at ERIM. The recorded data consists of a 50 pulse/mm pulsed modulation along scan lines with the scan lines written in a raster format. Figure B.5 is a much magnified view of a section of this recorded data. Figure B.6 shows a magnified view of a Moire fringe pattern caused by placing an optical reference grating against the recorded pulse modulation of the film. The highly uniform spacing of the Moire pattern is an indication of the linear scan capability of the recorder which is normally adjusted to at least 1:20,000 of perfect linearity. The optical Fourier transform of this data results in spots of light at the frequency plane locations corresponding to the input data frequencies. A magnified view of an individual spot is shown in Figure B.7. The spot distribution, ideally a jinc function squared for the circular input

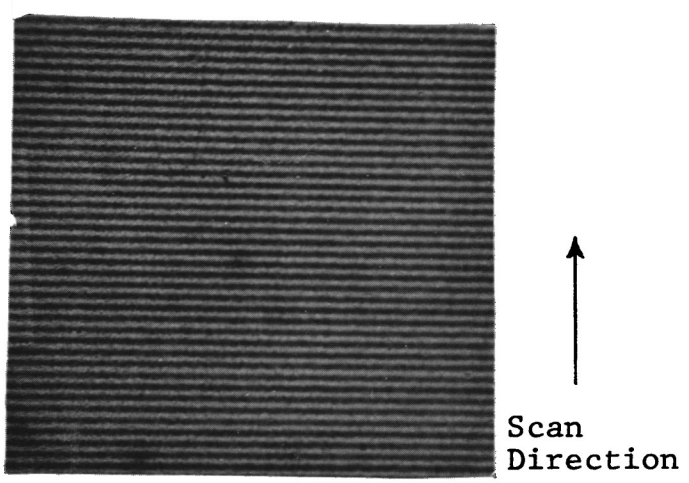

Figure B.5. CRT/Film Recorded Data (magnified) 50 pulses/mm in the Vertical (scan) Direction.

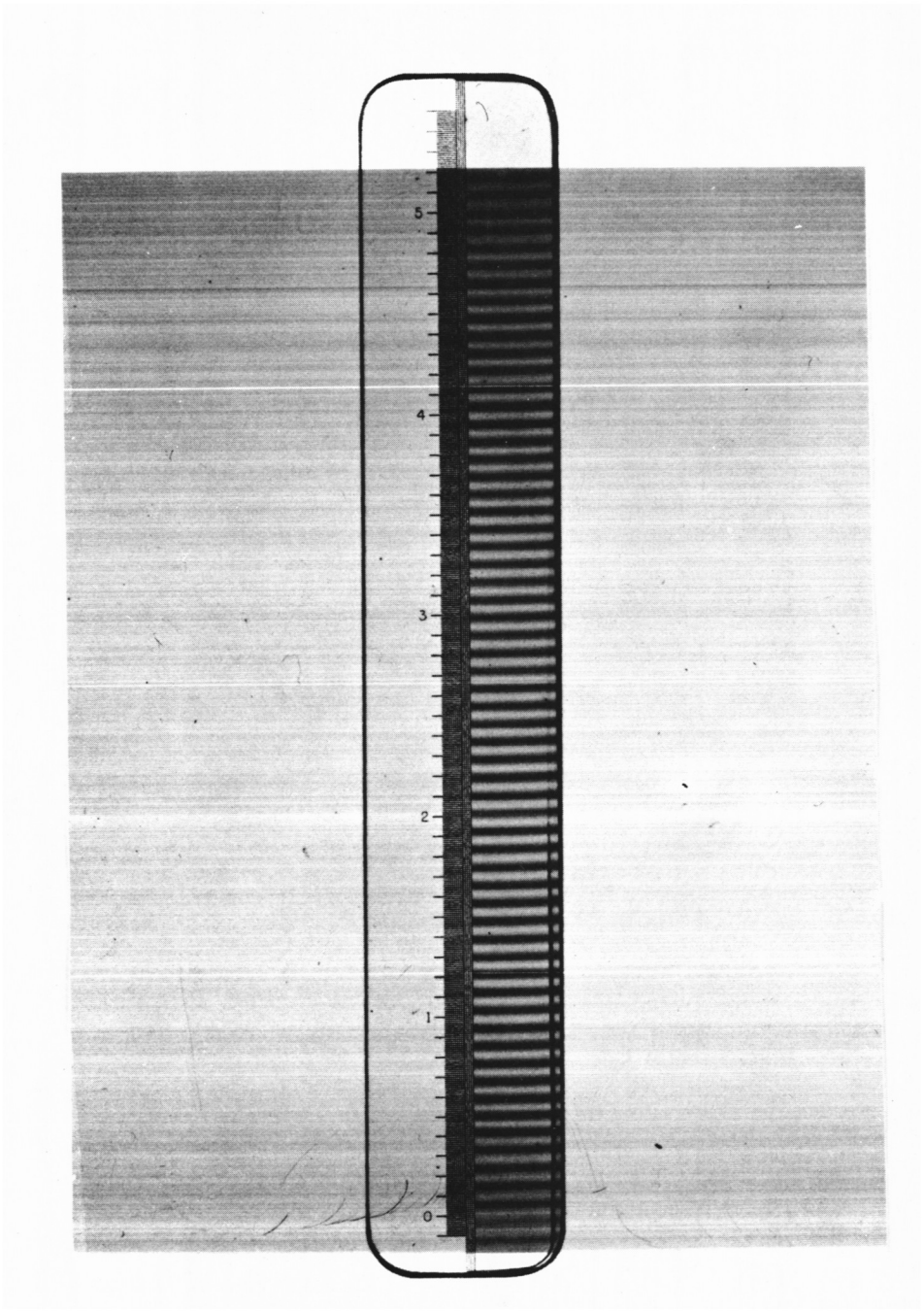

Figure B.6. Moire Fringe Pattern Between CRT/Film Recording and Reference Grating

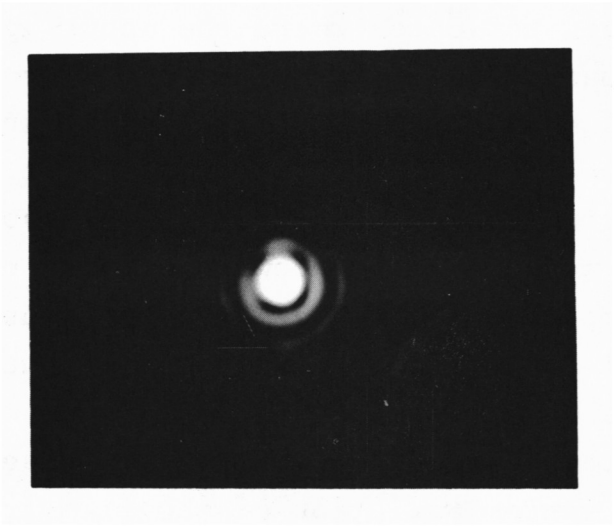

Figure B.7. Optical Fourier Transform Light Distribution for CRT/Film Recording of Figure B.6.

aperture used, agrees very closely to the theoretical jinc function.

A measure of the noise caused by the film is given in the data of Figure B.8. This data represents experimentally measured noise at the output of a Fourier optical channel when the input is a uniformly exposed film sample. Data is given for cases where the input aperture was circular and square. The input film had an average transmission of one-half and its inherent random variation due to its grainy nature. As mentioned earlier, the light intensity at the Fourier channel output plane (without a reference beam) is a measure of the power spectral density of the input film amplitude transmission variations. The average or DC level of the input gives rise to the large zero order peak in the data of Figure B.8 at x = 0. The low level away from the zero order peak is the noise power spectrum due to the random variation of the film transmission plus the far out sidelobes of the zero order.

The data was originally measured with a photodetector having an area eight resolution elements on a side, but has been normalized to an area of one resolution element. We see that the noise level in regions away from the zero order are at about -85 dB below the zero order peak. Interpreted at the input film, this means that over the spatial frequency bandwidth covered by a detector cell (at the output frequency plane) the mean square value of film noise is -85 dB relative to the average value of the film amplitude transmission. As a practical matter, this noise data includes noise due to scattering from dust particles present on optical surfaces and from scattering centers in the modest quality lenses used in the optical channel along with that cuased by the film grain scattering. We expect that an improvement down to at least the -95 dB level can be achieved.

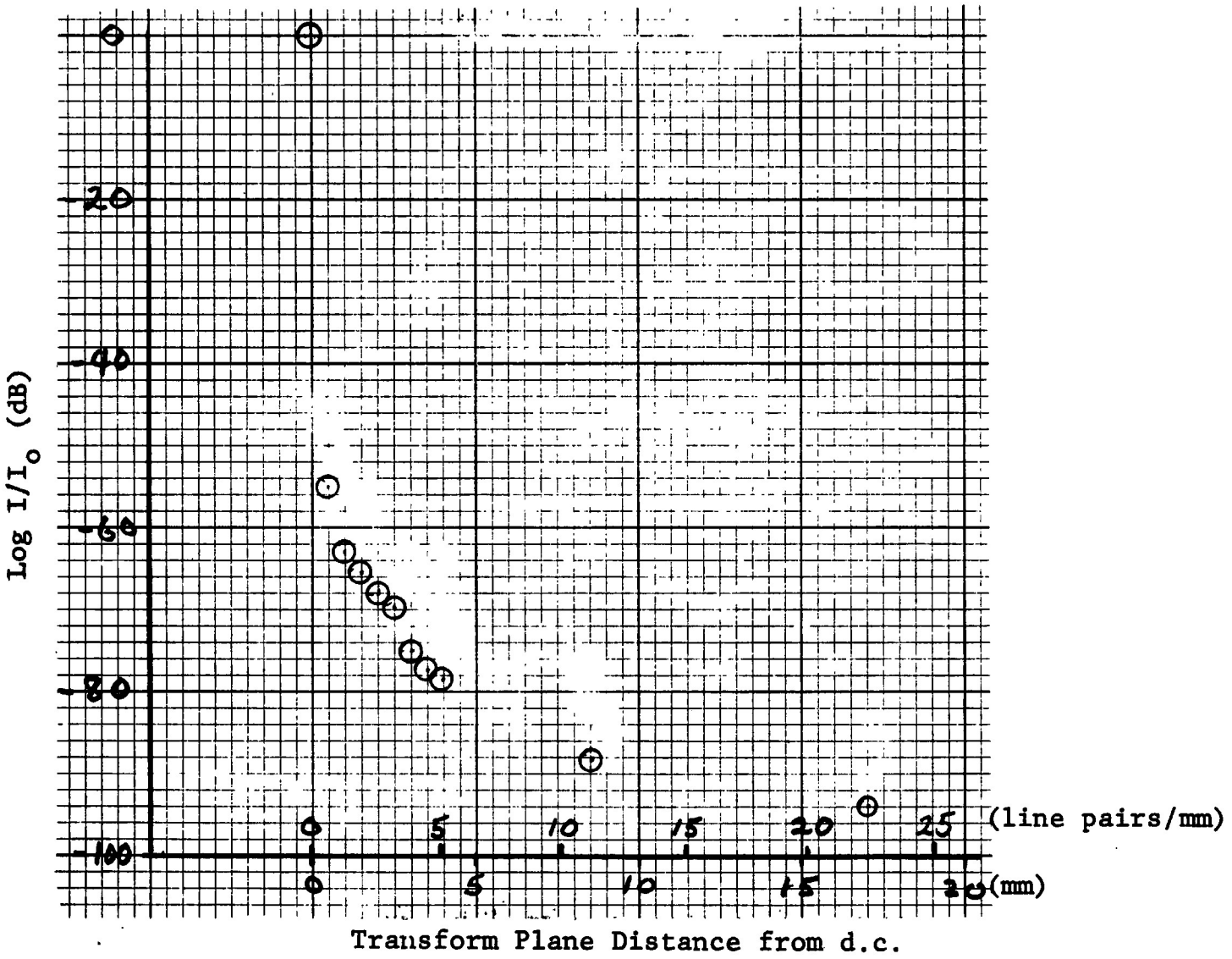

Figure B.8. Optical Processor Dynamic Range with 32½ mm Circular Aperture.

A further comment on the noise in the light intensity distribution at the optical processing channel output is warranted with regard to the phenomenon known as speckle noise. Speckle noise[10] is a random variation of a light intensity distribution associated with coherent light. It is caused by the coherent superposition of light from many scattering centers (as from an optically diffuse surface) with the scatterers contributing with a random phase. Scatterers of this type occur of course in the form of the films grainy structure and dust on lens surfaces. They are kept to a tolerable minimum by proper design as indicated by the noise data of Figure B.8 which was discussed above.

B.3 OPTICAL PROCESSING CHANNEL

In this section we will review the salient properties of an error free optical processing channel and then discuss its more exact characterization and design configuration.

The Fourier transformation is accomplished as an analog computation in the optical processing channel. Input data is entered as a two dimensional spatial recording having an optical transmission variation $\underline{t}(u,v)$ as depicted in Figure B.9. Illumination of the input with a coherent light beam causes the light beam field to be spatially modulated by the input data thus providing an optical analog which is operated on within the optical channel. For recorded data in the form of an optical amplitude transmission variation, illumination with a light wave having the field $U_i(u,v)$ provides the modulated light wave $U(u,v)$, where

$$U(u,v) = U_i(u,v)t(u,v)$$

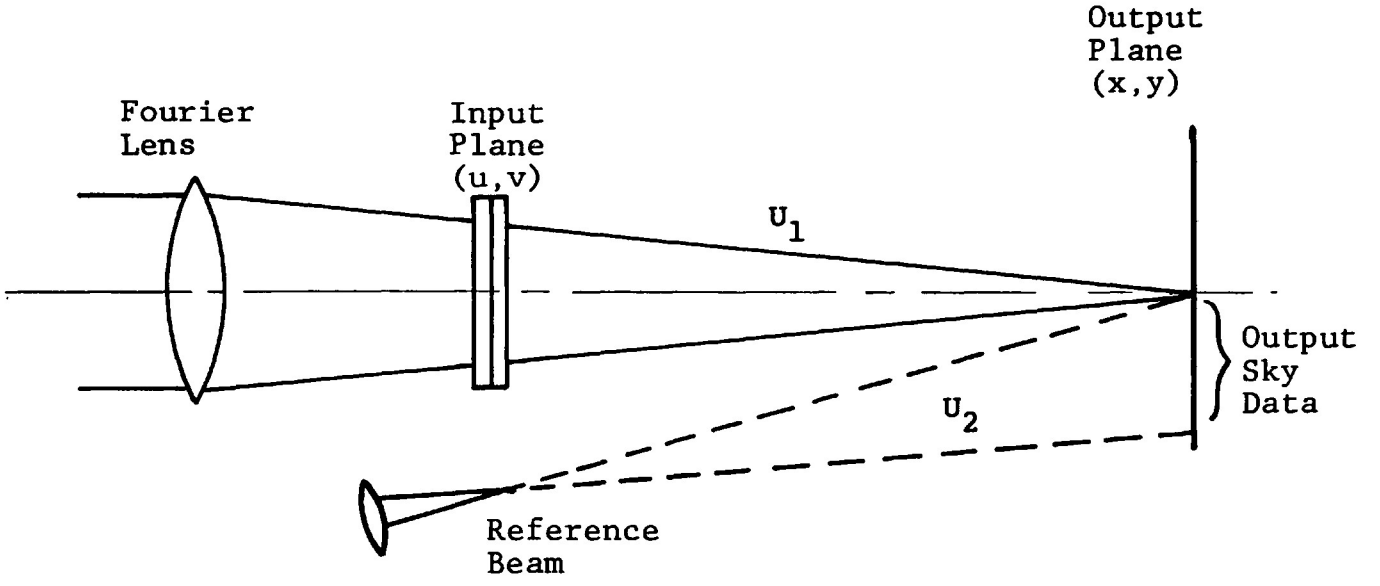

(a) After-the-Lens Input Optical Processing Channel

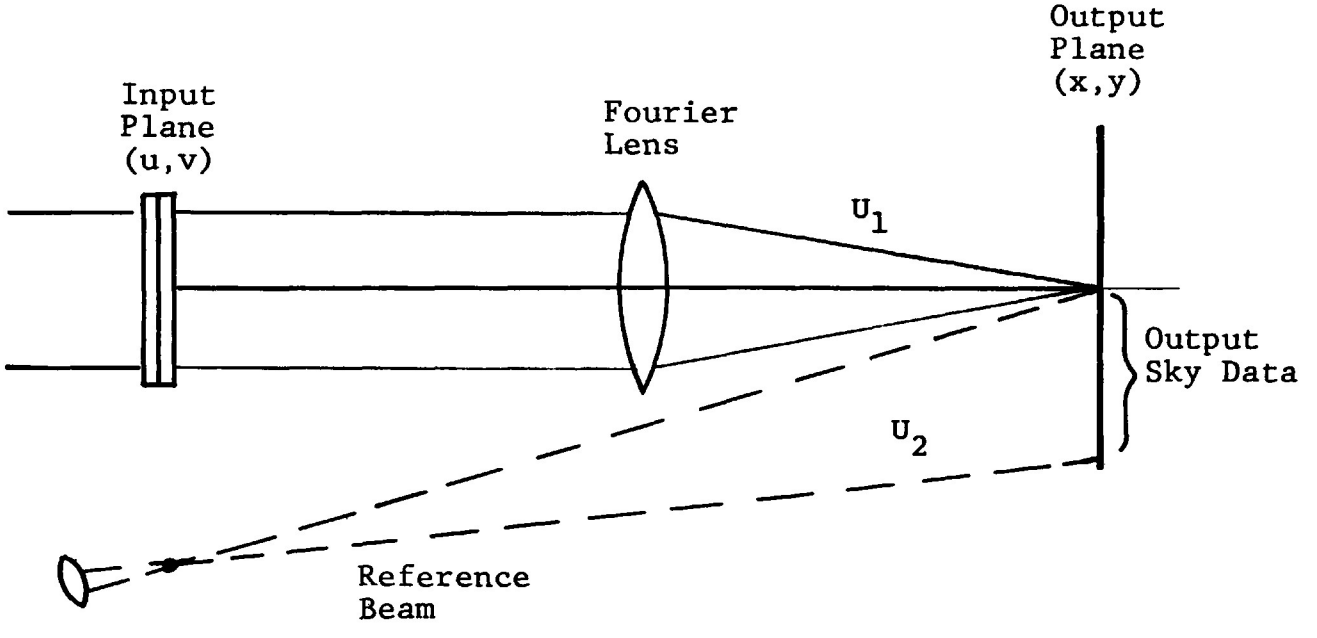

(b) Before-the-Lens Input Optical Processing Channel

Figure B.9. Optical Processing Configuration [Schematic]

This is the processing channel optical input. The processor accomplishes the optical Fourier transformation in terms of the light wave field and provides an output field $U_1(x,y)$ containing the desired transformed data. However, the optical field is not directly observable at the processor output; rather, as a practical matter, we can observe or measure the modulus squared, or intensity, of this light field. The output Fourier transform field is rendered accessible by use of a coherent reference light beam $U_2(x,y)$. Superposition of the reference light wave with the Fourier transformation channel output field provides a light intensity distribution $I(x,y)$ which is

$$I(x,y) = |U_1(x,y) + U_2(x,y)|^2$$

$$= U_1(x,y)\, U_2^*(x,y) + U_1^*(x,y)\, U_2(x,y)$$

$$+ |U_1(x,y)|^2 + |U_2(x,y)|^2$$

The Fourier output U_1 and the reference wave U_2 are expressed generally as

$$U_1(x,y) = A_1(x,y)\, e^{j\theta_1(x,y)} F[\underline{t}(u,v)]$$

$$U_2(x,y) = A_2(x,y)\ e^{j\theta_2(x,y)}$$

The error free expression for the transform $F[\underline{t}]$ is

$$F[\underline{t}(u,v)] = \iint \underline{t}(u,v)\ e^{-j\ \frac{2\pi}{\lambda z}\ (xu+yv)}\ dudv$$

The Fourier transform kernel $e^{-j(\ )}$ contains the processor output plane position variables x and y normalized by $1/\lambda z$, with z the operating focal length of the Fourier lens system and λ the optical wavelength.

Recall that the recorded data $\underline{t}$ is denoted as

$$\underline{t}(u,v) = t_o(u,v) + t(u,v) + t_*(u,v)$$

with

$$t(u,v) = \frac{1}{2}\ a_t(u,v)|V|e^{j[\omega_1 u + \phi(u,v) + \theta_o]} \otimes h_r(u,v)$$

$$t_*(u,v) = \frac{1}{2}\ a_t(u,v)|V|e^{-[\omega_1 u + \phi(u,v) + \theta_o]} \otimes h_r(u,v)$$

$$t_o(u,v) = [a(u,v)b + a_t(u,v)(b - b_t)] \otimes h_r(u,v)$$

The objective is of course the Fourier transform of the complex visibility function which is

$$a_t(u,v)\,|V|e^{j\phi(u,v)},$$

or its conjugate mate.

It is informative to examine the transform properties for a simple case at this point, that of a real input data aperture a(u,v) with a single sinusoidal fringe pattern or frequency f_1, i.e., let

$$\underline{t}(u,v) = a(u,v)e^{j2\pi f_1 u}$$

The optical transform will be

$$F[\underline{t}(u,v)] = \iint a(u,v)\; e^{j2\pi f_1 u}\; e^{-j\,\frac{2\pi}{\lambda z}\,(ux+vy)}\,dudv$$

$$= A(x - \lambda z f_1,\, y)$$

with

$$A\;(x,\,y) = \iint a(u,v)\; e^{-\frac{2\pi}{\lambda z}\,(ux+uy)}\,dudv$$

The result is the transform output function A with spatial location variables x and y at the processor output plane. The frequency component f_1 of the input data causes the output A(x,y) to be shifted by an amount proportional to that frequency. For this example we have an x dimension shift of

$$x = \lambda z f_1$$

The resultant transform A is shown in Figure B.10, in one dimension, for three types of aperture functions. For the input a(u,v) being square with sides L, the output A(x,y) is the sinc function. For a(u,v) circular with diameter L we get a jinc function for A. With $a(u,v) = a_t(u,v)$, the elliptical tracks of the visibility function, the resultant transform A(x,y), shown in its narrowest dimension in Figure B.10 denotes the synthetic beam. It is seen to have a lower level for the near-in sidelobe structure than does the sinc or jinc functions. The visibility track function $a_t(u,v)$ for this example was taken for the case of declination $\delta = 40^o$ and for a maximum aperture dimension the same as that for the square and circular functions.

The width of A(x,y) between the first zeros of the examples of Figure B.10, denoted ρ, is

$$\rho = \frac{2\lambda z}{L} \quad \text{(sinc function)}$$

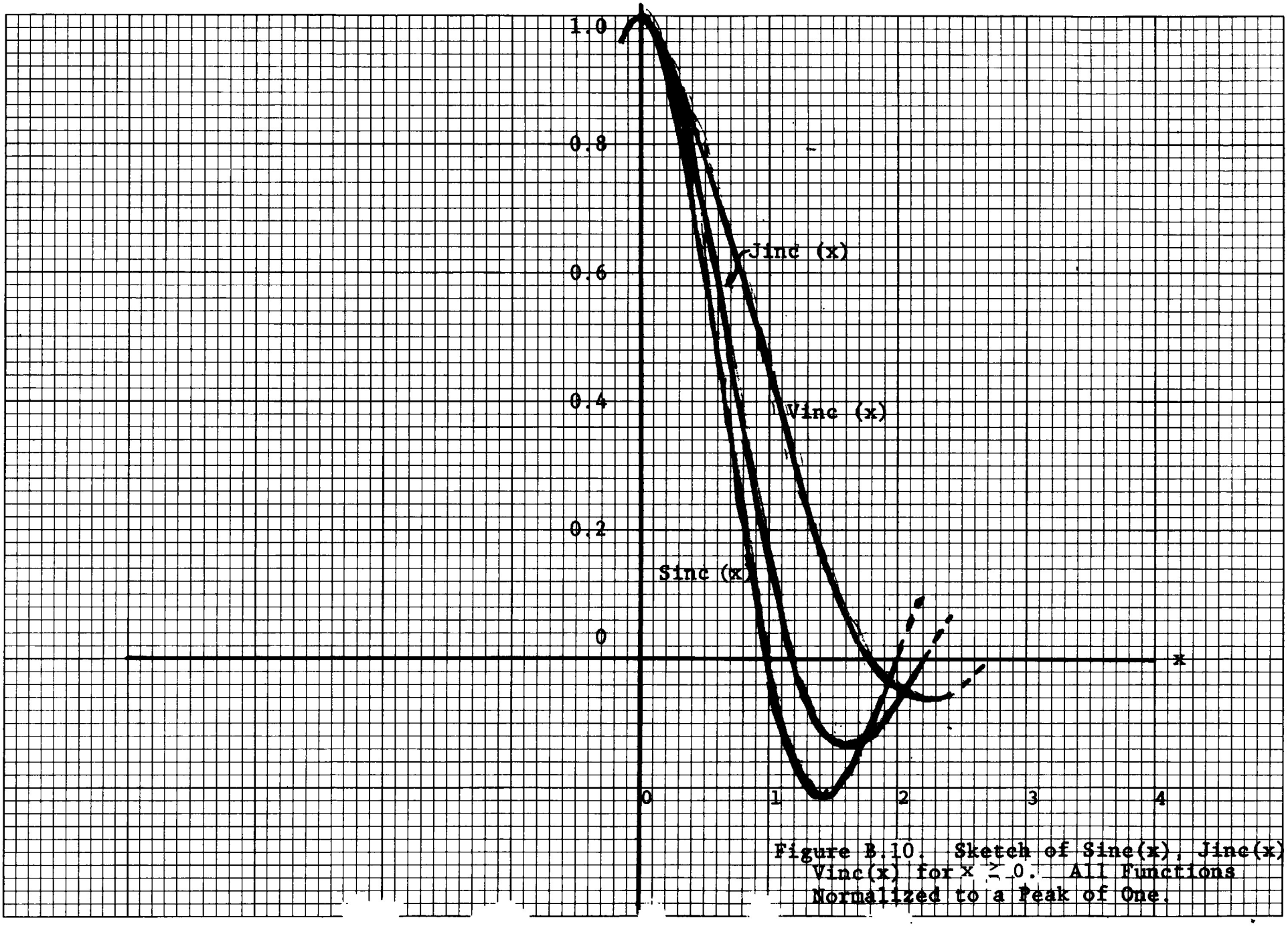

Figure B.10. Sketch of Sinc(x), Jinc(x), Vinc(x) for $x \geq 0$. All Functions Normalized to a Peak of One.

$$\rho = \frac{2.4\lambda z}{L} \text{ (jinc function)}$$

$$\rho \simeq \frac{3.8\lambda z}{L} \text{ (synthetic beam)}$$

B.3.1 OPTICAL DEFECTS

Small optical error effects can occur in the optical channel which can be identified with the input light field U(u,v), the optical Fourier transformation of F[t] and the reference wave $U_2(x,y)$. These errors include slowly varying amplitude weighting and phase aberrations and do not include scattering effects. Typically, the phase aberrations[13,14] are of primary concern as uncertainties in the amplitude spatial distributions can be kept suitably small. The errors can be characterized as multiplicative defect terms which will be denoted D_i, D_1 and D_2 for the input U, the optical transform operation F[t] and the reference beam U_2 respectively. The defect term represents a complex quantity with amplitude and phase representing the departure from the optically error free case. We will discuss here the phase error in terms of the components which cause them and leave for later their compilation and treatment on a system basis.

The input light beam U(x,y) can experience a defect mainly in the form of undesired optical path (phase) variation as it passes through the input recorded film data. This effect is brought under control by use of a liquid gate[11] shown in Figure B.11. Non-uniformities in the film thickness or surface scratches are compensated by

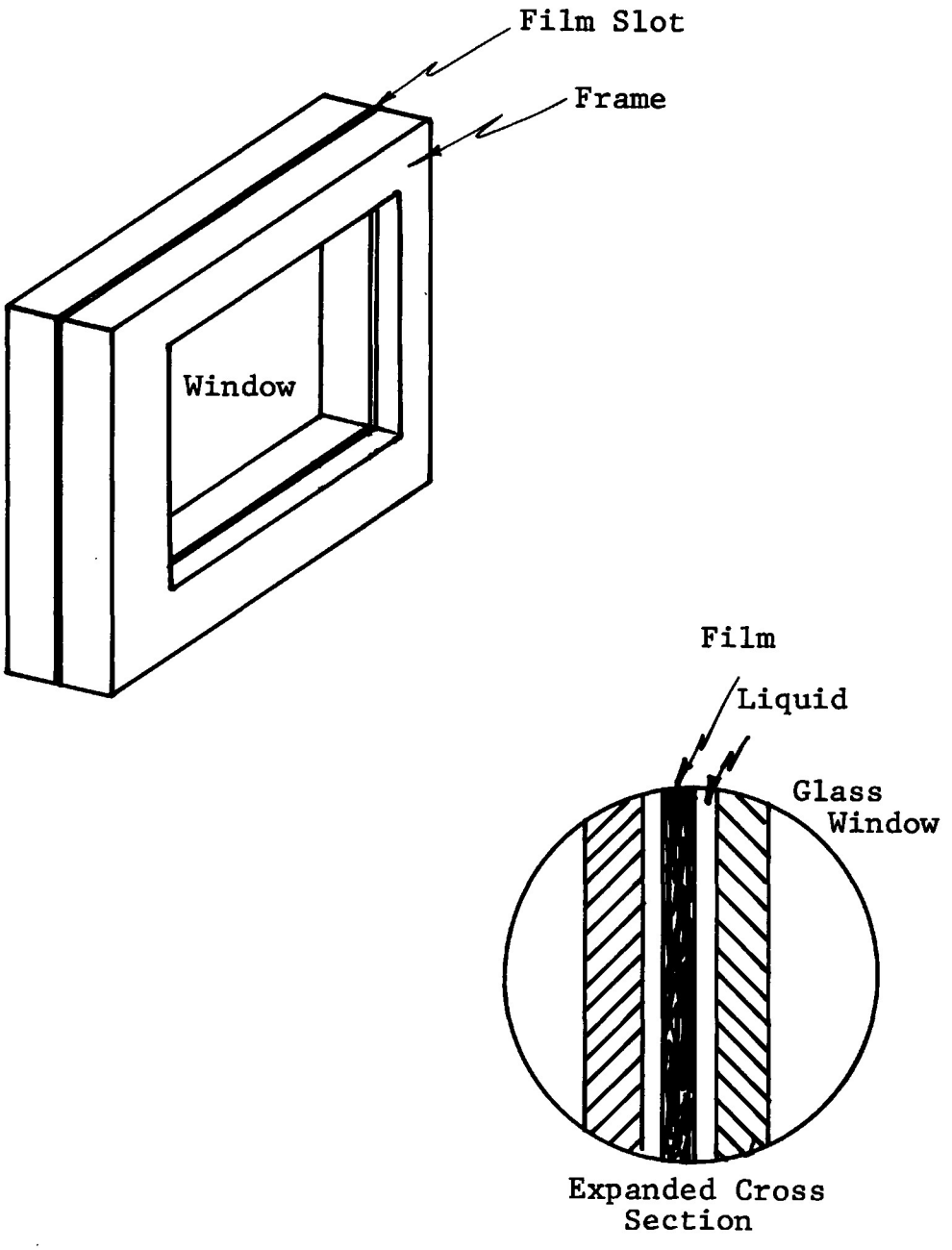

Figure B.11. Liquid Gate.

inserting the film in a liquid with a matching index of refraction. The film-liquid combination is held in the gate or cell by front and back windows of high quality glass. Index matching[11] between the liquid and film is required to 0.003 to constrain phase errors to less than $\lambda/40$. This can be provided by a mixture of xylene and alcohol. Considerable experience with the liquid gate indicates that film handling provisions and correction for optical path variations can readily be provided. Passage of the illuminating beam U_i through the gate must also be considered for spherical aberrations if the beam direction is not normal to gate (windows). Analysis[12] has shown that such aberrations are negligible for beam angles to about 20 degrees. The gate windows must of course be made of high quality glass and must have good flatness. These requirements are readily met particularly because the configuration is simple, i.e., non-curved surfaces and relatively small size (70 mm x 70 mm x 6 mm thick). As noted previously any defect within the liquid gate will be modeled as a complex multiplicative term D_i. The error free input field U(u,v) when expressed with the defect term included becomes

$$U(u,v)D_i(u,v)$$

Departure of the optical Fourier transform operator $F[\underline{t}]$ from the error free form shown below

$$F[\underline{t}] = \iint \underline{t}(u,v)\ e^{-j\ \frac{2\pi}{\lambda z}(ux+vy)}\ dydy$$

can occur as a change in the kernel or by a phase fluctuation of the light wave due to air gradients along the optical paths within optical processing channel. Air path gradients can be controlled to a suitable extent by properly enclosing the optical channel. Errors in the Fourier kernel can also be adequately controlled or compensated but do require careful consideration in the optical channel design. The two basic optical channel configurations will be discussed further relative to defects in the Fourier kernel[12,13].

After-the-Lens Input Plane

The after-the-lens input arrangement of Figure B.9a lends itself to a design having a minimum number of lens elements and is attractive for this reason. By its nature, however, the Fourier transform properties, if imperfect, are not corrected by use of correcting lens elements but rather by compensating for such imperfections, in the readout provisions. The defect in the after-the-lens system occurs when the diffraction angles of the light wave passing through the optical channel are sufficiently large. To establish the defect term D_1 for this case we start with an expression for the processor output in terms of the diffraction integral solution for the field at the processor output plane. The convergent spherical illumination at the input plane data will have amplitude A and be of the form

$$A \frac{e^{-jkr_1}}{jr_1}$$

The distance r_1 is measured from an arbitrary u,v location at the input plane to the focal point of this spherical

wave at the output plane. The Huygens-Fresnel diffraction integral defines the light field at the output x,y plane as the integrated sum of contributions from all points in the input plane, each input point being weighted by its initial complex amplitude U and also by a complex term of the form

$$\frac{z}{j\lambda r^2} \; e^{+jkr}$$

The distance r is measured between arbitrary input (u,v) and output (x,y) plane points. Thus, the Fourier channel provides an output field U_1 which is expressed as

$$U_1(x,y) = \frac{A}{\lambda} \iint \underline{t}(u,v) e^{jk(r - r_1)} \cdot \frac{z}{r_1 r^2} \, dudv$$

with

$$r_1 = [z^2 + u^2 + v^2]^{\frac{1}{2}}$$

$$r = [z^2 + (u - x)^2 + (v - y)^2]^{\frac{1}{2}}$$

Reforming the phase of the integrand kernel so that its defect term can be recognized, we get

$$U_1(x,y) = e^{j\theta_1(x,y)} \frac{A}{\lambda} \iint \underline{t}(u,v) e^{-j \frac{2\pi}{\lambda z} (ux + vy)} D_1(u,v,x,y)\,du\,dv$$

The defect term is

$$D_1(u,v,x,y) = \frac{z}{r_1 r^2} e^{j \frac{2\pi}{\lambda}(r - r_1)} \; j \frac{2\pi}{\lambda z}(ux + vy) \; e^{-j\theta_1(x,y)}$$

Binomial expansion of r_1 and r gives the term $(r - r_1)$ as

$$r - r_1 = \frac{1}{2z} (x^2 + y^2) - \frac{1}{8z^3} (x^2 + y^2)^2$$

$$- \frac{1}{z} (ux + vy)$$

$$+ \frac{1}{4z^3} [2u^3x - u^2 (3x^2 + y^2) + u(2x^3 + 2xy^2)]$$

$$+ \frac{1}{4z^3} [2v^3y - v^2(3y^2 + x^2) + v(2y^3 + 2x^2y)]$$

$$+ \frac{1}{4z^3} [2uv^2x - 4uvxy + 2vu^2y]$$

$$+ \text{higher order terms}$$

and

$$\theta_1(x,y) = z + \frac{1}{2z}(x^2+y^2) - \frac{1}{8z^3}(x^2+y^2)^2 + \ldots$$

This defect term, D_1, which we may refer to as the spherical wave defect at times, is deterministic. Those of its phase terms which couple between u,v and x,y terms must either be sufficiently small, or their effects must be compensated for when data is read out. The term linear in u will cause a scale distortion, the u^2 term causes the output to form an a curved surface rather than a plane and the u^3 term causes a distortion of the impulse response (lightspot) profile. Similarly for v dependent terms. Higher order terms are small enough to be insignificant. The phase terms with x or y dependence only, make up the phase term $\theta_1(x,y)$ used previously in the error free expression.

We will examine the magnitude of the phase of the defect term before considering its compensation. To do this a specific set of operating parameters for the optical channel must be used. A likely set of parameters are $z = 3.3 \times 10^3$ mm, $\lambda = 0.51 \times 10^{-3}$ mm, $u_{max} = 25$ mm, $x_{max} = 110$ mm, $v_{max} = 25$ mm, $y_{max} = 50$ mm. At the farthest edge of the output map plane (x = 110 mm) the term cubic in u reaches a maximum value of 1/20 (2π) or a twentieth wavelength. The term quadratic in u has a maximum of about 1/3 (2π) and the term linear in u has a maximum of 1.5 (2π). Note however that the output x,y plane is taken normal to the principal or central ray of the input plane illumination wave which is spherical.

Several methods of compensating for the phase defects are possible. If we maintain the same spherical illuminating wave while adjusting the location of the output plane we can affect the phase error terms just discussed. Such a

change in output plane location is identified with the distance $r - r_1$. Leaving the spherical illuminating beam unchanged means r_1 remains unchanged. Shifting the output plane location can be modeled as a change in the value of z in the distance variable r. If we let z go to $z + \alpha(x,y)$ in r and denote r as r' when $z = z + \alpha$ then we have (for small α)

$$r' = [(z + \alpha)^2 + (u - x)^2 + (v - y)^2]^{\frac{1}{2}}$$

$$\simeq [z^2 + (2z\alpha) + (u - x)^2 + (v - y)^2]^{\frac{1}{2}}$$

Denoting $2z\alpha \equiv \Delta$, the difference distance $r' - r_1$ can be written in terms of the unmodified distance $r - r_1$, as

$$r' - r_1 = (r - r_1) + \frac{1}{2}\frac{\Delta}{z} - \frac{1}{4z^3}(\Delta)(u^2 - 2ux + x^2)$$

$$- \frac{1}{4z^3}(\Delta)(v^2 - 2vy + y^2) - \frac{1}{8z^3}(\Delta^2)$$

$$+ \text{higher order terms}$$

The above terms of the form $\Delta(u^2 - 2ux)$ and $\Delta(v^2 - 2vy)$ can be used to, in part, cancel the error terms in $(r - r_1)$ which have quadratic and linear dependence on u.

Using a surface that is tilted relative to x axis at an angle whose tangent is k we have

$$\alpha(x,y) = kx$$

or

$$\Delta(x,y) = 2z(kx)$$

If we use a one dimensional parabolic surface we have

$$\alpha(x,y) = kx^2$$

or

$$\Delta(x,y) = 2z(kx^2)$$

Compensation for complete cancellation of the phase error terms is not required; the essential need is to reduce mainly the quadratic phase error, with either little or no compensation for cubic and linear phase errors. The cubic error of 1/20 wavelength is in a tolerable error range while the linear phase error causes a change of the output

map position that is compensated for with a calibration of the output.

A second method for compensation of the spherical wave phase defects of the after-the-lens optical channel is to record a prescribed deviation of the writing beam scan position from the error free or linear case that is normally specified. Departures from perfect scan linearity manifest themselves as a phase error which can have dependence on input and output plane variables u,v,x and y. They therefore can be used to negate, at least partly, the optical channel phase defects.

A third method for compensation is to design the illumination beam $A_1/jr_1\ e^{jkr_1}$ to have a modified phase, i.e.,

$$e^{j[kr_1 + \alpha(u,v)]}$$

with $\alpha(u,v)$ prescribed to have a phase which is equal and opposite in sign to that of $D_1(u,v,x,y)$ for one specified x,y position at the output plane. Since each of the phase terms of D_1 varies monotonically we can decrease the effective error to zero at a single output location and reduce the previous extremes over the map area by a factor of about 2.

The amplitude variation $1/r\ r_1^2$ in D_1 can be viewed as small amplitude weighting of the input data which is variant with the point of observation at the output plane. It is small but may be compensated upon readout of the output data.

Before-the-Lens Input Plane

For the Fourier channel configuration of Figure B.9b where the input data plane is placed before the transform lens we could consider a simple aspheric lens, however, a defect term will again occur and be somewhat similar to that for the after-the-lens arrangement of Figure B.9a. Instead we will discuss a Fourier lens set[9] design made by the Perkin Elmer company that utilizes five lens elements and is designed so that the defect term is minimized. Analytical data available for this design indicates an attractively low phase error. System performance is characterized with a u,v plane phase error function for each of several points of observation at the output x,y plane, and also with plots of the system impulse response. The input phase error function varies with the point of observation at the output plane. It appears to have nearly cubic dependence with the input plane variables and is quite low in all cases of interest (one fiftiety wavelength or less) as shown in the graph of Figure B.12.

This Fourier lens system with the before the lens configuration of Figure B.9b provides better performance than the beyond the lens spherical wave illumination arrangement of Figure B.9a in that compensation at the output plane for the defect term would not be required. It does however utilize several lenses and therefore requires more care in

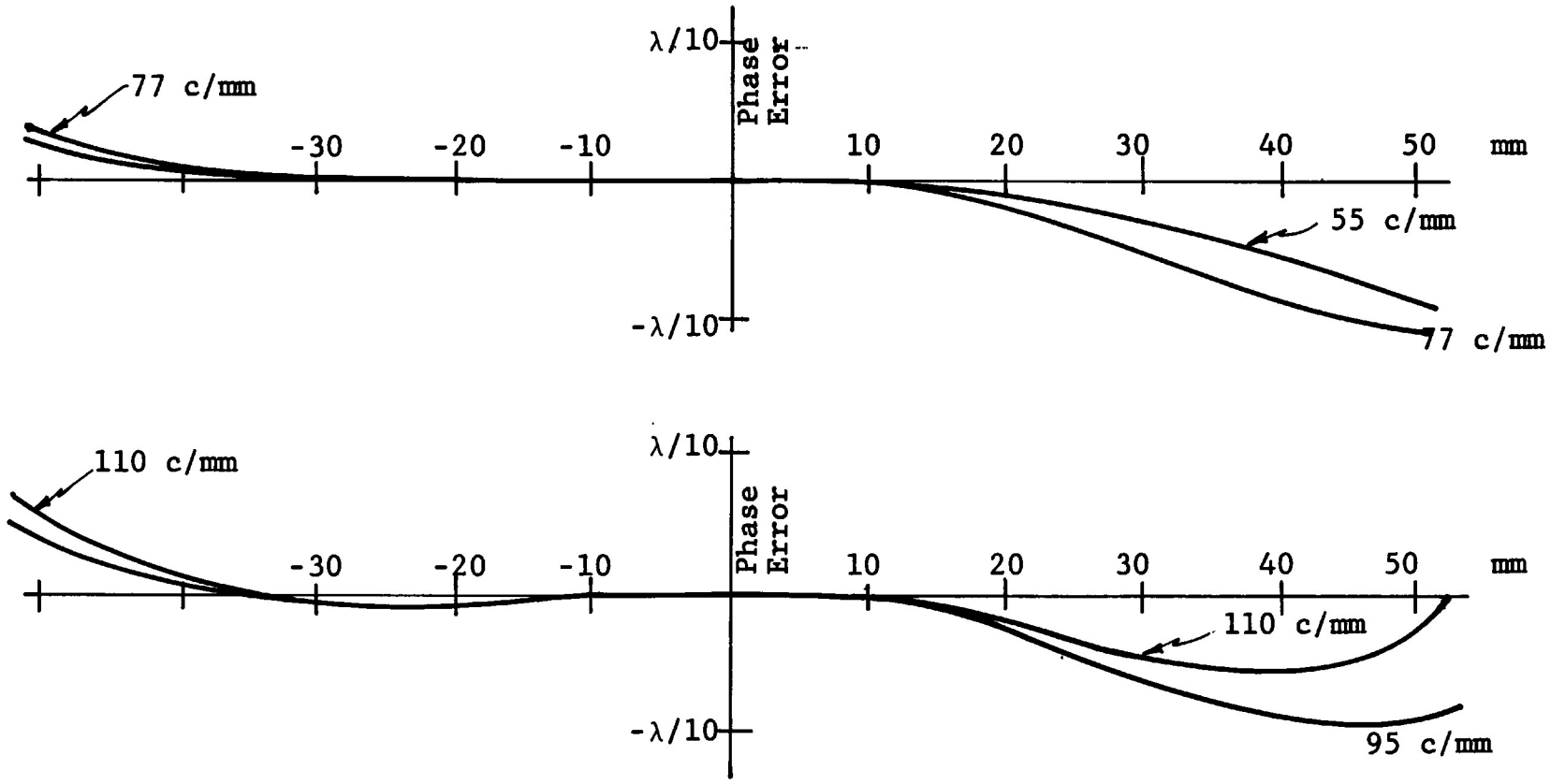

Figure B.12. Peak Phase Defect Equivalent at Input for P.E. FT Lens Design.

glass selection and fabrication to assure that its potential for high performance is realized and close attention to minimizing dust particles on its surfaces.

A defect D_2 in the reference wave would be identified with departures from the desired or prescribed phase θ_2 and amplitude A_2. With proper care in design this defect is expected to be insignificant and is included here for completeness.

In summary, we note that with the optical error defect terms included, the output plane optical waves U_1 and U_2 become

$$U_1(x,y) = A_1 e^{\theta_1(x,y)} \iint [t(u,v)D_i(u,v)]D_1(x,y,u,v)e^{-j\frac{2\pi}{\lambda y}(ux+vy)}dudv$$

and

$$U_2(x,y) = A_2 e^{j\theta_2(x,y)} D_2(x,y)$$

Recognize also that the recorded data $t(u,v)$ can have position errors i.e., $t(u + \varepsilon_u, v + \varepsilon_v)$. These positions will generate a phase error effect which will be described in Appendix C where the response function for the total system is discussed.

B.3.2 EXTRANEOUS OUTPUT TERMS

Recall that the output of the optical channel with the reference beam is expressed as

$$I(x,y) = 2A_1A_2\, F[\underline{t}(u,v)]\, \cos\,(\theta_1 - \theta_2)$$

$$+\ |U_1(x,y)|^2 + |U_2(x,y)|^2$$

with

$$U_1(x,y) = A_1 e^{j\theta_1(x,y)} F[\underline{t}(u,v)]$$

$$U_2(x,y) = A_2 e^{j\theta_2(x,y)}$$

$$\underline{t}(u,v) = t(u,v) + t_*(u,v) + t_o(u,v)$$

We will note for consideration at a later point that the term cos $(\theta_1 - \theta_2)$ can be prescribed to have a fixed phase either zero, $\pi/2$ or other values, whichever may have merit in handling the output data. Further, recall that a fixed phase term θ_o is buried in t and t_* of $\underline{t}$. This phase θ_o will enter the argument of cos $(\theta_1 - \theta_2)$ which then becomes cos $(\theta_1 - \theta_2 + \theta_o)$ for those terms in the expansion of I(x,y) which contain F[t] and $F[t_*]$.

The desired output F[t] will be separated from undesired terms at the output partly by its spatial separation and

partly by taking two scans through the sky map output light distribution in a way which allows cancellation of the remaining extraneous terms. It is important for an understanding of this extraction of F[t] to examine the nature of I(x,y) in further detail[14,15].

Expanding the terms $\underline{t}(u,v)$, $|U_1|^2$ and $|U_2|^2$ we have for I(x,y)

$$I(x,y) = 2A_1A_2\, F[t(u,v)]\, \cos\,(\theta_1 - \theta_2 + \theta_o)$$

$$+ 2A_1A_2\, F[t_*(u,v)]\, \cos\,(\theta_1 - \theta_2 + \theta_o)$$

$$+ 2A_1A_2\, F[t_o(u,v)]\, \cos\,(\theta_1 - \theta_2)$$

$$+ A_2^2 + A_1^2\; F[t]^2 + |F[t_*]|^2 + |F[t_o]|^2$$

$$+ A_1^2\, \{F[t]\, F[t_o]^* + F[t]^*\, F[t_o]\}$$

$$+ A_1^2\, \{F[t_*]\, F[t_o]^* + F[t_*]^*\, F[t_o]\}$$

$$+ A_1^2\, \{F[t]\, F[t_*]^* + F[t]^*\, F[t_*]\}$$

The very first term is the desired output since it contains F[t]. Of the remaining terms we recognize those containing the factor cos ( ) as opposed to those without the cos ( ) factor which can be cancelled upon subtraction of two separate scans of the output data as noted in Section 2.

Terms Containing cos ( )

Those terms with the factor cos ( ) will be retained in the resultant output after the subtraction of the two output scans; of these the second and third terms

$$2A_1A_2\ F[t_*(u,v)]\ \cos\ (\theta_1 - \theta_2 + \theta_o)$$

$$+\ 2A_1A_2[t_o(u,v)]\ \cos\ (\theta_1 - \theta_2)$$

are extraneous and must be avoided by being spatially separated or by being of a comparatively small magnitude. For the most part these second and third terms are spatially separated because of the use of the spatial carrier frequency f_1. The carrier frequency shifts the term containing the desired sky map data F[t] so that it is centered about the loaction $x = f_1\lambda z$, its conjugate mate $F[t_*]$ is centered at $x = -f_1\lambda z$ and the zero order term $F[t_o]$ is centered at x = 0. There can, however, be a certain amount of overlap due to the sidelobes structure of $F[t_*]$ and $F[t_o]$ since the carrier shift cannot be made arbitrarily large because this would place excessive demands for high spatial frequency response on the input recorder and the

optical channel. We will consider the sidelobe of the zero order term $F[t_o]$. The effect of $F[t_*]$ will be even less due to the combined effect of radio telescope antenna weighting on the output sky brightness data and spatial separation of $F[t_*]$ and $F[t]$.

Suppression of the $F[t_o]$ term is realized by proper choice of the phase of $\cos(\theta_1 - \theta_2 + \theta_o)$. The fixed phase θ_o is introduced when the original digital visibility data is converted to the analog form. The $(\theta_1 - \theta_2)$ part of this phase represents the phase of the optical waves at the processor output plane. If we let $\theta_o = \pi/2$ and prescribe $\theta_1 - \theta_2 = +\pi/2$ and $-\pi/2$ for the successive scans of the output data, then the zero order term $2A_1A_2F[t_o] \cos(\theta_1 - \theta_2 + \theta_o)$ will be retained.

A second appraoch to $F[t_o]$ suppression is the use of complimentary weighting of the input u,v data. This is accomplished by making the input illumination beam $A_1(u,v)$ the weighting function necessary to suppress the sidelobes of the zero order term $F[t_o]$. Noting, however, that $A_1(u,v)$ will also affect $F[t]$, the desired transform, the visibility function is weighted before recording in a way which causes cancellation of weighting provided by $A_1(uv)$. This is accomplished by dividing the visibility function amplitude $|V(u,v)|$ by a function of the same weighting as $A_1(u,v)$. This approach not only suppresses undesired sidelobes of the $F[t_o]$, it can also serve as a means of input data amplitude compression before recording with recovery during optical processing.

An additional suppression consideration lies in the alternative of allowing t_o to be the elliptical track function $a_t(u,v)$ or, if the bias level of a_t is matched with the

off track region bias by making $b = b_t$, we will have t_o take on the character of a(u,v) which can be rectangular, circular, etc. If t_o is governed by the track function $a_t(u,v)$ then the sidelobes level is down to about -25 dB from the peak of $F[t_o]$ over a major portion of the output plane in which we can expect our sky map data. If t_o is governed by a(u,v) then for a square aperture we can expect the sidelobes of $F[t_o]$ to be about -40 dB at locations displaced by about 25 sidelobe widths along a line at 45^o to the sinc function peak sidelobe line. This controlled location of the portion of the map data being readout, relative to the sinc function lobe lines, is achievable by use of the matched bias condition $(b - b_t)$ together with a rectangular (or parallelogram) boundary aperture a(u,v) which rotates in synchronism with the readout process.

Terms not Containing cos ( )

The remaining extraneous terms, those not containing the factor cos ( ), are cancelled in the subtraction of the two separate scans of the output data, i.e., $I_1(x,y) - I_2(x,y)$. However, the magnitude for those of these terms which occur specifically at the same spatial location as F[t] must not be so large as to dominate the available dynamic range of the readout photodetector used to scan the map data light intensity distribution. Those terms which are of significant relative magnitude and occur at the same spatial location as the map data are

$$A_1^2|F[t]|^2 + A_2^2$$

It is seen that one term contains the modulus squared of the map data and the other contains the reference beam squared. A_1 and A_2 represent the amplitude distribution of the Fourier channel illumination beam and the reference beam, respectively. We seek to minimize these terms while maximizing the desired map output term

$$2A_1A_2F[t] \cos (\theta_1 - \theta_2 + \theta_o)$$

The problem to be considered can be cast as one of maximizing the following ratio

$$R = \frac{2A_1A_2 \ |F[t]|}{A_1^2|F[t]|^2 + A_2^2}$$

To assess this matter further we let $A_2 = KA_1$ with K a constant and will write $F(t) \equiv F$, then the ratio in question can be formulated as

$$R = \frac{2}{F/K + K/F} \leq 1$$

This ratio has a maximum value of one when $F/K = 1$ and is less than one otherwise. This maximum occurs when $F = A_2/A_1$. However, since the Fourier transform F can take on a range of values depending upon the nature of the sky brightness map, we are left with the choice of maximizing the ratio R

for one value of F. We will make R a maximum when F is at its peak magnitude. This will allow the maximum of the output intensity, which is essentially $2A_1A_2F[t] + A_1 F[t]^2 + A_1^2$, to be well defined and therefore readily prescribed to have a value which will approximately equal the peak (saturation level) in the linear response range of the output ohotodetector. Recall that the measured sky brightness distribution for any one brightness map must preserve a dynamic range of a few hundred. With an expected photodetector dynamic range of at least 2000 the output map data will quite readily be detected without saturation of its peaks and yet with its lowest values well above detector noise, when using the above criterion for selecting the value of A_1 and A_2.

B.3.3 RELATIVE OUTPUT LIGHT INTENSITY LEVELS

The relative levels of the sky brightness data available at the light intensity distribution of the processor output is readily estimated in terms of the recorded input data properties. Recall that the output map has the form

$$2A_1A_2 \; F[t(u,v)] \cos (\theta_1 - \theta_2 + \theta_o)$$

with

$$t(u,v) = \frac{1}{2} a_t(u,v)|V|e^{j \phi(u,v)} \circledast h_r(u,v)$$

With A_1, A_2, cos ( ) a_t and h_r being fixed quantities, the output will vary as F[t] which we can relate to the recorded visibility data t. The visibility function is recorded as film amplitude transmission variations which are bounded by the values 0.9 and 0.1 and have an average or bias level 0.5. Thus, the available peak excursion for the input visibility data t is nominally 0.2.

For the case of a single star the fringe pattern for the visibility data can have a recorded peak of 0.2. For the case of one hundred equally bright stars we have a superposition of 100 fringe patterns whose sum is bounded by 0.2. They would not be expected to add in-phase. Taken as a peak summation each of the 100 fringe patterns would have an equivalent peak of $0.2/100 = 2.0 \times 10^{-3}$. The case of a visibility function for maximally distributed source will be approximated as a random or noise-like signal with a uniform spectral distribution which would be characterized by its RMS amplitude and space-bandwidth product. To accommodate the peaks of this type of recorded visibility data we would scale its RMS level to a recorded transmission value of 0.05.

Knowing the peak value of a recorded fringe pattern, or the RMS value and space-bandwidth product of random data, we can determine corresponding relative values of their light intensity distributions at the processor output plane. We assume here that the aperture at the input plane is the same for all cases, which is true. For the case of a fringe pattern input, the peak value of the corresponding output star distribution at the sky map plane will be proportional to the peak of the recorded fringe pattern. For a single star the output is proportional to 0.2 while for 100 equally bright stars each star in the sky brightness map will have

a relative peak value of 2.0×10^{-3}. For a distributed source recorded with a space bandwidth product of 10^4, the level of the sky brightness map within one resolution cell at the output plane will be proportional to 5×10^{-4}. This result for a distributed source is about what is expected for CAS-A which is an infrequent occurrence. Thus, the range of sky map intensity levels at the processor output for the three cases cited can vary, on a relative basis, from about 0.2 to 0.5×10^{-3}.

The spatially separated zero order output containing the term $F[t_o]$ has a peak proportional to 0.5. However, at the location of the sky map data, the zero order is down into its sidelobe structure and will be cancelled as part of data readout procedure as discussed in Section B.3.2.

An estimate of the noise contribution in the output light intensity distribution caused by film grain noise and optics scattering was given in the experimental data of Figure B.9 of Section B.2.1. On a single resolution cell basis the noise power spectrum was down to -85 dB. This noise was contributed about equally by film and optical surface scattering giving -88 dB level associated with each of these noise sources separately. Therefore the output film noise term containing the transform $F[n_r]$ will have a level proportional to about 4×10^{-5} or -44 dB.

In summary the relative levels for output light intensity terms containing $F[t]$, $F[n_f]$ and $F[t_o]$, based upon the values of the recorded transmission variation are listed below.

Single star	0.2	peak
100 stars	2.0×10^{-3}	peak
Distributed	5×10^{-4}	per resolution cell
Film noise	4.0×10^{-5}	per resolution cell

Use of an input aperture function which differs in area will scale the above results by the ratio of the new to the previous area.

Accuracy of the Phase $\theta_1 - \theta_2$

The accuracy of the relative phase term $\theta_1 - \theta_2$ affects the output sky brightness term $2A_1A_2F[t] \cos (\theta_1 - \theta_2 + \theta_o)$ and it also determines the amount of reduction of undesired zero order $2A_1A_2F[t_o]\cos (\theta_1 - \theta_2)$. We will estimate the required accuracy of setting for $(\theta_1 - \theta_2)$.

Regarding the accuracy of the sky brightness output, let an error in the setting of $\theta_1 - \theta_2$ be θ_ε then our output is

$$2A_1A_2F[t] \cos (\theta_1 - \theta_2 + \theta_o + \theta_\varepsilon)$$

Since $(\theta_1 - \theta_2 + \theta_o) = 0$ or π we can rewrite this expression as

$$2A_1A_2F[t] \cos \theta_\varepsilon$$

Thus, the error θ_ε causes an incorrect magnitude scaling of the output by the factor $\cos \theta_\varepsilon$. This error will be 0.1% or less for $\theta_\varepsilon \leq 2.4^o$.

Suppression of the zero order can be considered in terms of the ratio of the zero order to the sky brightness output, i.e.,

$$\frac{2A_1A_2F[t_o]\cos(\theta_1 - \theta_2 + \theta_\varepsilon)}{2A_1A_2F[t]\cos(\theta_1 - \theta_2 + \theta_Q + \theta_\varepsilon)}$$

Recall that we have $\theta_1 - \theta_2 = \pm \pi/2$ and $\theta_2 = \pi/2$ allowing this ratio to be expressed, for small θ_ε, as

$$\frac{1}{57.4}\ \frac{F[t_o]}{F[t]}\ \theta_\varepsilon$$

where θ_ε is expressed in degrees. The choice of the value for $F[t_o]$, and the sky brightness data $F[t]$, for this zero order suppression assessment depends in part on the system implementation. We take $F[t_o]$ the sidelobe level of the synthetic (dirty) beam 2.8×10^{-2} and for $F[t]$ we take the case of a highly distributed source (CAS-A) with output plane magnitude 5×10^{-4}. These are not actual values but rather the relative values described previously. Thus, we have the zero order sidelobe to sky brightness ratio as

$$\frac{1}{57.4}\ \frac{2.8 \times 10^{-2}}{5 \times 10^{-4}}\ \theta_\varepsilon$$

We want this ratio to be small to assume good accuracy for the sky brightness data. To realize a ratio of 0.01, or one percent, we require $\theta_\varepsilon \leq 0.01$ degrees. This phase

accuracy is quite demanding of hardware implementation. Therefore, rather than allow a dirty beam for the zero order we can use the matched bias condition $b = b_t$ which cuases the zero order to be defined by the Fourier transform of the boundary aperture function a(u,v). Using a rectangular function for a(u,v) which is rotated in synchronism with the output scanning detector we will have for $F[t_o]$ a value of about 4×10^{-4} at the 25^{th} sinc sidelobe at 45^o to the sidelobe ridge, giving a zero order sidelobe to sky brightness ratio of

$$\frac{1}{57.4} \quad \frac{4 \times 10^{-4}}{5 \times 10^{-4}} \theta_\varepsilon \simeq \quad 3.4 \times 10^{-2} \theta_\varepsilon$$

In this case we require that $\theta_\varepsilon \leq 0.75$ degrees for a ratio of 10^{-2}, or one percent. However, the use of complimentary weighting, which reduces the sidelobe level of the zero order, may be used to further reduce the requirement on accuracy for the relative phase, possibly a factor of at least 3. With complimentary wieghting included, at least for CAS-A type situations where F[t] is quite low, we expect a phase error limit between reference and Fourier waves of about $\theta_\varepsilon \leq 2^o$.

Accuracy and stability of the setting for the relative phase $\theta_1 - \theta_2$ is required in order to realize output sky brightness data that is accurate to one percent. Provisions for this purpose include both an accurate means for setting $\theta_1 - \theta_2$ to a prescribed value and good stability of the setting. Stability is realized by mechanical rigidity of optical components in the optical processing channel and utilizing a common optical path for both the reference and Fourier light waves to the extent possible. Further, air

gradients in the optical paths must be minimized and use of an enclosed and possibly partially evacuated housing for the optical channel would be used for this purpose. In addition the relative phase of the two beams can be sensed and then stabilized by closed loop control of the phase of the reference beam. Phase shift control for this provision can be accomplished with an electro-optic or acousto-optic device which would also provide for the basic $\pi/2$ and $-\pi/2$ settings for $(\theta_1 - \theta_2)$.

B.3.4 OPTICAL CHANNEL LASER REQUIREMENT

The laser light source which serves as the illuminating light beam for the optical processing channel must provide an output of a suitable power level, wavelength and power stability. The argon laser is well suited to the VLA optical processor requirements. At the wavelength of 0.5140 μm, single transverse mode power outputs of 4 watts and 1.4 watts are available with the Spectra-Physics Models 170 and 165 respectively. Power output stability, using closed loop stabilization provisions built into the laser by the manufacturer, can limit the RMS output variations to 0.2% in the 10 Hz to 2 MHz range, and long term stability of 0.5% over 10 hours is available.

The power required at the laser can be estimated from the expression for twice the light intensity of the output sky map which is

$$I(x,y) = 4A_1A_2F[t(u,v)]$$

where we have taken cos ( ) = 1.

The laser power P_o is related to the amplitude product A_1A_2 as follows. A_1 and A_2 represent amplitudes of two beams at the output map plane which are obtained by division of the original laser beam. Defining the ratio of these beam amplitudes as $K = A_2/A_1$, and taking $K = F$ as discussed earlier, we have for map data + modulus squared,

$$I(x,y) = 4A_1^2 F^2$$

Here we have taken $|F[t(u,v)|]^2 \cong F^2$. The field amplitude A_1 at the processor output is related to the field A at the processor input by $A_1 = A/\lambda z$. The magnitude F has a relative value γ discussed earlier multiplied by the area β_T of the input visibility track function. Therefore we can write the output intensity I(x,y) as

$$I(x,y) = 4A^2\gamma^2 \frac{\beta_T^2}{(\lambda z)^2}$$

The input plane power distribution A^2 is the total input plane power P normalized to the input plane area β giving

$$I(x,y) = 4 \frac{P}{\beta} \gamma^2 \frac{\beta_T^2}{(\lambda z)^2}$$

The input plane power P is equal to the laser source power P_o multiplied by a loss factor α(which is due to beam

forming optics) giving

$$I(x,y) = 4P_o \frac{\alpha \gamma^2 \beta_T^2}{\beta(\lambda z)^2}$$

This expression has units of power per unit area. Multiplying by the area per output map resolution cell which is $(3.8)^2(\lambda z)^2/\beta$, and by the ratio of the number of map resolution elements per detector cell δ, we have the power per detector cell as

$$I = \frac{4P_o \alpha \gamma^2 \beta_T^2 (3.8)^2}{\beta^2}$$

With a detector integration time Δ the energy sensed by a detector cell is

$$E = \Delta \cdot I$$

Solving for the laser source power P_o we have

$$P_o = \frac{E}{4\alpha\gamma^2 (\frac{\beta_T}{\beta})^2 \delta\Delta(3.8)^2}$$

The Reticon detector array requires about 9×10^{-12} joules to saturate a single 15 x 15 μm detector cell. As a worst case estimate for laser power we solve for the P_o

which will cause saturation of the detector, using the following parameters

$$E = 9 \times 10^{-12} \qquad \delta = 6 \times 10^{-2}$$
$$\alpha = 2 \times 10^{-1} \qquad \Delta = 10^{-2}$$
$$\beta_T/\beta = 0.2$$
$$\gamma = 5 \times 10^{-4}$$

The laser power required with these operating parameters is $P_o = 1.3$ watts which is readily available with Argon lasers.

B.4 SKY BRIGHTNESS MAP DATA READOUT

The sky brightness data I(x,y) is converted to an electronic signal using a scanning photodetector then digitized and processed to obtain the difference between two successive scans which have been phase shifted relative to one another.

A number of image detectors are available. Silicon arrays, although still not a mature technology development, offer excellent geometric fidelity and a photo response and MTF adequate for the readout of the processor light intensity distribution output. Of the silicon diode arrays available a Reticon self-scanned linear array and a Fairchild charge-coupled linear array device were used experimentally. An important advantage of the self-scanned array by Reticon is its capability to withstand a high intensity exposure (beyond saturation) in a single detector element with only a minor effect on the remaining elements of the array. Only the elements immediately adjacent to the element under saturation are affected.

Large two dimensional image arrays are not available therefore a linear array in a push-broom arrangement would be used to scan the sky brightness data. An array length of 7200 elements would be used and would be built up using arrays of shorter length. A number of these linear arrays are used to further reduce total readout time.

The array would be electronically scanned along its length and mechanically stepped in the orthogonal direction with a precision electrical stepping motor similar to our experimental breadboard processor detector which is shown in Figure B.13.

The response of the array can be defined on an individual element basis by an impulse response function $h_d(x,y)$. This response function is comprised of the product of a gain constant K_d and spatial distribution $g_d(x,y)$ which describes the variation in response over the extent of an individual detector element, i.e.,

$$h_d(x,y) = k_d g_d(x,y)$$

K_d can be tailored to be a constant but only over a finite range of input light levels and $g_d(x,y)$ is approximately rectangular in its spatial distribution as depicted in Figure B.14. The linear detector array elements provide a discrete sampling of the light intensity along the array direction at a spacing d_x while mechanical stepping in the y-direction is accomplished with a step size d_y. An integration time Δ seconds long is realized by allowing the array to dwell for that duration at each step of the mechanical

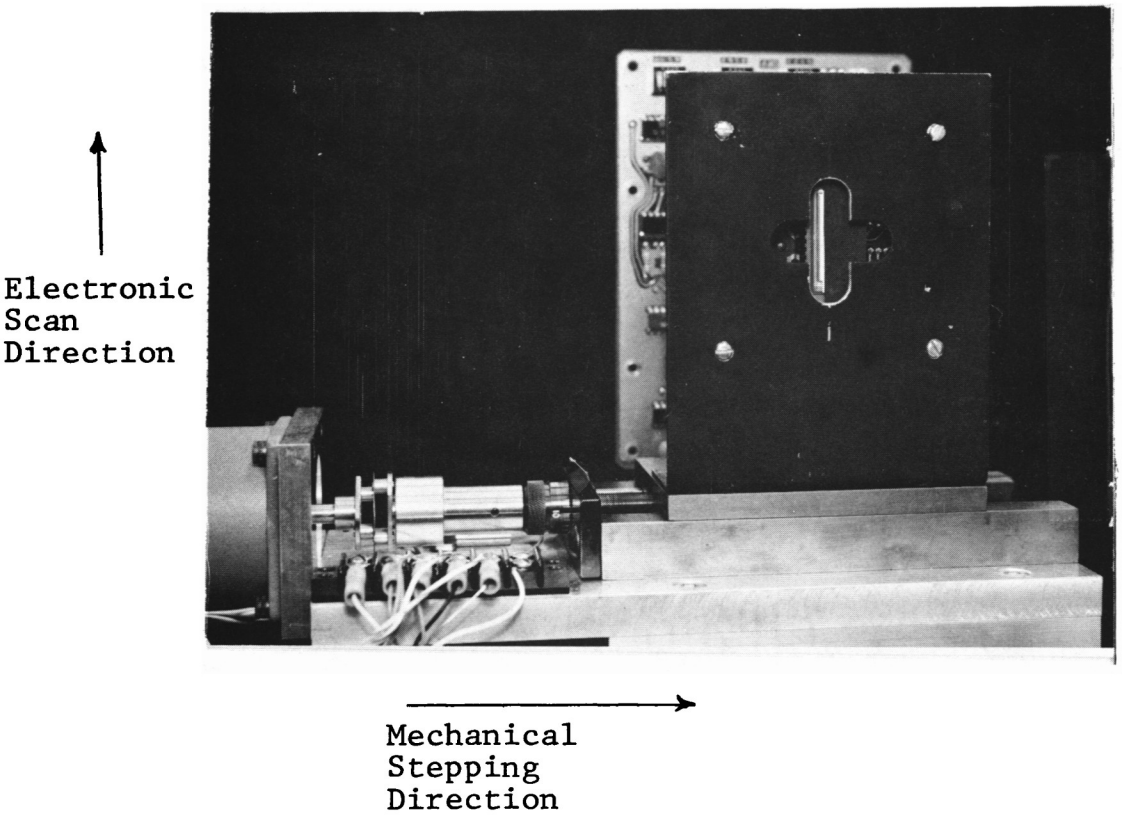

Figure B.13. Linear Detector Array

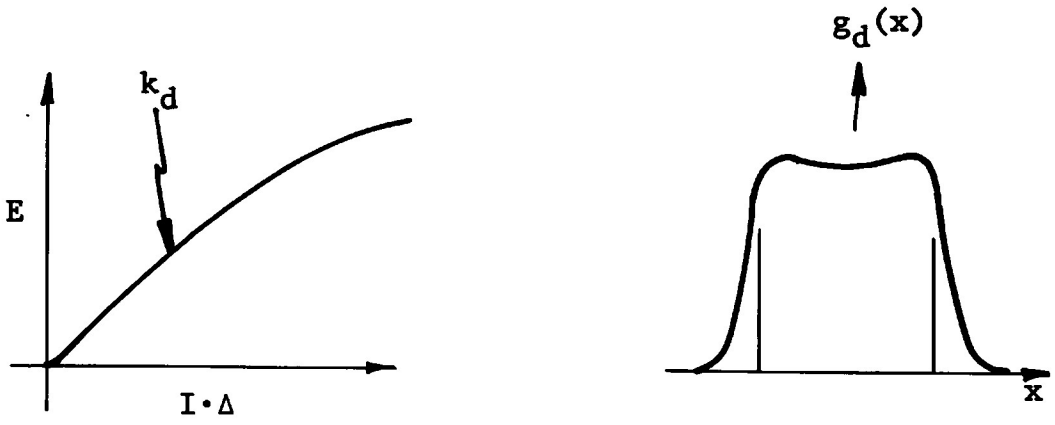

Figure B.14. Photodetector Impulse Response Properties.

stepper. The sample positions taken by the detector array in x and y can be expressed as a series of delta functions denoted as

$$\text{Ш}\left(\frac{x}{dx}\right)\text{Ш}\left(\frac{y}{dy}\right)$$

Given the light intensity distribution I(x,y), the detector output may be written as the voltage signal E(x,y) plus the detector noise η_d which is expressed as

$$E(x,y) = \Delta\{I(x,y) \circledast h_d(x,y)\}\, \text{Ш}\left(\frac{x}{dx}\right)\text{Ш}\left(\frac{y}{dy}\right) + \eta_d(x,y)$$

A scan of the output data I(x,y) is taken for each of two phase conditions in the optical channel as discussed in Section 2. We denote these two outputs I_1 and I_2. The scanned and digitized output is provided for I_1 and I_2 on a line by line basis so that the subtraction $I_1 - I_2$ can also be done on a line basis. The final output is the difference of the two readout voltages which we denote as B(x,y) the sky brightness data, i.e.,

$$B(x,y) = E_1(x,y) - E_2(x,y)$$

with

$$E_1(x,y) = E_2(x,y) = \Delta\{[I_1(x,y) - I_2(x,y)] \circledast h_d(x,y)\}$$

$$\cdot \text{Ш}(\frac{x}{dx}) \text{Ш}(\frac{y}{dy}) + \eta_d(x,y)$$

Digitization and subtraction of the pair of output data frames is a post-processing step of the readout process which provides digital sky brightness map data.

The process of digitizing an image proceeds as follows. The reference beam is set to $\pi/2$ relative phase and a line is integrated by the image sensor. The output is converted to a digital from and stored. The phase of the reference beam is shifted by $-\pi/2$ relative phase. The residual integrated signal in the Reticon is dumped prior to the start of the scan since it will have sensed some of the non-phase shifted signal during the phase change period. The new line is integrated by the sensor and A/D converted. This second digital output is subtracted from the first and stored. The sensor gain variations are digitally corrected and the data is transferred to the output storage device. The residual signal integrated by the image sensors during the slewing of the sensor is dumped prior to beginning readout of the next line.

The time required to perform the above operations is as follows:

$+\pi/2$ phase integration	10 ms
shift phase time	01 ms
$-\pi/2$ degrees phase integration	10 ms
mechanical shift to next line	05 ms
	26 ms total per line

Using only a 7200 element linear array the total time to produce a 7200 by 7200 cell image is 240 seconds. Use of fifteen parallel arrays allows a 16 second readout time.

The image sensor is composed of four Reticon 1872 element image sensors placed in series. The total one-dimensional number of elements is 7488 (4 x 1872). The extra elements provide for sensor overlap and an outside boarder. A beamsplitter is used to deflect half ot the incoming light to one pair of sensors, and the other half of the light to fall directly through to the other pair. A set of four sensors rather than a custom single sensor is proposed due to the expected high cost of a single IC containing over 7000 cells.

The Reticon image sensors are cooled to produce a more uniform and consistent output. Studies at Kitt-Peak have indicated that the Reticon is more consistent from frame to frame with its fixed pattern and gain variations. The noise from the device is also lowered somewhat with cooling.

Since the device will be operated in a partially evacuated chamber, cooling is made easier. Without convection by air, cooling can be provided by circulating cooled brine water through the base of the sensor mouth. A temperature of -10C should be sufficient for the require-

ments of the VLA. Cooling will reduce the dark current from an unimportant 1% at room temperature to an insignificant 0.07%.

The evacuated chamber also provides an additional benefit to the Reticon sensor devices. Without airborne contaminants and dust, the cover can be removed. This allows fewer surface-to-surface reflections in the system. Multipel surface reflections can cause interference patterns which can reduce the accuracy of the data. The devices will require a removable cover for use during maintenance periods where the vacuum is broken.

The analog outputs of each of the image sensors is fed to a high speed 12 bit A/D converter. The shift rate of each 1872 element sensor is 300 KHz which allows an integration time of 10 ms. The 300 KHz shift rate of the sensors is well below the maximum rate of the devices (20 MHz) but near the maximum for optimum signal-to-noise operation. A shift rate of 300 KHz with 1872 elements results in a 6.24 ms period for shifting. The difference between 10 ms and 6.24 allows time for mechanical movement between lines and phase shifting of the reference beam. Note that the dumping of the integrated image during line-to-line movement and phase shifting must be performed at the same rate as the subsequent valid image output rate in order to make the integration periods of all of the cells equal.

There are four integrations per output line. Two of these are required to sense the two images which have the phase of the reference beam shifted by 180 degrees. These two images must be subtracted prior to sending the data

out to the final output storage device. For the first integration, the output from the 4 A/D converters is fed directly into a multiplexer and then to a line buffer. For the second integration (where the phase of the reference beam has been shifted by 90 degrees) the digital outputs are multiplexed through an arithmetic unit (AU). The second input to the AU is the result of the first integration. These two digital data streams are subtracted and stored in the line buffer. The other two integrations are not digitized and are used only for dumping unwanted integrated data.

The resulting data in the line buffer has not yet been corrected for fixed pattern and gain variations. For subtracted lines, the fixed pattern (a variable dc shift from cell to cell) need not be compensated since the process of subtracting scan lines has removed this pattern. The fixed pattern buffer is provided for diagnostic purposes only. The gain variations (form cell-to-cell) must be removed and this is performed by feeding AU the data stored in the line buffer and the gain constants associated with each cell. The data in the line buffer is then read for transmittal to the final output storage device (tape drive, disc, etc.)

Detector Performance

The performance of the detector array readout and electronics should not be the limiting component of the VLA optical processor in terms of performance and accuracy. The signal-to-noise ratio of the sensors is expected to exceed 1000 to 1, and will likely be at least 2000 to 1 as reported in work at the Kitt-Peak Observatory. Additional performance can easily be obtained by averaging scans

(which reduces noise by the square root of the number of lines in the average) and by longer integrations which allows weaker signals to integrate to a larger fraction of the dynamic range. A longer integration could cause the brightest portions of the sky map data to saturate but fortunately, the Reticon image sensor has a well controlled blooming characteristics which will allow observation of weak returns everywhere except very close to the saturating points.

Spatial positioning of each cell is as accurate as the mask used to produce the image sensor IC. These masks are digitally formed and are accurate to much better than a single cell. Nevertheless, the spatial accuracy of the sensors will be verified during calibration testing.

The gain linearity of the Reticon can be made essentially as good as it can be measured. There are two types of linearity which must be considered. The first is the relationship between input intensity and output voltage with the integration period a constant. Both of these parameters were measured for an experimental unit at ERIM but were measurements limited by the accuracy of the reference equipment. Non-linearities which do exist will be removed in the same manner that gain variations are removed after digitization of data that was read out.

The effects of cell-to-cell fixed pattern and gain variations are easily removed by the means described previously. The values of each are derived at the beginning of each day by exposing the sensors with a controlled intensity uniform light. Several integrations are averaged to reduce the effects of noise and the averaged result is stored in the appropriate buffer. The time required to

perform this calibration sequence is less than a minute and is automatically performed.

Slowly varying changes in sensor gain functions will be accomplished by periodic recalibration. In order to determine the absolute changes in the detector gain, a fiber optic light source coupled to several detector cells outside the imaging area will provide an absolute reference.

Appendix C
SYSTEM RESPONSE AND ERROR AFFECTS

The overall system response can be defined in terms of the expressions for the input-output relations of each of its subsystems which were described previously in Appendix B. For the error-free case, we have the difference of two photodetector scans of the output giving the sky map data B as

$$B(x,y) = E_1(x,y) - E_2(x,y)$$

The photodetector readout E, as a function of the optical channel output I:

$$E_1(x,y) - E_2(x,y) = \left\{\left[I_1(x,y) - I_2(x,y)\right] \otimes k_d g_d(x,y)\right\} \Delta \cdot \text{Ш}\left(\frac{x}{dx}\right) \text{Ш}\left(\frac{y}{dy}\right)$$

The optical channel output I in terms of the recorded data t:

$$I_1(x,y) - I_2(x,y) = 4\, A_1 A_2\, F\left[t(u,v)\right]$$

The film recorded data t as a function of the recorder input s:

$$t(u,v) = s(u,v) \otimes k_r g_r(u,v)$$

The prefilter output s in terms of the visibility data V:

$$s(u,v) = \frac{1}{2}\, a_t(u,v)\,|V|\; e^{j[\omega_1 u + \phi(u,v)]}$$

After substitution through the above sequence of expressions, we have (leaving out the sample function for convenience) the sky brightness as

$$B(x,y) = 2\Delta A_1 A_2\; k_r k_d\; F\left[a_t(u,v)\,|V|\; e^{j\phi(u,v)}\right] G_r(x,y) \circledast g_d(x,y)$$

$G_r(x,y)$ is the transform of the recorder spatial response term $g_r(u,v)$, k_r is the recorder gain, k_d is the gain of the output photodetector and $g_d(x,y)$ is the photodetector spatial response.

The sky-map data is scaled in magnitude by $2\Delta A_1 A_2\; k_r k_d$, weighted by $G_r(x,y)$ and smoothed by $g_d(x,y)$. The sampling functions provides map data sampled as spacing d_x and d_y.

C.1 ERROR EFFECTS

We summarize here the results of our error studies. The vocabulary we use is as follows:

Defects are defined as imperfections associated with the processor or the u,v plane data. They are the source of errors in the map.

Errors are defined as the point by point difference between a perfect map and the map which results from the inclusion of a particular defect.

Phenomenologically, errors are the consequence of a defect.

There are a number of important defect sources:

Amplitude defects -	optics & recorder
Phase defects -	optical aberrations
Position defects -	film & recorder
Spherical wave defect -	the difference between spherical and plane waves in the processor

These have all been considered in detail analytically and numerically and are discussed below. Note that the map errors due to other light sources, e.g., the zero order dirty beam associated with the bias, are not considered here; see Appendix B.

The significant amplitude defect changes slowly over the x,y plane and is deterministic; therefore, it can be

compensated for by calibration at the readout photodetector. The phase defect, must, however, be properly constrained or its errors removed by calibration at the output plane. Phase terms linear in u and v cause an output scale change or a map position shift and can be accounted for by scale factor calibration. Quadratic and cubic terms can also be partially compensated by sensor plane orientation and position shift. Higher order terms are lower in magnitude and have been found to have an insignificant effect by comparison.

Phase defects originate in the usual wave aberrations of an optical system. Position defects originate in scan-position defects in the film and recorder. As will be seen, we are most concerned with the low-order, odd-power (1,3,5) terms in the power series, the even powers (2,4,6) contributing significantly less error to the outupt map. We have simulated the low-order even and odd terms and calculated the resulting map error for both the VLA aperture $a_t(u,v)$ and a clear circular aperture. By the VLA aperture we mean an aperture of unit transmission at the locus of points in the u-v plane sampled by the telescope. A clear aperture, in contrast, has unity transmission everywhere. "Uniform" aperture weighting was always simulated.

The sperhical wave defect has its origin in the Huygens spherical wavefronts which diverge from every point of the input plane to every point in the output plane. These wavefronts can only be approximated by plane waves (i.e., the Fourier kernel) over a finite region. This leads to the concept of a finite space-bandwidth product. The magnitude of this product depends on the magnitude and type of error acceptable in the processor output.

A computer analysis of map errors due to phase defects was made to establish a specification on allowable phase defects. For this analysis, the direct Fourier transform of the visibility function was computed for cases with and without phase defects. Comparison data was generated by taking the difference between the real part of the resultant Fourier transforms. The calculation was of the form,

$$\text{Error} = \text{Re}\left\{F\left[a_t(u,v)\ e^{j\omega_1 u}\right]\right\} - \text{Re}\left\{F\left[a_t(u,v)\ e^{j\omega_1 u}\ e^{j\theta(u,v,x,y)}\right]\right\}.$$

The real part only was used since the imaginary part will cancel in the two-scan subtraction process used to generate the output map data.

C.1.1 MINIMIZING MAP ERRORS DUE TO DEFECTS

Compensation and calibration to remove map errors due to certain important defects can be accomplished completely or in part depending on the defect. The spherical wave defect is represented by terms of the form

$$\frac{e^{jkz}\left(1 - \frac{4u^3x}{8z^4} + \frac{6u^2x^2}{8z^4} - \frac{4ux^3}{8z^4} + \text{H.O.}\right)}{R_1R_2^2R_3}$$

It is possible to compensate for the linear phase shift term by positioning the sensor array to the corresponding displacement in the output plane. Similarly, the focal shift term can be compensated by a shift of focus being applied to the sensor array. The cubic phase shift can be partially compensated by a displacement in the output plane corresponding to a linear approximation to the cubic. Note that the shift of focus can be partially implemented with a plane image sensor array of proper orientation.

In the numerical results to be described, we have simulated these compensations by removing the corresponding defect. The linear phase shift compensation is referred to as "linear", the quadratic as "focus". In both these cases the gain change due to $1/R_1R_2^2R_3$ is also included.

Turning to the phase defect simulations, these too can be partially compensated (as described for the spherical wave defect terms of power 1, 2, and 3). We have not included such compensation in these simulations however.

Errors due to position defects can also be reduced by calibration techniques. Conceptually (and in practice) these are implemented by adding a few test stars to the visibility data being mapped and calibrating the processor based on error signals derived from the image of these stars. In the numerical simulation of position defects we have not allowed for any calibration removal of map error.

C.1.2 MAP ERROR CRITERIA

We are concerned with the difference between the true Fourier transform and the output of the optical processor.

This error is to be less than 1% of the peak response to a point source anywhere in the map. The error criteria applies to the center of the point image and everywhere beyond the maximum of the first sidelobe. It does not apply between the first sidelobe and the center of the response. We have also included in this study the errors beyond the second null of the point source image. In terms of a synthesized beam, these regions of interest are shown in Figure C.1.

The errors we have studied have been primarily in the region of the point image; e.g., four to six sidelobes in all directions. We have found that the errors (error maps) are well behaved with peaks near the 3 dB point of the main-lobe and falling monotonically to small values within a few beam diameters. DFT calculations of dirty beams at many hundreds of beam diameters from the central lobe have also been performed.

The difference between the DFT and the FFT results (of Figure C.2) is due in part to the finite grid size used in the FFT, the form of "uniform" weighting used with the FFT grid and the form of "uniform" weighting used with the DFT. The weighting for the DFT was made "uniform" in terms of sample density along a baseline.

C.1.3 NUMERICAL RESULTS

The principal results from polynomial phase defect simulations are presented in Figure C.2. Digital computations were performed using both a fast Fourier transform (FFT) algorithm and a direct computation of the Fourier transform (DFT). The results from FFT simulation are on the left and the results from DFT simulation are on the

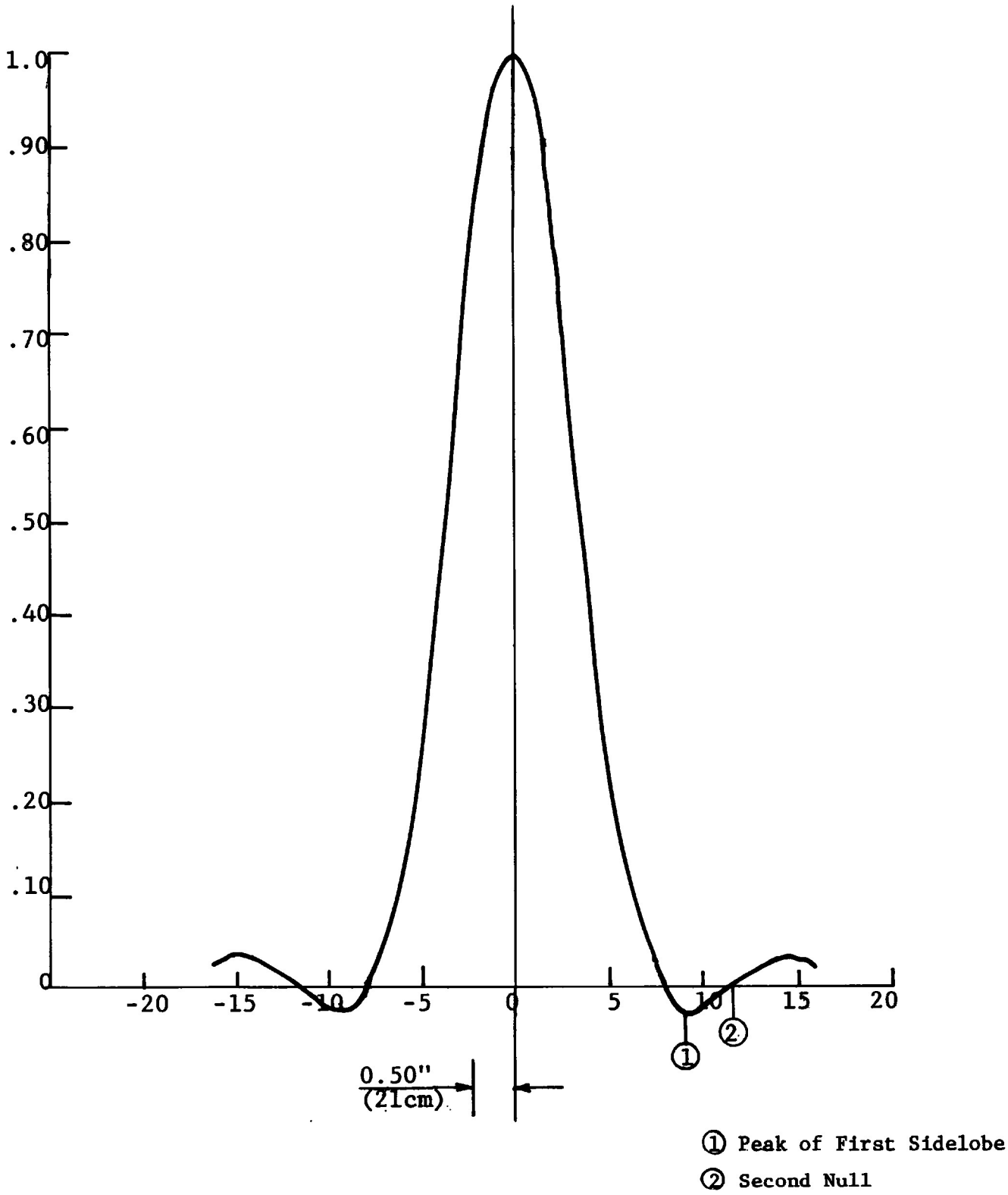

Figure C.1. VLA Synthesized Beam

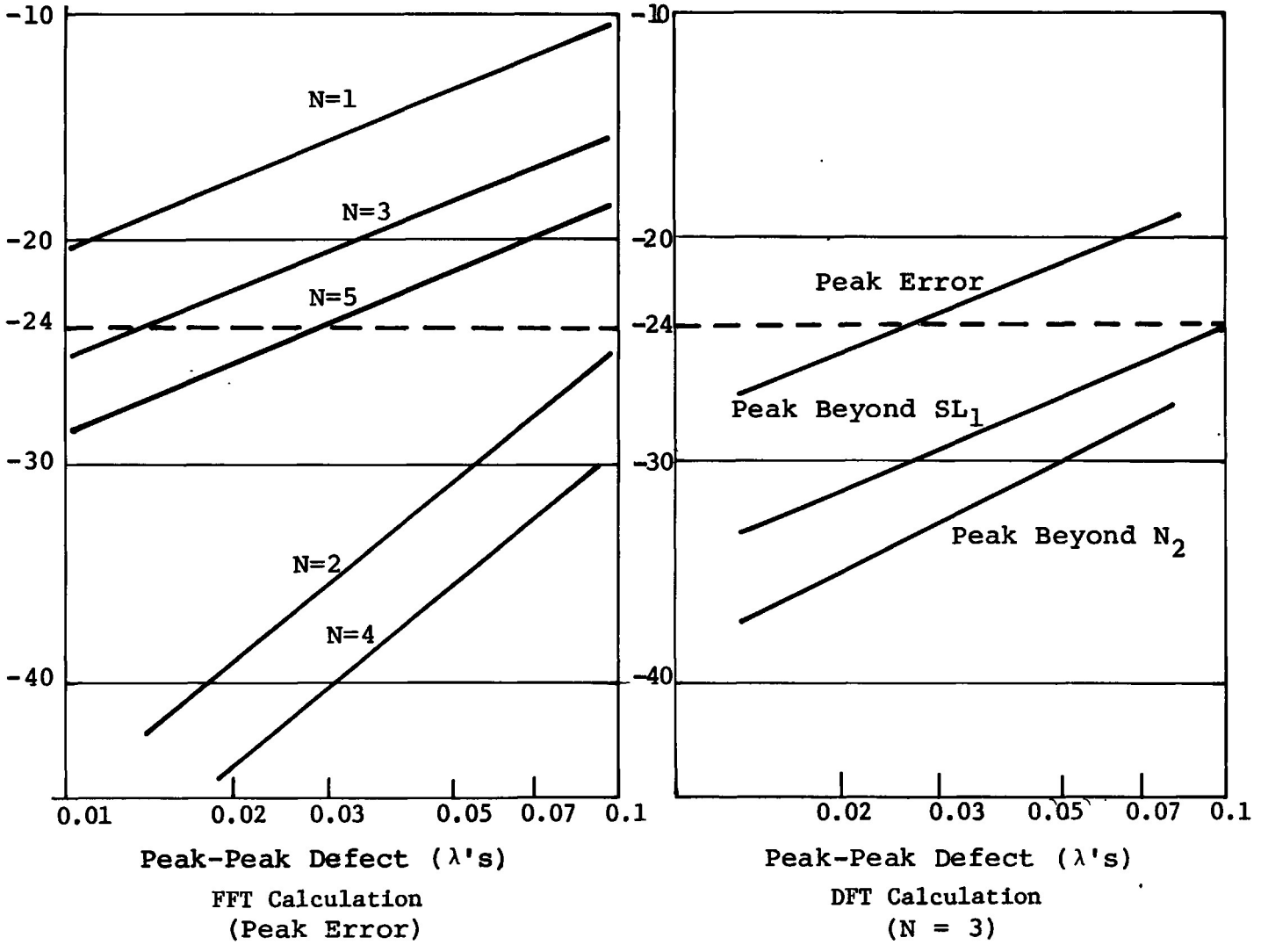

Figure C.2. Map Error Versus Polynomial Phase Defect

right. The FFT results are the first five terms in a power series (N = 1, 2, 3, 4, and 5). The odd power defects cause a larger map error than the even powers. The case, N = 1, is readily compensated by repositioning of the readout photodetector and is not discussed further.

The cubic term, N = 3, is the most troublesome. The result of simulations studies are shown in the right side of Figure C.2 where the peak map errors, as well as those beyond the first sidelobe (SL_1) and the second null (N_2) are shown.

From these results we see that the peak map error beyond the first sidelobe is -24 dB at a peak-peak cubic phase defect of 0.1 revolutions ($\lambda/10$ and -27 dB at the equivalent of $\lambda/20$). These can be taken as reasonable phase defect design specifications. The system can be manufactured and the error is acceptably small.

Turning to the spherical wave defect simulations, Figures C.3 and C.4 show the various map error values (peak, SL_1, N_2) as a function of location in the output plane. Figure C.3 demonstrates the various map errors when the processor is compensated for gain and the linear phase shift defect (sensor position calibration); Figure C.4 demonstrates the various map errors when the processor is compensated for gain and both the linear and quadratic (shift of focus) terms.

Figures C.3 and C.4 simulate a representative optical processor design operating with a VLA input array. The design parameters and VLA observing configurations are tabulted in the figures. These simulations include the

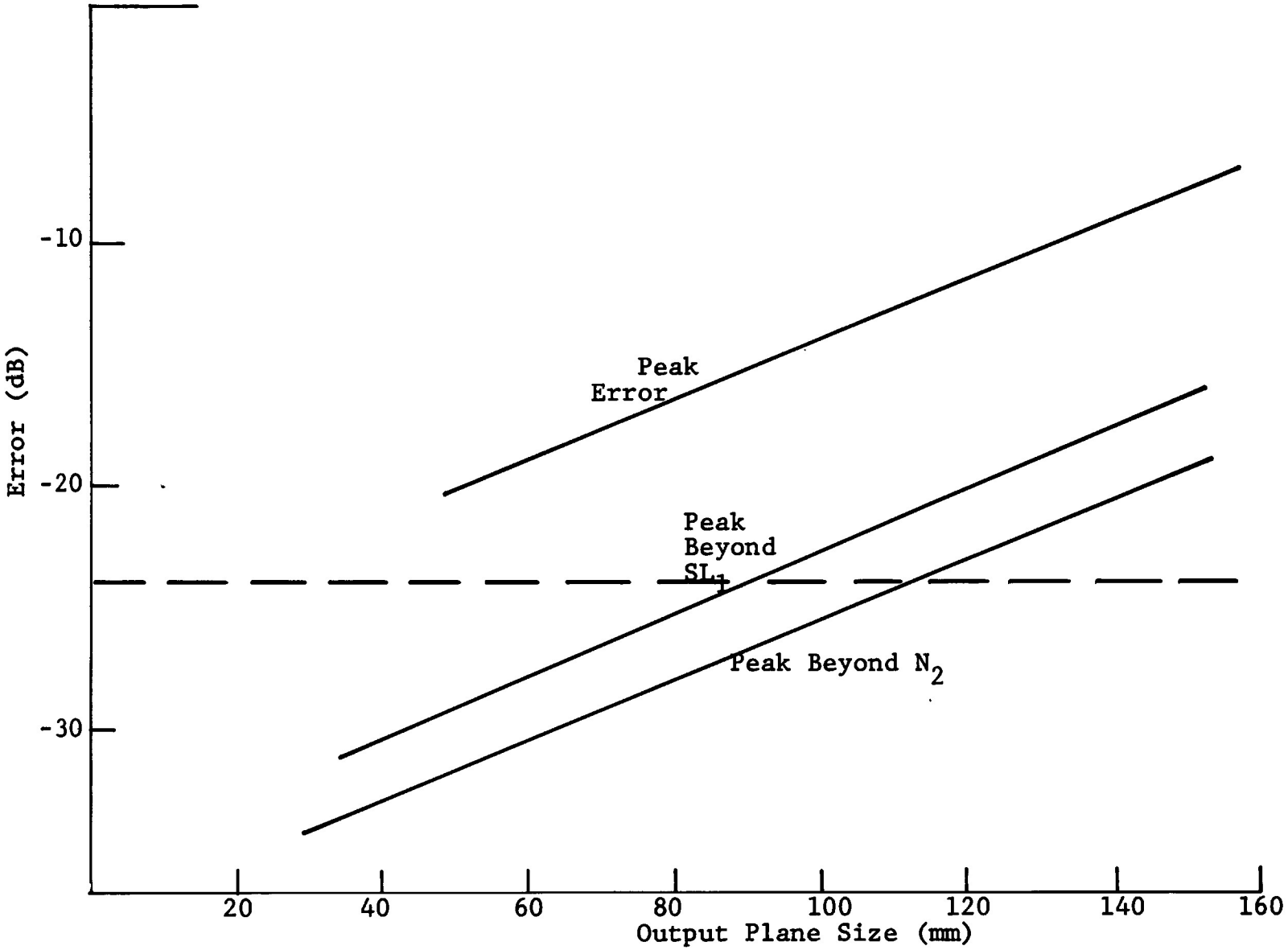

Figure C.3. Map Error versus Spherical Wave Defect (with gain and linear defect compensation).

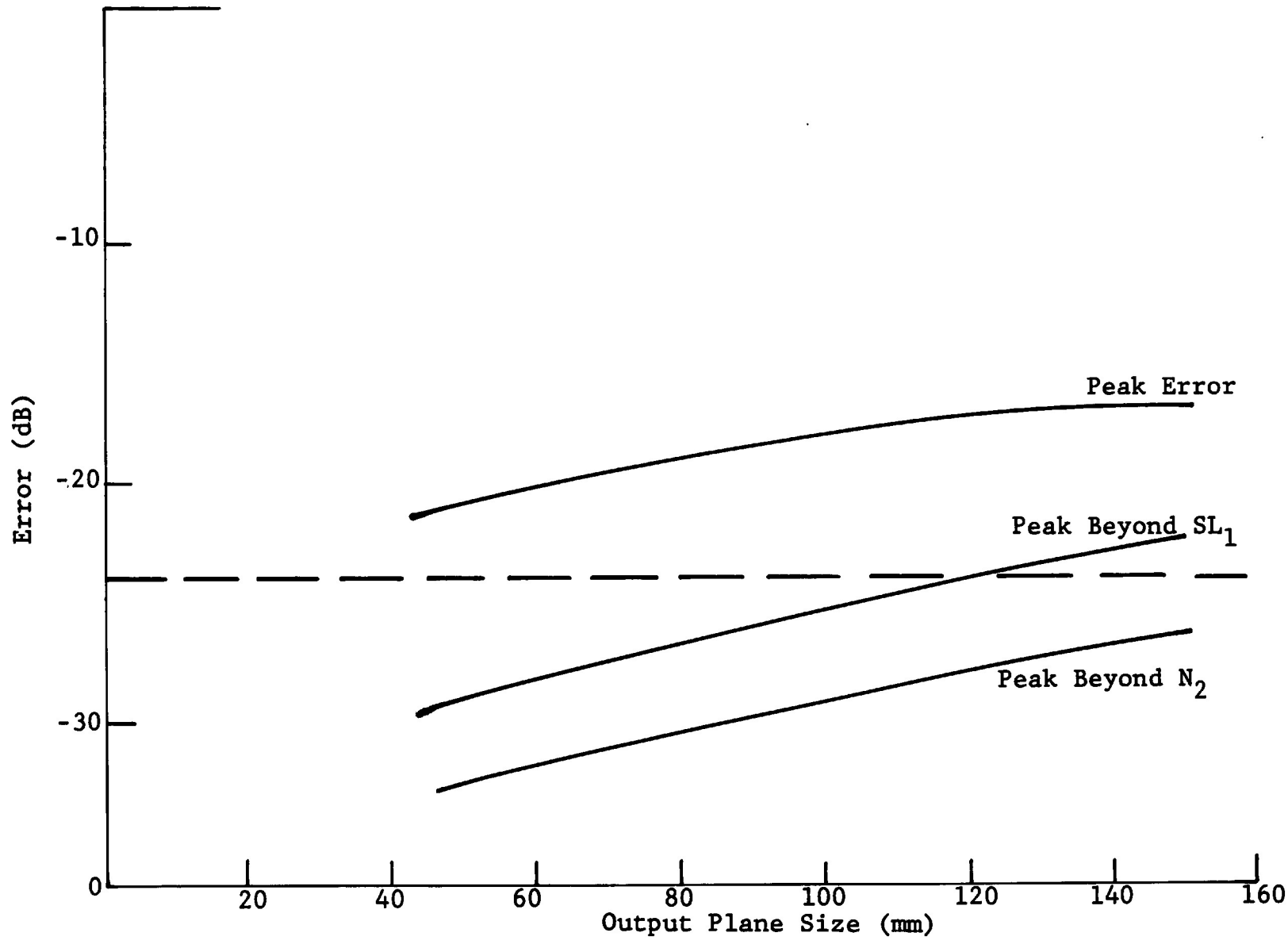

Figure C.4. Map Error versus Spherical Wave Defect (with gain, linear and quadratic phase defect.

slowly changing amplitude defect which arises in the diffraction integral as well as the much more important phase defect due to the difference between spherical wavefronts (the processor) and plane wavefronts (the Fourier transform).

From these results we see that the first sidelobe error curves pass through -24 dB at an output plane radius of 90 mm for the gain and linear compensated case. The same error contour passes thorugh 123 mm for the gain and linear and focus compensated case. This suggests that both linear and focus compensation are required to obtain a 100 mm square map area. This could be implemented but will not be necessary.

Discussions with optical designers confirm that an aberration can be introduced which will displace the center of the spherical wave defect from the optical axis to the center of the map. This would then center the required 100 mm map interval in the region of minimum error due to SWD.

We would choose to keep the map center where it is for MTF reasons in the film recorder. This would result in a map edge at about 52 mm (in Figure C.4) and have an error due to linear and gain compensated SWD of not more than -28 dB.

The above design concept is suggested as reasonable for the VLA processor.

Turning finally to recorder beam and film position defects, we note that the shrinkage in film will be a simple magnification effect and is calibrated out from test signals written on each film frame. The shrinkage is known

to be space variant but with a small random value by our standards. The beam position defect is another question however.

Complete information on residual beam position errors, after linearity correction has been applied, is not readily available. What is available suggests that a combined random and deterministic model would apply. Some idea of recorder requirements can be obtained from a simulation of beam position defects using a power series. This has been done and the results are shown in Figure C.5.

These simulations have been performed for the usual 40^{o} δ VLA aperture function by means of a direct Fourier transform. As expected from the polynomial phase defect studies, the cubic term is most troublesome. From these results we conclude that a 1:30,000 PP cubic position defect results in a -24 dB error for a point object at the map edge furthest from the optical origin. That is, at the position in the output plane which is 1000 optical beam diameters (first null) from the origin. At 1:20,000 PP cubic position defect the resulting map error will be -22.5 dB, again at the map edge.

It is interesting to note that while position and phase defects are different, their difference is relatively small in some circumstances. For example, a point source at the 1000 beam diameter position has less than 1 dB difference between the map error due to 1:30,000 position defect and (λ/10) phase defect. The (λ/10) phase defect is 1:30,000 of the total optical aperture phase or space bandwidth of 3000 cycles.

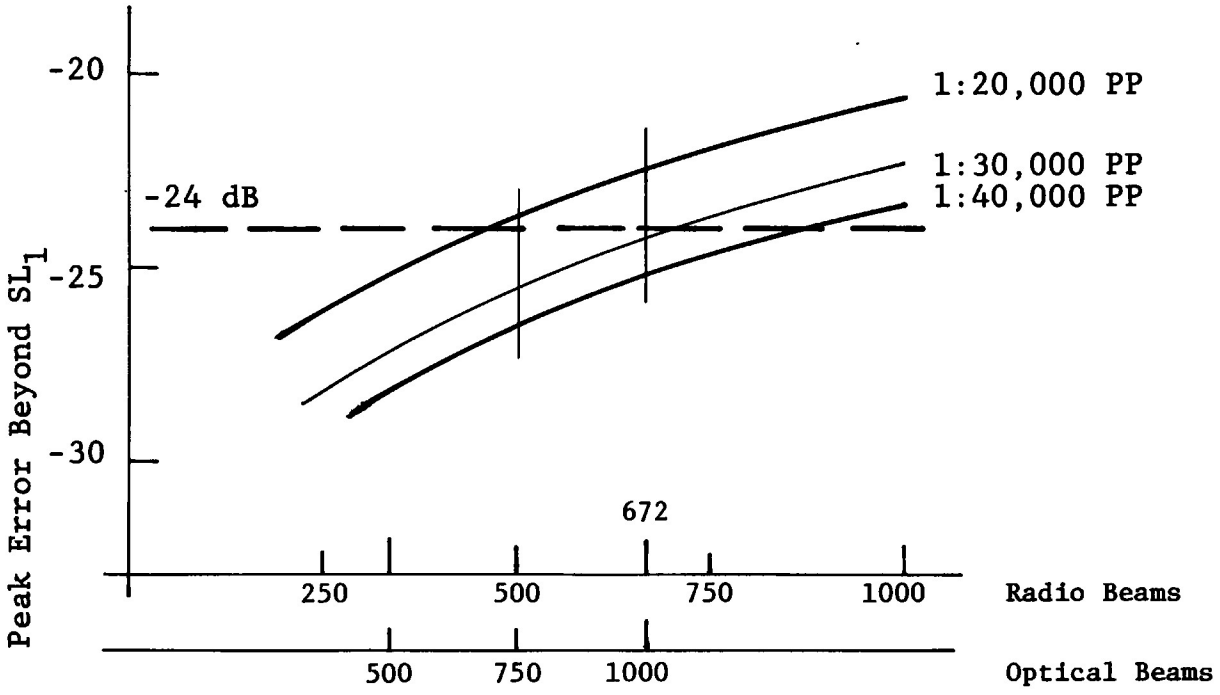

Figure C.5. Peak Map Error Beyond First Sidelobe versus Synthesized Beam Number or Map Size.

The recorder position defect was modeled as a cubic with a p-p value at the edge of the uv plane equal to 1 part in 20,000, 30,000 and 40,000 of the uv plane.

Further study of position defects is currently underway at NRAO. Some modeling based on experimental residual position defect data (MIT) may further delineate recorder position specifications.

Discussion with recorder system manufacturers (Celco Corporation) indicates confidence in system stability (temporal and spatial) of 1:60,000. The implication is that the desired linearity can be obtained if it is possible to measure the deviation from linearity, calculate and implement suitable deflection correction wave forms. Experience at ERIM, and with users of the Celco equipment (MIT and oil companies) indicates this is reasonable.

Note that the clear optical aperture will generate 1000 null beam diameters in the 3 dB primary beam diameter and that the VLA will generate 672 synthesized beam diameters (null) in the same space (FOV).

C.1.4 CONCLUSIONS AND DESIGN CONSIDERATIONS

A reasonable design concept follows. It is based on the assumption that cubic phase and position defects are the principal problem and that they will all add coherently to generate a worst case. The results are interesting.

A design concept:

1. Specify the optical system to have less than $\lambda/20$ PP cubic phase defect. This can be achieved with current manufacturing capability and should not be expensive.

2. Further, specify the optical system to have an intentional aberration which to first order shifts the center of the spherical wave defect from output plane center to map center. This will increase the cost of the optical system but not significantly.
3. Specify the recorder to have a 1:20,000 PP or less cubic position defect.

The corresponding phase defect budget can be tabulated as follows:

1. The cubic phase defect is $\lambda/20$ or	$.05\lambda$
2. The spherical wave defect at 52 mm for linear and gain compensation only -28 dB. This defect, if conservatively estimated as due solely to an uncompensated cubic phase term would correspond to	0.04λ
3. The recorder cubic position defect is as mentioned earlier within 1 dB of being equivalent to a scaled phase defect. Thus it is possible to interpret the -22.5 dB error associated with 1:20,000 PP cubic at the 1000 beam diameter map edge as equilavelent to	0.15λ

4. Assuming all phases add to form the worst case the total equivalent cubic phase defect would be 0.24λ

5. From the cubic phase defect study, this corresponds to a map error of -20 dB for a point object at the map edge.

The coherent superposition of all phase and phase-like errors can be prevented with proper design. Thus these results are somewhat pessimistic.

In conclusion we can say:

1. Cubic phase defects are the most critical. They arise naturally in the optics and in the linear compensated SWD.
2. Position defects are phenomonologically similar to (but not the same) as phase defects. The map errors they generate are about equal when the position defect is scaled via the u,v fringe period into an equivalent phase defect.
3. The spherical wave defect (SWD) has linear, quadratic and cubic terms in it and they can be partially compensated with sensor repositioning.
4. An optical system aberrations specification of $\lambda/20$ is reasonable from the map error and manufacturing point of view.

5. The SWD should not be a significant problem with recentering to the map.
6. A simple, but conservative, calculation of total equivalent cubic phase defect due to the various sources suggests that a -20 dB can be achieved everywhere in the full 1000 beam diameter map field (equivalent to the 3 dB FOV for the primary beam).
7. More information on the distribution of errors in highly corrected recorders is required.

In summary, a $\lambda/20$ optical system with an aberration suitable for SWD-offset to map center, combined with a "1:20,000 PP" recorder is capable of mapping the full 3 dB FOV from the full A-array u,v coverage.

APPENDIX D
SYSTEM CALIBRATION AND PRE-SETTINGS

D.1 CALIBRATION

The calibration of the processing system is conveniently viewed in terms of the expression for the system output data $E(x,y)$ made available from the photodetector.

$$E(x,y) = 2\Delta A_1 A_2 \, k_b k_f k_d \, F[t(u,v)] \cos(\theta_1 - \theta_2 + \theta_o) \, G_r \circledast g_d$$

Amplitudes A_1 and A_2

The optical field amplitudes A_1 and A_2 are not directly measurable but their modulus squared or power can be. To measure A_1 we block the reference beam, use a clear (no film) input aperture, and measure the power P_1 in the zero order light spot at the output plane with a single detector array element. We divide this measurement P_1 by the area β of the processor input plane which is known a priori. This gives A_1^2; then taking the square root of this quantity we have $A_1 = \sqrt{P_1/\beta}$. To measure A_2 we block the light in the Fourier channel and measure the power of the reference beam at the output plane with a single detector array element which gives us the power reading $P_2 = A_2^2$ and taking its square root gives A_2.

Recorder Gain k_r

The gain term for the film recorder $k_r = k_b k_f$ defines the relation between the recorder input voltage and the film optical transmission. To measure k_r we measure a set of test points in the gain relationship between input voltage

and the optical transmission of the film. The input voltage is a sinusoid of fixed frequency. At four separated prescribed locations or apertures on the film, we record a sinusoidal pattern using a raster scan, the sinusoid being written in one direction only giving a grating pattern. Each of the four gratings is recorded with an input voltage of a different prescribed peak voltage, V_a, V_b, V_c, V_d. Once recorded, the film is entered at the optical channel input and the power at the peak of the diffracted spot of light is measured with a single detector array element. This is accomplished separately for each of the four input gratings giving four peak power measurements, P_a, P_b, P_c, P_d. The reference beam would be blocked during this measurement. The power illuminating the aperture of the input gratings is determined from knowledge of the full input aperture power P_1, the area of the full aperture β, and the individual grating aperture area β_a which are known. The grating illumination power is $P_1\ \beta_a/\beta$. The peak-to-peak amplitude transmission variation for these sinusoidal film recordings corresponding to the input voltage peaks V_a, etc., is

$$t_a = 4\left[P_a\left(\frac{\beta}{\beta_a P_1}\right)\right]^{1/2}$$

$$t_b = 4\left[P_b\left(\frac{\beta}{\beta_b P_1}\right)\right]^{1/2}$$

$$t_c = 4\left[P_c\left(\frac{\beta}{\beta_c P_1}\right)\right]^{1/2}$$

$$t_d = 4\left[P_d\left(\frac{\beta}{\beta_d P_1}\right)\right]^{1/2}$$

The desired points on the recorder gain curve are simply the above optical transmission values divided by their respective input voltages t_a/V_a, etc. This entire procedure can be fully automated and the gain curve points computed and stored for use as calibration data in the output photodetector read-out procedure.

Spatial Scale Factor

The spatial scale factor for the output x,y coordinates is governed by the combination of the recorder scaling of frequency at the input u,v plane and the optical Fourier transform scaling of the input to the output plane. Calibration is accomplished by recording several prescribed input frequencies and then Fourier transform processing of this recorded data. The optical Fourier channel would be operated with the reference wave absent (blocked). The output photodetector would measure the spatial location of the peak of the output light spots corresponding to the recorded input frequencies. The measured positions would be used to establish the spatial scale factor for sky map data B(x,y). The recorded frequencies would be selected for a suitable sampling of the output plane in both x and y dimension, e.g., for x = 11, 56, 101 mm and y = 0, ±25, ±50 mm. The entire procedure would be automated.

Output Weighting G_r

The output weighting factor $G_r(x,y)$ can be measured in normalized form and, if desired, its weighting affect can be removed. Measurement of G_r^2 at several sample points in the output x,y plane is accomplished at the same time that the spatial scale factor measurement described in the preceding paragraph is made. What is done is to measure the peak of the diffracted light spots corresponding to each input frequency that is recorded. The peak value of the input signal that is recorded for this procedure must be set accurately to the same value for each of the frequencies recorded. The peak power at the center of the out-light spot for the lowest recorded frequency is measured and this measurement is used to normalize the measurements obtained for all frequencies. Taking the square root of each of these normalized measurements gives data which describes the weighting caused by $G_r(x,y)$ over the sky map data. Again, this can be accomplished automatically.

Photodetector Gain k_d

Calibration of the detector element responses k_d is done by illuminating the array with a light source of known power. Rather than attempting to illuminate the full detector array with one broad light beam, we use a fiber optic feed which is coupled to a light source of known intensity at one end. The opposite end is moved over the photodetector array by a mechanical translation stage. The detector array elements each make a measurement of the calibration light source. The gain of individual elements is the ratio of the detector output voltage divided by the known input light intensity. The gain of each detector is

corrected or normalized by multiplying each detector output signal by a correction factor. The correction factor for a given detector element is the ratio of its output measurement of the calibration light source divided into the output of one detector element which is taken as a reference. This correction factor is stored and is applied to the data routinely obtained by the detector array after the detector output has been digitized.

D.2 PRE-SETTINGS

Prior to calibration discussed in Section D.1 several elements of the system must be checked to assume proper operating condition or pre-scattering. The optical recorder, the recorder film developer and the laser in the optical processing channel require the check-out discussed below.

Recorder Scan Linearity

The u,v plane spatial scale factor is governed by scan position control of the optical recorder writing beam. Scan control in the recorder is designed to have a linear correspondence to u,v position coordinate of the visibility data. This linear scale factor does not have to be exact in an absolute sense because of the use of a scale factor

calibration procedure discussed in the preceding paragraph. It is, however, expected to be settable to a prescribed value to within 0.005% by use of a scan position test and monitoring provisions built within the recorder. Of equal and possibly greater importance is any departure from a linear scan over the u,v plane. Such departures, or scan nonlinearity, are present but are constrained to a tolerable level. The scan nonlinearity is sensed and adjustment made if needed by use of the scan position test and monitoring provisions built within the recorder system. These provisions can be described in terms of a linearity test procedure. A single precise frequency is written on the recorder's CRT phosphor using a two-dimensional raster format. The pattern on the phosphor is projected onto a precision optical grating and the light pattern seen through the grating is sensed by a photomultiplier. This light pattern is defined by the difference in phase between the phosphor writing and the reference grating. The photomultiplier output is amplified and displayed on an oscilloscope monitor. Departures from a linear scan are seen as a modulation of the light collected by the photomultiplier. The reference grating and the pattern written on the CRT phosphor are both two-dimensional. The phosphor pattern consists of a set of resolvable parallel scan lines with a fixed-frequency modulation along the scan lines. The optical grating has the same spatial structure in the form of clear and opaque regions. It is expected that a once-a-day check for possible minor adjustment of recorder scan linearity will be required by the system operator.

Recorder Focus

Focus of the recorder writing beam is accomplished using the provisions for scan linearity setting Readout of the writing beam through the reference grating for the linearity check generates a bias level which reaches a peak when the writing beam is in best focus. A potentiometer control located at the recorder for focus of the writing beam spot is adjusted for best focus as determined from the grating readout bias level.

Recorder Writing Beam Bias

The bias level of the writing beam of the optical recorder is checked in terms of the beam current level of the recorder CRT. A beam current meter and adjustment control are provided at the recorder for measurement and control of beam bias level. This is done once each day.

Film Developer and Film Supply

The film developer for the optical recorder must be checked to assure that the chemical film developer is at a proper temperature and that the developer solution is at the proper supply level, clean and of a proper chemical composition. Temperature is indicated by a temperature sensor at the film developer equipment chemical developer level and condition are read from a direct viewed sample tube. Film developer checkout is done one per day.

The film frame supply at the CRT recorder must be checked to assure an adequate supply.

Laser

The laser used as the coherent light source for the optical processing channel should be examined briefly once each day to check for proper optical, electrical and cooling conditions.

REFERENCES

1. G. W. Swenson and N. C. Mathur, The Interferometer in Radio Astronomy, Proc. of IEEE, Vol. 56, No. 12, December 1968.
2. R. G. Strom, G. K. Miley and J. Oart, Giant Radio Galaxies, Scientific American, August 1975.
3. C. Aleksoff, Anti-hermitian Input Possibilities, ERIM Internal Memorandum, 7 December 1976.
4. J. Fienup, Phase Modulation Encoding, ERIM Internal Memorandum, 2 September 1976.
5. J. Fienup, Method for Imaging Both Halves of u-v Plane on Film Simultaneously, ERIM Internal Memorandum, 11 November 1976.
6. J. Fienup, Basic Limitations of Encoding Methods, ERIM Memorandum, 21 September 1976.
7. I. Cindrich, Scanning Beam Model with Scan Position Errors, ERIM Internal Memorandum, 19 July 1976.
8. I. Cindrich, Optical Processor System Model, ERIM Internal Memorandum, 5 November 1976.
9. A. Klooster, VLA Laboratory Measurement of Fourier Transform Using π Shift of Reference Beam, ERIM Internal Memorandum, 16 August 1976.
10. C. Aleksoff, Phase Error Plots, ERIM Internal Memorandum, 16 August 1976.
11. C. Aleksoff, Output Calibration Correction for Phase Errors, ERIM Internal Memorandum, 9 November 1976.
12. C. Aleksoff, Relating Phase and Ray Aberration Error, ERIM Internal Memorandum, 7 September 1976.
13. C. Dwyer, Film Coherent Optical Quality Considerations, ERIM Internal Memorandum, 26 October 1976.
14. C. Aleksoff, Film and Film-Gate Considerations, ERIM Internal Memorandum, 6 October 1976.
15. L. Somers, F. Schwab and C. Aleksoff, Spherical Wave Defects for a Particular Optical Fourier Transform Configuration, ERIM Internal Memorandum, 25 October 1976.

REFERENCES
(continued)

16. L. Somers, F. Schwab, and J. Garalund, Errors in an Optical Fourier Transform Processor Due to Certain Phase Error Effects, ERIM Internal Memorandum, 11 November 1976.

17. I. Cindrich, Fourier Transform Lens Design, ERIM Internal Memorandum, 19 November 1976.

18. J. R. Fienup, Detected Signal, ERIM Internal Memorandum, 27 July 1976.

19. J. Fienup, On-Axis Impulse Response, ERIM Internal Memorandum, 7 January 1977.

20. R. Dallaire, Preliminary Test Comparisons Between the Reticon and Fairchild Sensor Arrays, ERIM Internal Memorandum, 28 September 1976.

21. R. Dallaire, Preliminary Detector Array Evaluation, ERIM Internal Memorandum, 1 September 1976.

22. R. Harrison, Reticon Information Summary, NRAO Internal Memorandum, 23 August 1976.

23. R. Harrison, Optical Processor Detection Characteristics, NRAO Internal Memorandum, August 1976.

24. C. Aleksoff, Sampling Considerations, ERIM Internal Memorandum, 8 September 1976.